Journal of Jnde
Non Destructive Testing and Evaluation

ISSN 0973 - 9610

September 2023
Volume 20 ● Issue 3

An Official Journal of the Indian Society for Non Destructive Testing



NDE of Civil Infrastructures

Indian Society for Non-Destructive Testing
ISNT
www.isnt.in

An ISNT Publication

jnde.isnt.in

SIUI

Total Focusing Method
32:128PR / 64:128PR PAUT
4-channel TOFD





Ultrasonic flaw detector & thickness gauge

PA low-profile scanner

Compatible with Olympus.



www.siui.com/ siui@siui.com

Contents

2 LETTERS
- President Talk
- Managing Editor's Talk
- Guest Editor's Talk

3 CHAPTERS

4 NGC/NCB MEMBERS

6 CHAPTER ACTIVITIES

18 TRAINING MANAGEMENT BOARD

25 TECHNICAL PAPERS

- **Acoustic Emission-Based Non-Destructive Technique for Integrity Assessment of Heavily Reinforced Typical Trunnion Beam of Spillway Structure**
  A. Thirumalaiselvi, M. Kannusamy, Srinivas Voggu and Saptarshi Sasmal
- **Enhancing Corrosion Monitoring in Bolted Steel Joints Through Ultrasonic Inspection**
  Jay Kumar Shah, Subhra Majhi and Abhijit Mukherjee
- **Monitoring Stress Concentration Using Ultrasonic Signals**
  Saurabh Agarwal, Surendra Beniwal and Debdutta
- **Assessment of Residual Compressive Strength of Geopolymer Concrete Exposed to Elevated Temperature Using Artificial Neural Network Approach**
  Kishor S. Kulkarni, Sana D. Sayyad and M. Reyazur Rahman
- **Robotic Ultrasonic Pulse Velocimetry for Submerged Concrete Assets**
  Susheel Patil, Ashish Antony Jacob, Vineet Upadhyay, Tanuj Jhunjhunwala, Prabhu Rajagopal and Krishnan Balasubram
- **Ultrasonic Imaging for Detection and Mapping of Complex Pattern of Subsurface Cracks in Concrete**
  Suhaib Ul Reyaz, Surendra Beniwal

81 NDE PATENTS

Journal of Non Destructive Testing and Evaluation

SEPTEMBER 2023
Volume 20 - Issue 3

JNDE EDITORIAL Team

Managing Editor : **Bikash Ghose,** HEMRL-DRDO

Chief Editor : **Prof. Krishnan Balasubramaniam** IIT Madras

Editorial Team : **Bikash Ghose,** HEMRL-DRDO
Debasish Mishra, GE Global Research
Digendranath Swain, VSSC
Diwakar Joshi, IQS
Menaka M, IGCAR
Paritosh Nanekar, BARC
Phani Mylavarapu, DMRL-DRDO
Prabhu Rajagopal, IIT Madras
Ravibabu Mulaveesala, IIT Delhi
Sarmishtha Palit Sagar, NML-CSIR
Shyamsunder M T, Azereri Pvt Ltd
Surendra Beniwal, IIT Jammu

on the COVER Page



NDE of Civil Infrastructures

OBJECTIVE - This Journal of Non Destructive Tesing & Evaluation (JNDE) is published quarterly by the Indian Society for Non Destructive Testing (ISNT) for promoting NDT Science & Technology. The objective of this Journal is to provide a forum for dissemination of knowledge in NDE & related fields. Papers will be accepted on the basis of their contribution to the growth of NDE Science & Technology.

The Journal is for the private circulation to members only. All rights reserved throughout the world. Reproduction in any manner is prohibited. Views expressed in the Journal are those of the authors' alone.

PUBLISHED BY: Mr. Bikash Ghose - Managing Editor, JNDE

For JNDE Subscription / Advertisement / New / Renewal of ISNT Membership Inquiries Contact:
Indian Society for Non-Destructive Testing (ISNT)
Modules 60& 61, 3rd Floor, Readymade Garment Complex,
SIDCO Industrial Estate,
Guindy, Chennai - 600 032, India
Tel: 044-2250 0412 / 4203 8175 Email: headoffice@isnt.in

LETTERS

PRESIDENT TALK



DIWAKAR JOSHI

Dear Friends

Greetings!

June 2023 issue of JNDE was on "Emerging Technologies in NDE". It was well received by the readers,thanks to Dr. Debashish Mishra, our guest editor.The current issue is on "NDE of Civil Infrastructure" which is a very important topic in the current scenario.

You will be happy to note that the first program of PFMB on the subject of '2D & 3D Industrial Radiological Imaging and their applications' was completed at Trivandrum Chapter with excellent participation. You can expect many more programs from PFMB in the near future.

NCB has completed the successful audit of certification body (NABCB) to include all sectors in ICN, meeting the requirements of ISO 9712:2021. NCB is making efforts to connect to the regulatory bodies and Industries to promote our certification schemes. I sincerely appeal all members to ensure that ICN scheme is promoted at all places.

The TMB's work on training course time tables, study materials, course notes, practical training books, train the trainers and practice questions is in full swing. The final authorization of the chapters and training centers is in progress.

There are a lot of activities happening in the chapters including webinars, training programs and workshops, which is a good sign. Many chapters have started releasing E-Bulletins regularly.

Preliminary work of NDE 2023 has already been started. The theme this time is "Transformative NDE : Unleashing the Power of Advanced Technologies". The focus will be on NDE 4.0 and topics such as artificial intelligence, robotics, and advanced sensors, which have the potential to revolutionize NDE practices and enable more efficient and effective inspection processes. I appeal all of you to promote and spread the word to ensure maximum participation in the conference to make it a grand success.

I thank all authors, the editorial board, advertisers, and the whole team for releasing this issue in time. I am sure the readers will enjoy this issue.

Diwakar D. Joshi
President
president@isnt.in

MANAGING EDITOR TALK



BIKASH GHOSE

Warm greetings from Indian Society for Non-destructive Testing (ISNT).

We at ISNT are delighted to bring out a special issue of the Journal of Non-Destructive Testing & Evaluation (JNDE) on "NDE on Civil Infrastructure." This issue features six original technical papers that delve into the latest advancements in non-destructive testing techniques and their application in safeguarding the integrity of civil structures.

I would like to express my sincere gratitude to our guest editors, Dr. Surendra Beniwal from IIT Jammu and Dr. Debdutta Ghosh from CBRI-CSIR, for their dedicated efforts in shaping this special issue and helping us to release on time. Their expertise has been invaluable in curating a collection of articles that highlight the crucial role of NDE of civil infrastructure.

In addition to the technical contributions, this issue also provides insights into the vibrant activities of ISNT chapters over the past three months. These activities reflect the commitment of our chapters and members to advancing the field of non-destructive evaluation and promoting knowledge exchange within our community.

Once again, my heartfelt thanks to the guest editors, the authors, advertisers, and our readers for their continued support. I hope this special issue serves as a valuable resource for researchers, practitioners, and enthusiasts in the field of non-destructive testing.

One can now submit the original research articles to JNDE through the online portal of JNDE https://jnde.isnt.in.

Looking forward meeting you at the ISNT's Flagship 33rd Annual Conference and Exhibition on Non Destructive Evaluation (NDE 2023) to be held from 7-9 Dec 2023 at Hotel Orchid in Pune.

Bikash Ghose
Managing Editor, JNDE
me.jnde@isnt.in

GUEST EDITOR'S TALK



DR. SURENDRABENIWAL



DR. DEBDUTTA GHOSH

Civil infrastructure forms the backbone of modern society. This volume of JNDE contains six research articles contributing to non-destructive testing of civil infrastructure from eminent scientific community of India and abroad.

The aim of this special issue is to provide the readership with state of the art non-destructive evaluation techniques and advances in the current progress in the field. The applications involve acoustic emission based assessment, ultrasound based corrosion footprint monitoring, residual compressive strength assessment, stress concentration monitoring analysis of transmission signals, spatial mapping of complex subsurface crack patterns, and underwater concrete inspection in various forms of civil infrastructure.

Overall, all the articles have contributed towards addressing very interesting problems related to non-destructive testing and evaluation of civil infrastructures, and it is expected that readers will be benefited from these articles. Finally, we thank the authors for contributing their research work to be part of this issue. We also hope the readership will find this issue interesting and enjoying.

Dr. SurendraBeniwal
Email: surendra.beniwal@iitjammu.ac.in

Dr. Debdutta Ghosh
Email: debdutta@cbri.res.in

CHAPTERS

CHAPTER Chairmen & Secretary

CHAPTER CHAIRMEN/SECRETARIES

Shri Hemant Kumar
Chairman– ISNT-Ahmedabad Chapter
Head – Reliability Static
CAB-1st Floor, SEZ Refinery,
Reliance Industries Ltd, VP-CES,
Jamnagar-361142, Gujarat, India,
(Off)+91 288 6621826 / Mobile:0'9998215033
hemantk.kumar@ril.com / hemant.ril2013@gmail.com

Shri Jayesh Prajapati
Secretary– ISNT-Ahmedabad Chapter
CEO, Ultratech Engineers, 28, N.K. Industrial Park Part-1,
Bakrol-Dhamatvan Road, Bakrol (Bujrang),
Ahmedabad-382430
Mobile: 9824396155
jayeshprajapati82@gmail.com

Shri Shashidhar P. Pallaki
Chairman- ISNT-Bangalore Chapter
CEO, Pallakki NDT Excellence Center
No-411, A, 4th Phase, Peenya Industrial Area
Bangalore – 560058 / Cell: 0'9448060717
pallakki@pallakkindt.com

Shri Prakash Balasubramanian
Hon. Secretary, ISNT-Bangalore Chapter
Mb:9845192860
prakash@sasthascientific.com

Shri RG. Ganesan
Chairman- ISNT -Chennai Chapter
"Chief Executive,
BETZ ENGINEERING & TECHNOLOGY ZONE,"
"Door # 21, Dharakeshwari Nagar,
1st Street, Sembakkam, "
Tambaram to Velacherry Main Road, .
Chennai – 600 073
Mb: 9840175179
rg_ganesan@yahoo.com

Shri P. Anandan
Hon. Secretary, ISNT-Chennai Chapter
Technical Manager & NDT Level-III
Scaanray Metallurgical Services, Plot C-12,
Industrial Estate, Mogappair West, Chennai – 600 037
Mb: 9884036985
ap@scaanray.com

Shri P. Murali
Chairman, ISNT- Coimbatore Chapter
Mb: 9443491823
murlinaveen@gmail.com

Shri A. Rathinam
Hon. Secretary, ISNT-Coimbatore Chapter
Cell:0'9843011031
everestndt@gmail.com
isntcoimbatorechapter@gmail.com

Shri Raj Kumar Singh
Chairman, ISNT-Delhi Chapter
Cell : 0'9312433853
rajinspection001@gmail.com

Shri F. Siddiqui
Hon. Secretary, ISNT-Delhi Chapter
541/2, Group-I, Hastal, Uttam Nagar,
New Delhi – 110059
Cell: 0'9811466220
isntdelhi@gmail.com / delhindt@yahoo.com

Dr. Komal Kapoor
Chairman, ISNT Hyderabad Chapter
Chief Executive, NFC.
Hyderabad-62
Office: 040-2718 4300
Mb: 9100033949
cenfc@nfc.gov.in

Shri K. Somasekhar Reddy
Hon. Secretary, ISNT Hyderabad Chapter
SM,Quality Assurance Group(MT)
Nuclear Fuel Complex,
Hyderabad-62.
Office: 040-2718 3213
Mb:9985546729
ksreddynfc@gmail.com

Shri S Balamurugan
Chairman, ISNT- Jamshedpur Chapter
Head, Non-Destructive Testing & Sensors (NDT&S) Research Group
Research & Development Division, Tata Steel Limited
Jamshedpur 831001 / Ph: 0657 2648915
Mb:9204651390 / s.balamurugan@tatasteel.com

Shri Rohit Kumar Agrawal
Hon. Secretary, ISNT- Jamshedpur Chapter
Principal Researcher, Non-Destructive Testing & Sensors (NDT&S) Research Group
Research & Development Division, Tata Steel Limited
Jamshedpur 831001 / "PH: 0657 6648915
Mb:9897521586 / rohit.agrawal1@tatasteel.com

Shri S. Athmalingam
Chairman, ISNT Kalpakkam Chapter,
Associate Director, HSEG & Head - QAD
IGCAR, Kalpakkam - 603 102
Ph: 044-27480071/27480500 (Ext.23490)
Cell:0'9444501819
athma@igcar.gov.in

Shri M.V. Kuppusamy
Hon. Secretary, ISNT Kalpakkam Chapter
Head-QA Projects Section
Quality Assurance Division, SQ & RMG,
IGCAR, Kalpakkam 603 102
(Off) Phone:044-27480500 Extn. : 22388
Cell:0'8056090071
masikuppu@igcar.gov.in

Shri Sathyan V
Chairman, ISNT- Kochi Chapter
SM (Project), Bharat Petroleum Corp. Ltd. (Kochi Refinery)
PO Ambalamugal 682 302, Ernakulam, Kochi
0484-2822109 (O)
Cell:0'9446086345
sathyanv@bharatpetroleum.in

Shri Sibi Ignatius
Hon. Secretary, ISNT-Kochi Chapter
BPCL Kochi Refinery,
Ambalamugal 682302, Ernakulam, Kochi
Ph. No. 0484-2821121 / Cell:0'9446385611
sibiignatius@bharatpetroleum.in

Shri Dipankar Gautam
Chairman, ISNT- Kolkata Chapter
AB 121, Salt Lake, Kolkata – 700 064
Ph. No. 033 23581072
Cell: 98048 13030 / 98302 03223
dgautam1956@gmail.com / dipankargautam@yahoo.co.in

Shri Ajoy Kumar Chandra
Hon. Secretary, ISNT- Kolkata Chapter
134/2 Baruipara Lane,Kolkata -700 035
Cell : 9433728438
chandraak42@gmail.com

Shri S.K. Verma
Chairman, ISNT- Kota Chapter
NPCIL, PO - Anushakti,
Via - Kota (Raj) - 323 307
Cell:0'9413356402
surendrakverma@npcil.co.in

Shri Ranjeet Singh Rajpurohit
Hon. Secretary, ISNT Kota Chapter
Scientific Officer-E, -Quality Assurance Section
Rawatbhata Rajasthan Site, Unit 3&4
Nuclear Power Corporation of India
Ph. No. 01475-242052
Cell:9413358189
rsrajpurohit@npcil.co.in

Dr. P.P. Nanekar
Chairman–ISNT Mumbai Chapter
Head, Post Irradiation Examination Division
BARC, Trombay, Mumbai – 400 085
Off: 022-25594867 / 25564258
Cell: 0'9892161750
pnanekar@barc.gov.in / paritoshn@yahoo.com

Shri Samir K. Choksi
Hon. Secretary, ISNT - Mumbai Chapter
Choksi Imaging Ltd., 4 & 5, Western India House,
Sir P. M. Road, Fort, Mumbai- 400 001
Ph. No. 022-2610 1113 / Cell: 0'9821011113
Choksiindia@yahoo.co.in

Shri Jeevan Ghime
Chairman, ISNT-Nagpur Chapter
M/s. Becquerel Industries Pvt. Ltd.
33, Rushikesh Modern Co-op. Hsg. Society
Ingole Nagar, Wardha Road, Nagpur - 440005
Cell: 0'9822565879 / jeevan@biplndt.com

Shri Parag W. Pathak
Hon. Secretary, ISNT - Nagpur Chapter
M/s. NDT Solutions Saket - Pruthvi Appt
Plot No-. A+ B, Second Floor, Surendra Nagar, Nagpur - 440015
Cell: 0' 7709047371/ paragwpathak@yahoo.com

Shri Jayaprakash Hiremath
Chairman –ISNT Pune Chapter
C2, 301, Woodsville Phase 1,
Borhadewadi , Near Gail Pump
House, Moshi, Pune, Maharashtra, 412105
Mb: 9423569802
hiremath@tuv-nord.com

Shri Rahul Kulkarni
Hon. Secretary –ISNT Pune Chapter
C / O - KQSPL, Plot No. 55, Scheme
No. 4, Sector No. 4, Yamunanagar, Nigdi, Pune- 411044
Mb: 9822547797
hon.secretaryisntpune@gmail.com / rahul.kulkarni@kqspl.com

Shri P.V.S. Kurmanath
Chairman , ISNT Sriharikota Chapter
Dy. Gen. Manager, I&T, SMPV Unit-1&2
SHAR, Sriharikota – 524124
Ph-08623-223382
Mb:9490271743
Krumanath.pvs@shar.gov.in

Shri V. Rajasekhar
Hon. Secretary, ISNT Sriharikota Chapter
Chapter Sci/Eng.-SD, NDT, SPP,
SDSC – SHAR, Sriharikota – 524124
Off) Phone:08623-225923 / (Mobile):0'9989898932
rajasekhar.v@shar.gov.in /vrajasekhar55@gmail.com

Shri R.Murali
Chairman –ISNT Tarapur Chapter
Scientific Officer H+ and Chief Superintendent,
Tarapur Atomic Power Station 1&2 ,
Nuclear Power corporation of India Limited.
Mb:9423081628
rmurali@npcil.co.in

Shri Nagendrakumar,
Hon. Secretary –ISNT Tarapur Chapter
Scientific Officer F,
Bhabha Atomic Research Center, Tarapur
Mb: 9518952721
nagendrak@barc.gov.in
nagendragc@gmail.com

Dr. T. Gurunathan
Chairman, ISNT -Trichy Chapter,
General Manager/Quality & BE,
BHEL/Trichy, Tamilnadu, PIN-620014
Mobile: 9442627082 /Ph-0431-2575877
tguru@bhel.in

Shri H. Nikhil
Hon. Secretary, ISNT-Trichy Chapter
Deputy Manager/ATP-NDTL Quality
BHEL, Trichy, Tamilnadu, Pin-620014
Mb:9489320982
hnikhil@bhel.in / trichy@isnt.in

Dr. Mohan Kumar L
Chairman-ISNT- Trivandrum Chapter
GENERAL MANAGER, ROCKET PROPELLANT PLANT,
VSSC, ISRO P.O. THIRUVANANTHAPURAM, PIN – 695 022
Ph. No. 0471-256 3822 (O)
Mob. No. 94461 77376
l_mohankumar@vssc.gov.in / lmkdrn@yahoo.com

Shri Girish N Namboodri
Hon. Secretary, ISNT- Trivandrum Chapter
SCI/ENGR SE, NDTF/RPP,
VSSC, ISRO P.O. THIRUVANANTHAPURAM-PIN – 695 022
Ph. No. 0471-256 2599/3340
Mob. No. 75618 39768
girish.nampoothiri@gmail.com / isnttvm@gmail.com

Shri R. Venkatasubramanian
Chairman-ISNT-Vadodara Chapter
"C/o Industrial X-Ray and Allied Radiographers India Pvt. Ltd.,"
C-17 / 78, Krishana Industrial Estate,
Opposite to BIDC, Gorwa,
Vadodara – 390 016 Gujarat, India
(O) 0265 – 2280756 / Mb: 9825244941
rmani1511@gmail.com / chairmanisntvc@gmail.com

Shri Kashyap Niranjan Bhatt
Hon. Secretary, ISNT - Vadodara Chapter
Rushikesh Engineering Resources
306, Vrajsiddhi Tower, Market Char Rasta,
Rajmahel Road, Vadodara: 390001
GUJARAT, INDIA.
(Mb:) 9825245886
info@rushikeshengg.com / secretaryisntvc@gmail.com

NGC/NCB Members

NATIONAL GOVERNING COUNCIL (NGC)

1. **Shri Diwakar D. Joshi**
   President - ISNT
   Mb- 9822263475
   president@isnt.in

2. **Dr. Krishnan Balasubramaniam**
   President Elect - ISNT
   Mb: 9840200369
   balas@iitm.ac.in

3. **Dr. Jaiteerth R. Joshi**
   Vice President - ISNT
   Mb: 9440049272
   joshidrdl@gmail.com

4. **Shri Rajul R. Parikh**
   Vice President - ISNT
   Mb: 9820192953
   rajulparikh@eecindia.com

5. **Dr. M.T. Shyamsunder**
   Vice President - ISNT
   Mb: 9880508266
   mandayam.shyamsunder@gmail.com

6. **Shri Bikash Ghose**
   Hon. Gen. Secretary - ISNT
   Mb: 91 9890127524
   secretary@isnt.in

7. **Shri R. Vivek**
   Hon. Jt. Secretary - ISNT
   Mb: 9840023015
   vivek@electromagfield.com

8. **Shri Nerurkar K.A**
   Hon. Treasurer - ISNT
   Mb: 9822525518
   treasurer@isnt.in

9. **Shri S. Viswanathan**
   Hon. Co-Treasurer - ISNT
   Mb: 9894945482
   viswa@igcar.gov.in

10. **Dr. B. Venkatraman**
    Immediate Past President - ISNT
    Ph: (Off) 044-27480240
    qadbvr@gmail.com

11. **Dr. R.J. Pardikar**
    Past President - ISNT
    Cell: 9003096843
    r.j.pardikar@gmail.com

MEMBERS

12. Shri Anil V. Jain
13. Shri Anandan. P
14. Balamurugan. S
15. Shri V. Deepesh
16. Shri Dharmveer Singh
17. Shri R.G. Ganesan
18. Prof. S. Gopalakrishnan
19. Shri S. Hari Krishna
20. Shri P. Mohan
21. Shri Mukesh Arora
22. Ms. Menaka. M
23. Ms. Navita Gupta
24. Shri Bhausaheb Krishnaji Pangare
25. Shri Partha Pratim Brahma
26. Dr. Ravibabu Mulaveesala
27. Shri Ravindran S.R
28. Shri Sadasivan. N
29. Shri Samir K. Choksi
30. Shri Shashidhar Pallaki
31. Shri M. S. Shendkar
32. Shri Uday Kale
33. Shri Umakanthan Anand
34. Shri R. Venkatasubramanian
35. Shri M.N.V. Viswanath
36. Shri G. Surya Prakash (Co-opt)
37. Shri Raja Narendra Mallampati (Co-opt)

Permanent Invitee:

38. Shri G. Ramachandran

PAST PRESIDENTS

39. Shri V.R. Deenadayalu
40. Shri K. Balaramamoorthy
41. Shri A. Srinivasulu
42. Shri K. Viswanathan
43. Shri S. I. Sanklecha
44. Shri Dilip P. Takbhate
45. Dr. P. Kalyanasundaram
46. Shri V. Pari
47. Shri D.J. Varde

ALL CHAIRMAN/SECRETARY OF CHAPTERS

EX-OFFICIO MEMBERS

48. Dr. P. P. Nanekar, Chairman, NCB
49. Shri V. Manoharan, Chief Controller of Exams
50. Prof. Krishnan Balasubramaniam, President, QUNEST Fdn.

NATIONAL CERTIFICATION BOARD (NCB)

1. **Dr. Paritosh P. Nanekar**
   Chairman, NCB
   Bhabha Atomic Research Centre
   Chairman.ncb@isnt.in

2. **Shri M.V. Kuppusamy**
   Hon. Secretary, NCB
   Indira Gandhi Centre for Atomic Research
   secretary.ncb@isnt.in

3. **Shri V. Manoharan**
   Chief Controller of Examinations, NCB
   Principal Technologist
   VisiConsult-X-Ray Systems & Solutions
   coe.ncb@isnt.in

4. **Shri S. Viswanathan**
   Hon. Treasurer, NCB
   Indira Gandhi Centre for Atomic Research
   treasurer.ncb@isnt.in

MEMBERS

5. Shri G.V. Shiva Rao, DRDL, Hyderabad
6. Shri A.K. Das, National Thermal Power Corporation Ltd.
7. Shri S. Ramakrishnan, Brakes India Ltd.
8. Shri Umakanthan Anand, Reliance Industries Ltd.
9. Shri Tushar Mukherjee, Reliance Industries Ltd.
10. Shri Anand Bagdare, Godrej & Boyce Mfg. Co. Ltd.
11. Shri Sathyan. V, BPCL Kochi Refinery
12. Shri Sanjay Narang, Larsen & Toubro Ltd.
13. Shri Raghvendra. P, Larsen & Toubro Ltd.
14. Shri Muraleedharan Nair, IRClass, Indian Register of Shipping
15. Shri Jayaprakash Hiremath, TUV India Pvt. Ltd.
16. Shri Uday Kale, KUB Quality Services Pvt. Ltd.

POTENTIAL NCB AUTHORIZED EXAMINATION CENTER

17. Shri R.G. Ganesan, ISNT Chennai Chapter
18. Shri N. Sadasivan, ISNT Mumbai Chapter
19. Ms. Navita Gupta, Satyakiran School for NDT, Delhi

EX-OFFICIO MEMBERS

20. Shri Diwakar D. Joshi, President, ISNT
21. Prof. Krishnan Balasubramaniam, President-Elect, ISNT
22. Shri Bikash Ghose, Hon. Gen. Secy., ISNT
23. Dr. B. Venkatraman, Immediate Past President, ISNT
23. Dr. M.T. Shyamsunder, Chairman-Training Management Board -ISNT
24. Shri Parthapratim Brahma, Controller of Authorisation -ISNT

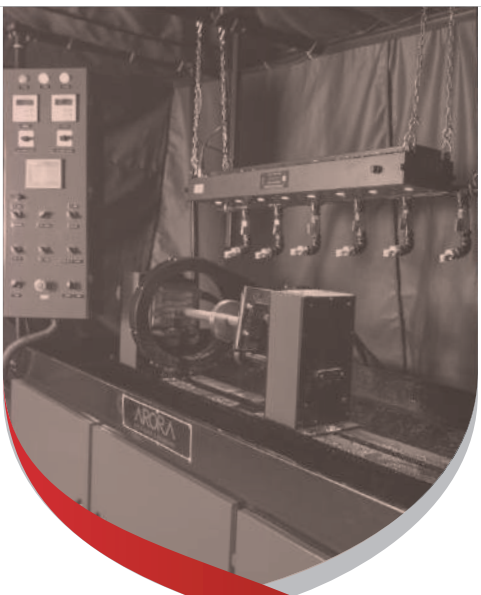

ARORA
Arora Technologies (P) Limited

MaNufacturing | Distribution | AuTomation

Manufacturing of NDT Products

ABM Magnetic Bench Machine

- Designed for magnetic particle inspection
- For surface & subsurface defects in ferromagnetic material
- Offers 1500 Amps to 6000 Amps range of AC and HWDC
- Wide range application in manufacturing industry, Iron & steel metallurgical industries, metal working, aerospace, railways, etc.



Distribution of NDT Solutions

WAND system

- Thin Battery-free ultrasonic sensors
- Permanently installed to the surface of pipework & vessels
- Sensor with unique RFID for traceability & automated data management
- Comes with hand-held and remote data collector



Automated NDT Systems

Eddychek 605

- Eddy current testing system for advanced quality and process control
- Reliable semi-finished product testing
- Up to 5 channels at 3 best positions
- Intuitive graphical user interface
- Major application for tubes, bars & wires

Plot No. D-183/8, MIDC, TTC Nerul, Navi Mumbai, Maharashtra 400706, India.
+91 22 6138 0600 info@arorandt.com www.arorandt.com

CHAPTER ACTIVITIES

Ahmedabad

Technical Talk :

Technical Meet on: Helium Leak Testing

Session I: NDT Helium Leak Testing

Session II: Sponsors Presentation

Session III: ISNT & Forthcoming National Conference Dated 22/07/2023

Seminar

1. Inspection and maintenance Training of Sentinal Brand Delta Camera
2. Demo Of DS702 UT machine
3. Newly Launced EECI RAD Equipment
4. New MPT products Date 29/07/2023

Other Activities :

EC Meeting held on 08/07/2023.

















Flaw-Guide®

NDT Products

(Manufactured By Pradeep Group of Industries)

Contact Address : 707, Lodha Supremes Bldg.1, Road 22, Wagle Estate, Thane 400604 (India)
Email : sales@pradeepndt.com Tel.Nos 91 22 25836001 / 2 / 3 Website www.pradeepndt.com

Flaw Guide
NDT Products

Fluorescent Penetrants

Water & Solvent Removable
Post Emulsified
Hydrophylic & Lipophylic





0.5 x 10 u Ni-Cr Panel

Approved By
NPCIL / RDSO

ISO 9000-2015 Certified

Flaw Guide
NDT Products

Magnetic Powders

Dry & Wet Application

Colours
Black-Red-Gray



Packings
1, 5 & 25 Kg.

Flaw Guide
NDT Products

Red (Visible) Penetrants

Solvent Clean Type
Water Washable
Dual Mode
High Temp.Application



Aerosol & Bulk Packings

High Quality Products

Meet Requirements of all International Specifications

Distributors For Local Requirements at all Industrial Locations

Flaw Guide
NDT Products

Fluorescent Powders For MPI

Water & Oil Suspended Carrier Oil



Packings
1 / 5 / 20 Kgs

Flaw Guide
NDT Products

White Contrast Black Ink
Fluorescent Ink

For MPI



Ready to Use
Aerosol Sprays
&
Powders in Bulk

CHAPTER ACTIVITIES

Bengaluru

Course & Exam :

RTFI Training program conducted at Reliance Industries Ltd between 19-25 June 2023 at Vadodara, Gujarat. 10 candidates attended.

Other Activities:

AGM on 19th Aug 2023



Hyderabad

OTHER ACTIVITIES:

3rd July 2023:

ISNT Hyderabad Chapter's New Executive Committee (EC) Meeting was held at NFC, Hyderabad. Dr. Komal Kapoor, Chairman, ISNT-Hyderabad Chapter welcomed EC members and asked for active participation in the ISNT activities to make the chapter more vibrant with effective planning and execution of programs.



15th July 2023:

1. **Paying floral tributes to Bust of late Dr. N. Kondal Rao at NFC :**

ISNT Executive Committee Members, NFC's Senior Officials, and Former Chief Executives paid floral tributes to the bust of Late Dr. N. Kondal Rao, NFC's Founder Chief Executive and Former Chairman, ISNT Hyderabad Chapter. Shri K. Balaramamoorthy, NFC's former Chairman & CE, and Founder member of ISNT (standing immediate next to the bust) and Dr. C. Ganguly, NFC's former Chairman and CE (standing at extreme right) were also present.



Multiple applications

Research & Development
Corrosion Mapping
Immersion Tanks
Weld Inspection
With Scanners
& Crawlers
& Robots

Explorer 128/ 128



EXPLORER

INTEGRATION MADE EASY
for all inspection systems

contact@tpac-ndt.com

TPAC

Explorer 64/128

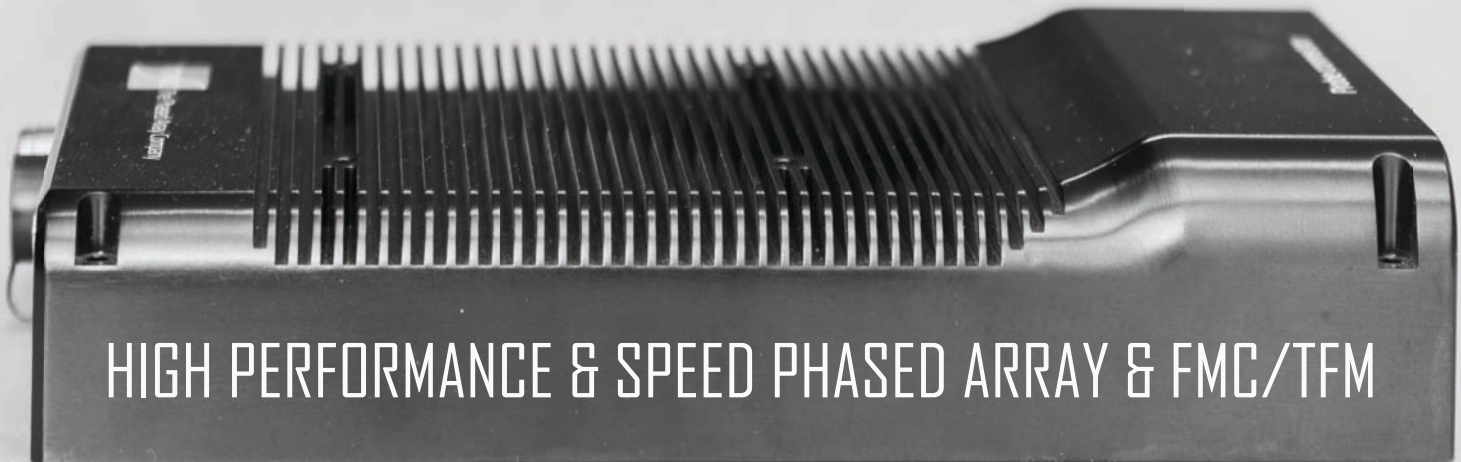

HIGH PERFORMANCE & SPEED PHASED ARRAY & FMC/TFM

2. Dr. N. Kondal Rao Memorial Award Lecture:

Prof. Krishnan Balasubramaniam delivered Dr. N. Kondal Rao Memorial award Lecture titled "NDE 4.0 for Manufacturing Industries". The lecture was attended by largely ISNT fraternity and NDT working personnel. Prof. Krishnan Balasubramaniam was conferred with "Dr. N. Kondal Rao Memorial award" for this year.

The lecture program was started by lighting the lamp by the dignitaries.



From left to Right: (1) Dr. Komal Kapoor (Chairman, ISNT Hyd. Chapter and Chairman & CE, NFC), (2) Shri N. Sreedhar (elder son of late Dr. N. Kondal Rao), (3) Shri G. V. S. Hemantha Rao(Former Chairman, ISNT Hyd. Chapter and NFC's Ex-ACE), (4) Prof. Krishnan Balasubramaniam(Head, CNDE, IIT Madras), (5) Shri. N. Prabhakar (Younger son of late Dr. N. Kondal Rao), (6) Padma Shri Dr. C. Ganguly (NFC's Ex-Chairman and CE) (7) Dr. N. Saibaba (Former Chairman, ISNT-Hyderabad Chapter and NFC's Ex-Chairman& CE) and (8) Dr. Dinesh Kumar Srivastava (Ex-Chairman& CE, NFC).



Prof. Krishnan Balasubramaniam is being felicitated by Dr. Komal Kapoor, Chairman, ISNT Hyderabad Chapter. Sons of late Dr. N. Kondal Rao are also present.

EXERTUS CIRCA 80



Se-75 Close Proximity Projector

SILFLEX SHIELDING MATERIAL



EXERTUS DUAL 120



Ir-192 & Se-75 compatible Projector

REPLACEMENT SOURCES



IRIDIUM	COBALT	SELENIUM
192	60	75

SPEC-150

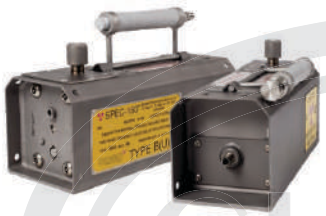

Iridium-192/Se-75 Projector

SPEC-300



Cobalt-60 Projector

LASER INDUSTRIAL X-RAY FILM & CHEMICAL



RADAC LEAD INTENSIFYING SCREEN



TELEDYNE ICM



Portable X-ray Systems
Digital Radiography Solutions
For NDT Applications

CHOKSI ASIA PVT. LTD.

(Formerly known as Hi-Tech Imaging Pvt. Ltd.)
Choksi Bhuvan, Nehru Road, Vile Parle (E), Mumbai 400057

Tel: +91 90224 45544 / 93228 94243 Email: choksindt@gmail.com Website: www.choksi-asia.com

spec SOURCE OF QUALITY | LASER X-Ray Film & Chemical | Silflex SHIELDING | TELEDYNE ICM Everywhereyoulook | RADAC | oserix POWER OF CONFIDENCE

3. Release of 1st Issue of ISNT Hyderabad Chapter's Newsletter

ISNT Hyderabad Chapter has taken initiative to bring out Quarterly Newsletter covering various Technical articles, Programs, Events and Awards & Honors relevant to ISNT. 1st issue of the Newsletter was released on 15th July 2023, Birth Anniversary of late Dr. N. Kondal Rao.



From left to Right: Shri G. V. S. Hemantha Rao, Padma Shri Dr. C. Ganguly, Shri N. Sreedhar, Dr. Komal Kapoor, Prof. Krishnan Balasubramaniam and Shri N. Prabhakar

4. Dr. N. Kondal Rao Memorial NDT Professional award:

This award for the year 2023 was given to Shri S. Chakradhar, Technician, Quality Assurance Group (SSTP) for his contribution in Eddy Current Testing of Steam Generator Tubes for PHWRs.

Kota

Course & Exam :

VT Level- L-I & L-II; MT-L-I and LT-L-II practical examination for recertification of NDT certificate. (09 participant) 17.8.2023.

Technical Talk:

- Lecture on Eddy current inspection of Calandria Tube by IGCAR Engineer (Dr. B. Sasi) at RAPS-3 & 4 Conference Hall to ISNT members and Station management. (Date-02.06.2023).
- Line management training on "Introduction on NDT methods" for new joined QA personnel of RR Site QA By ISNT NDT L-III engineers. (07.08.2023 to 11.08.2023).



NDT-L-I&II Practical Exam for recertification 17.8.2023

35+ Years of Impeccable Performance
In Precision, Reliability and Innovation



Radiation Detectors, Monitors & Alarms



Coating Thickness Gauge



Leak Detectors



Ultrasonic Thickness Gauges



Smart Radiation Detectors

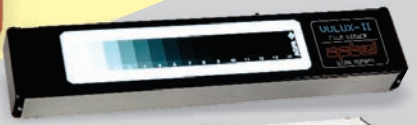

Film Viewer



UV-Meter



Vibration Meter



Optical Densitometer



Sound Level Meter & Calibrator



Block

Hardness Tester

www.pulsecho.com
www.optel.in

Pulsecho Systems established in 1976 as SSI Unit making highly reliable instruments for maintenance & upkeep of industrial units and plants. Our main products are for preventive and predictive maintenance and quality assurance.

Pulsecho Systems and **Optel** have developed more than thirty different portable products for field use with highest reliability and quality. Thus they enjoy a wide customer acceptance and reputation. The shear population of some of these instruments have made them industry standard.

We have earned many laurels and awards of many a forum like ISNT, Chambers of Commerce & Industry etc. **Pulsecho Systems** & **Optel** products are in use in the more than ten countries. Giving an excellent "After Sales Services with an Urgency" we enjoy customers' trust and respect.

Fully illustrated, detailed catalogues and enquiry form are posted on www.pulsecho.com & www.optel.in

PULSECHO SYSTEMS (BOMBAY) PVT. LTD
Unit 110, Nirmal Industrial Estate, Near Sion Fort, Sion (E), Mumbai-400 022.
Fax : +91 22 2407 4244 Phones : +91 22 2407 1055, 2409 2087
E-mail: pulsecho@vsnl.com / optel@pulsecho.com

optel

creativeconcepts11-2013

Mumbai

Course and Examination :

- LPT Level II was conducted at NPCIL from 06th June – 10th June, 23 for 24 nos. candidates.
- MPT Level II was conducted at NPCIL from 13th June – 17th June, 23 for 22 nos. candidates.





Vadodara

Course and Examination :

ISNT Vadodara Chapter supported ISNT Bengaluru Chapter for conducting RTFI training course for their customer M/s. Reliance Industries Limited.

Members of ISNT Vadodara Chapter supported as training faculty for the course.

ISNT Vadodara Chapter also supported by providing equipment for practical demonstration / training during this RTFI Course.

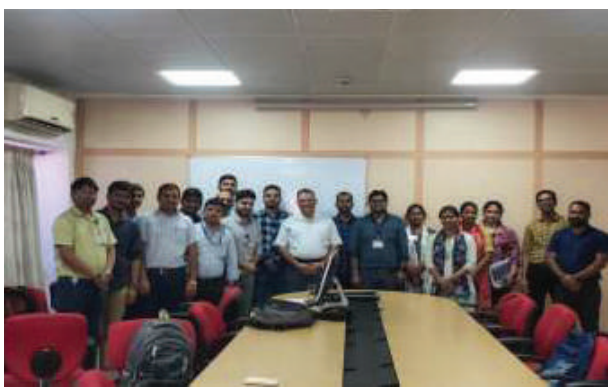

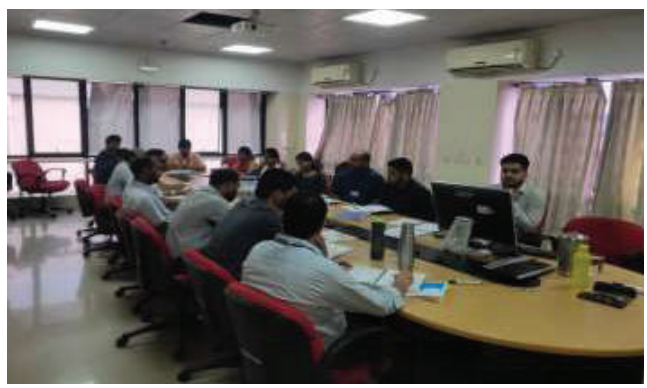

LEVERAGE THE POWER OF
FLAW DETECTION
DIGISCAN DS-702

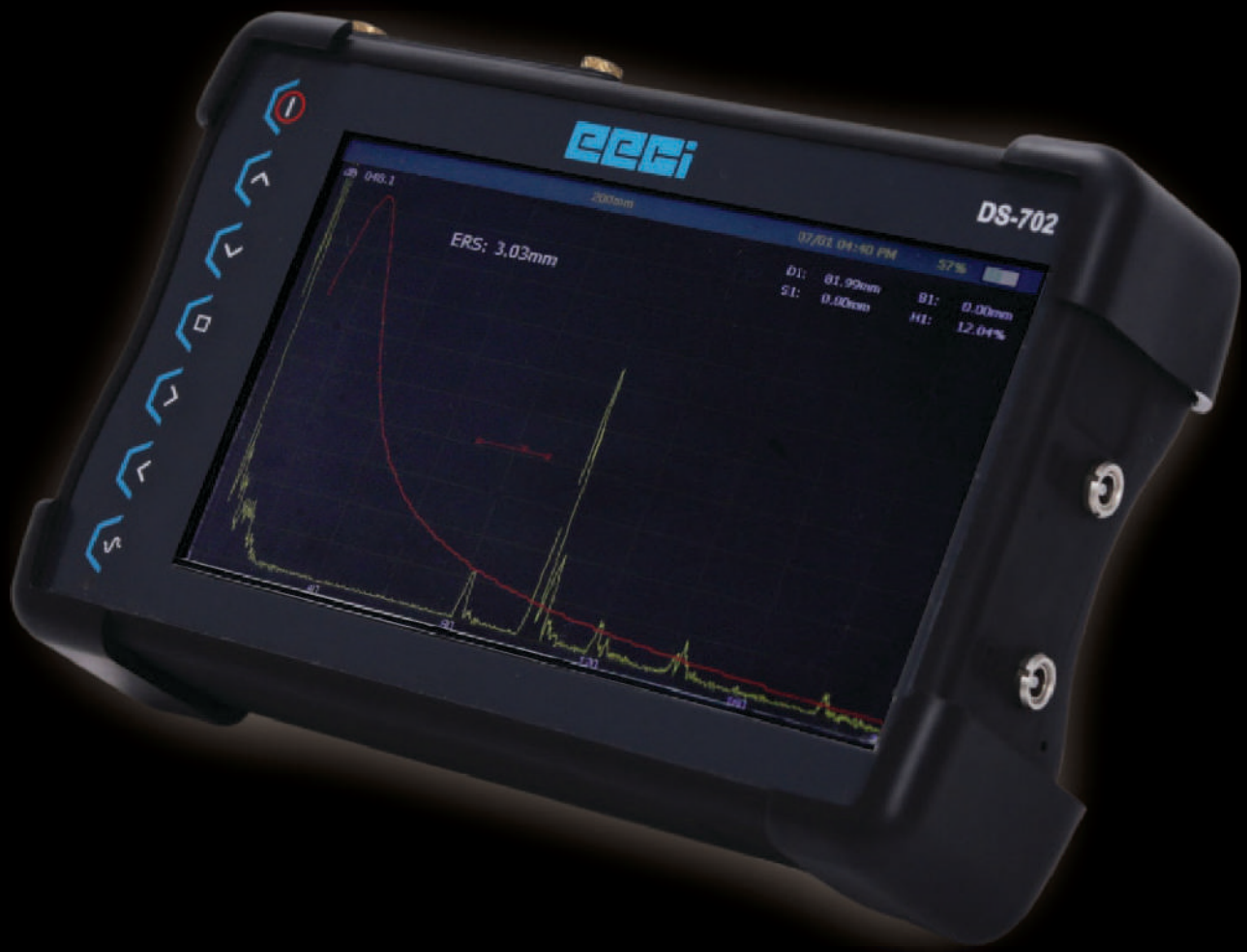

- 7" — Large Display
- IP65 — Rugged Design
- 120 dB — Dynamic Gain
- Adjustable Pulser Voltage
- Upto 2Khz PRF
- Square & Spike Pulser
- 0.01 mm — TOF Resolution
- Zero Cross Detection
- PDF — On Board Reporting
- Mp4 — Continuous Video Recording

eeci the best in ndt

ELECTRONIC & ENGINEERING CO.[I] PVT. LTD

EEC House, C-7, Dalia Industrial Estate, Off New Link Road, Andheri (W), Mumbai 400 053. India
Tel No.: +91-22-6150 3800 ♦ Email: ndtsales@eecindia.com ♦ Web: www.eecindia.com

TRAINING MANAGEMENT BOARD

Training Management Board (TMB) – ISNT

The Training Management Board (TMB) was officially formed by ISNT in February 2022 to act as a nodal agency to address all NDT training related activities (which lead to formal certification as Level 1, 2 or 3 personnel under IS 13805 and ICN schemes of ISNT). Over the period of nearly 15 months since its formation, TMB has made good progress on several fronts by creating multiple Task Forces focussing on different tasks including creation of harmonized timetables, Training material for course instructors, Course notes for trainees, Question Bank / Mockup exams, Train-the-Trainers programme. The other major activity which was the focus of TMB was to establish a robust process with appropriate guidelines, mechanisms and teams to establish Authorized Training Centres (ATC) of ISNT across the country (and later abroad) who can conduct effective and harmonized training courses for both the schemes in all the NDT methods at all Levels of certification. This was achieved by the dedicated Task Force set up for the purpose under the leadership of "Controller of Authorization". This enabled empanelling a several ATCs under the "Interim Authorization" scheme till June 30, 2023. The "Call for Applications" from interested entities for Full Authorization as an ATC valid for 5 years through an audit and assessment process is out now and we welcome all to take advantage of the same. Through its focused efforts, TMB envisages a standardized and harmonized training system to be in place in the near future which ensures a world class NDT training ecosystem in all aspects.

We also welcome volunteers to join and contribute to TMB activities in whatever way they can to help accelerate the fulfilment of our objectives.

To learn more about TMB and its activities please visit https://isnt.in/

For any queries related to TMB, please send an email to tmb@isnt.in

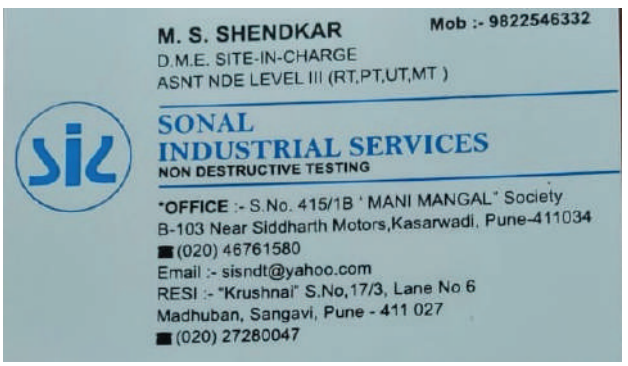



SATYAKIRAN ENGINEERS PRIVATE LIMITED

For all your needs in NDT

TRAININGS/ TESTING SERVICES/ MANPOWER

- ISNT
- ASNT
- NAS410/ EN4179
- ISO 9712

UT, MT, RT, PT, VT, LT

& advanced

EDDY CURRENT, RVI,
MFL, DR, PAUT,
TOFD

admin@satyakiran.com 9899241107





ELECTRO-MAGFIELD CONTROLS & SERVICES

Manufacturer of
Magnetic Crack Detectors, Demagnetizers,
Accessories and Dye Penetrant Systems.

Authorised Distributors BASF SPECTRO-UV Chemetall



L.G. INSPECTION SERVICES LGI

NDT Inspection (MT, PT & UT)
Eddy Current Testing

Authorised Distributors MR CHEMIE NDT-materials ARORA NDT Products & Accessories

Plot No. 165, Kattur Women's Industrial Estate, Vellanur Village,
Thirumullaivoyal, Chennai - 600 062.

sales@electromagfield.com

Mob:9840023015

+91 44 26366013 / 14 / 17 vivek@electromagfield.com www.electromagfield.com

PROGRAM FORMULATION AND MANAGEMENT BOARD (PFMB)

I wish to inform you that the Program Formulation and Management Board of ISNT (PFMB) has been constituted with Shri V. Manoharan as the Chairman, Dr. Deepesh Vimalan as Hon. Secretary and 14 technology/industry experts as members of the board.

PFMB has formed 4 technology groups –Radiological Imaging, Electromagnetic NDE, Thermal Imaging, and Acoustic NDE and Chairman for each working group were identified.

Office Bearers

Shri V. Manoharan, Chairman

Shri Deepesh Vimalan, Hon. Secretary

Members :

Dr. S. Thirunavukkarasu
Mr. A.K. Das
Dr. Phani Suryakiran
Mr. Bhausaheb Pangare
Dr. Arumugam. M
Prof. Prabhu Rajagopal
Dr. Menaka
Prof. Kavitha Arunachalam
Mr. P. Vijayaraghavan
Prof. Ravibabu
Mr. Komma Reddy Vamshi
Dr. Debasish Mishra
Mr. Umankanthan Anand
Dr. Ramadas Chennamsetti

Ex-Officio Members

Mr. Diwakar D. Joshi, President -ISNT
Mr. Bikash Ghose, Hon. Gen. Secretary -ISNT
Mr. Kalesh Nerurkar, Hon. Treasurer ISNT

Invitees

Dr. Paritosh Nanekar, Chairman-NCB
Dr. M.T. Shyamsunder, Chairman -TMB

Objectives

The main Objectives of PFMB are as follows:

- To conceptualize, formulate and organise various non-certification programs such as Webinars, Workshops, Conferences, Seminars etc. to create platform for constant interaction with ISNT members, meet the requirement of industry, academia and research community.
- To interact with other international NDT societies, National technical societies to formulate and organise joint programs.

Scope

- To plan and organise two annual conferences of maximum 2 days' duration (other than NDE) and execute through an organizing committee nominated by PFMB
- To conceptualize, formulate and execute programs such as Webinars, Workshops, Conferences, Seminars etc. of relevance to the NDT community to be organised by ISNT throughout the year across the country.
- To publicize the proposed program
- Develop and implement mechanism for executing the programs along with ISNT Chapters or independently (only if no chapter is interested).
- Create various topical working groups within PFMB and formulate programs as stated above for meeting specific requirement.
- To connect with various industries / institutes and formulate program to meet the specific needs
- Interact with international NDT societies (ISNT partner societies with MOUs) for conducting joint programs, pre-dominantly Webinars
- Interact with national technical societies for conducting joint programs
- Establishing a model for sustained revenue generation for continued operations and growth of PFMB

Insight Quality Services

INSIGHT QUALITY SERVICES

28 YEARS ANNIVERSARY

Office No.507/508, 5th Floor, Building No.1, Siddharth Towers,Sr. No. 12/3B, Near Sangam Press, Kothrud, Pune : 411 029, Maharashtra, India.
E-Mail: support@iqs-ndt.org | Website : www.iqs-ndt.org
Mobile: +91 9689928561 / +91 9881244118

Insight Quality Services is a pioneering institute in the field of Training, Consultancy, Inspection & NDT Services.

TRAINING COURSES

- Certification Courses in NDE Level II (RT,PT,UT,MT,VT,LT,ET)
- NDT Level III Preparatory (RT,PT,UT,MT,VT,LT,ET)
- EN ISO 9712 Level 2 & 3 Preparatory (RT,PT,UT,MT,VT)
- Welding inspectors / Welders, QC managers' certification
- Fabrication Inspector
- CSWIP 3.0, 3.1,3.2 & Bgas Preparatory Training
- Management Systems - Internal Auditor, and Awareness
- ASME codes awareness, NDT Awareness
- Preparatory for API (510, 570, 653, 580, 577,571,936,1169, SIFE)
- AWS CWI & CWEng Seminar & Exam
- Computerized mock exams for API and ASNT Level III modules

CONSULTANCY SERVICES

ASME Certification (U, R, U2, S, N, PP Stamps) Preparatory Work
ISO 9001, 14001, 45001 Certification preparatory work
Developing Management Systems - quality manuals
Setting up NDT labs, Procedures & Work Instructions
Welding procedures & Welders' review / approval
Vendor assessment & development
Developing QA / QC systems
Setting up internal quality systems
Quality & Safety audits (HSE)
Liaison with third party / statutory inspection agencies
ISO 3834 & ISO 15085 Certification Consultancy Services

INSPECTION SERVICES

- Pressure vessels, Heat exchangers
- Storage tanks, Casting, Forging, Static & rotary equipment, Pumps & Valves, Equipment of nuclear projects
- Positive Material Identification Inspection

NDT SERVICES

NDE services for VT, PT, MT, UT and RT film interpretation by NDE Level II / III or EN ISO 9712 Level 2 / 3.
PAUT & TOFD Level 2 & 3 Services
Borescopic Inspection & Hardness Testing

SHUTDOWN INSPECTIONS

- Team of managers and inspection Engineers for Shutdown Inspections

WELDING TRAINING AND TESTING CENTER

Basic and Advanced Level Programs in SMAW, GTAW

"It is good to have Education, it is better to have Experience, but it is essential to have Training!"

First Programme of PFMB :

Topic : "2D/3D Industrial Radiological Imaging and it's Applications"

The first ever PFMB workshop after its formation was conducted successfully by ISNT Thiruvananthapuram Chapter on August 4th and 5th, 2023, on the theme, "2D/3D Industrial Radiological Imaging and it's Applications", at the beautiful campus of Liquid Propulsion Systems Centre (LPSC), Valiamala. This program received an overwhelming response with a total of 119 Participants attending the Workshop. Dr. Narayanan V, Director, LPSC inaugurated the program and welcomed all participants to LPSC. He mentioned the important role played by NDE in aerospace sector and its relevance. Shri M.S. Suresh, Associate Director/ LPSC, Dr. Arumugam. M, Dy. Director/LPSC and the Program Coordinator, Shri V. Manoharan, Chairman, PFMB, Dr. Mohan Kumar. L, Chairman, ISNT Thiruvananthapuram Chapter, and Shri Roykuttan K.K, Organising Committee Chairman addressed the gathering. The concise Workshop Course Note was also released during the inaugural function.

The workshop started off with a lecture on 2D digital imaging by Shri V. Manoharan, Visiconsult, Bangalore. This was followed by a session by Shri. Samaresh Changdar, Baker Hughes. Both stalwarts in the field of Radiography gave an overview of the principles of 2D/3D digital Radiography. Dr. Deepesh Vimalan, BHEL elaborated the applications of 2D radiography for manufacturing and Service Sectors and gave a detailed account of the requirements of RT in various Codes and standards.

After the morning sessions, participants were treated with a grand lunch at LPSC campus. The highlights of the post lunch sessions include the extensive presentation on 2D Xray Imaging of Solid Rocket Motors and Space Ordnance systems by Dr. Girish N Namboodiri, VSSC, followed by the presentations by Shri Roykuttan which covered the applications of CR/DR in the aerospace applications, and the presentation by Shri P. Vijayaraghavan, Ex-HAL on the applications and case studies on 2D X-Ray imaging applications in aerospace sector.

Delegates were offered a technical demo session and grand gala dinner at a palatial venue in the city. Shri. Krishna Bhuta, Topaz NDT delivered a brief presentation on the CR systems and it's applications, followed by the demonstration of the flat Bed Type CR Scanner (Model HPX 1 PLUS) by Carestream team.

On day 2, Dr. Esha Sen Guptha in her lecture spoke about CT and it's applications, and the role of GE in introducing the Artifact corrections which had improved CT imaging to a great extent. Dr. Arumugam, LPSC presented various case studies on 3D CT using Computed Metro Tomography system at LPSC. Dr. TVL Narasimha Rao, Sundaram Clayton gave a scrupulous account of the applications of CT&DR in the automotive sector. In his second lecture Dr. Arumugam M, shared some significant case studies on the applications of CT for Additive Manufacturing components. After a sumptuous lunch, participants were provided an exhaustive practical session at the 3D Computed Metro Tomography facility, CR, DR facilities of LPSC, Valiamala.

The session concluded up after the practical. The hospitality and explanations given by the Organisers of workshop was well commented by the participants. Participants expressed their tremendous appreciations regarding various facets of the workshop including the transportation to the venue, Guest house accommodation arrangements, Coordination of the event, delicious food, Workshop kit and course Notes etc.













M : 9979895022
9051121211



R. K. DEY
Founder
SIGMA NDT GROUP
Specialised NDT Services, Training & Manufacturing
L64/21, Aishwarya Colony, Indira Nagar,
Adyar, Chennai - 600 020 INDIA.
E-Mail : sigmandtservice@yahoo.com
Website : www.sigmandt.com

Branch Offices :

Jamnagar Office :
Mirambika Complex, Opp. Reliance Main Gate,
Moti Khavdi, Jamnagar, Gujarat - 361 140.

Kolkata Office :
26, Kalachand Patitundi Lane,
Paikpara, Kolkata - 700 002.

Mumbai Office :
D-518, Vashi Plaza,
Navi Mumbai - 400 703

Our Esteemed Life Corporate Members

- P -Met High-Tech Company Pvt. Ltd
- Indian Airlines Ltd.
- Crompton Greaves Ltd.
- Hindustan Photo Films
- Pulsecho Syastems (Bombay) Pvt. Ltd.
- Alpha X-Ray Tech. Pvt. Ltd.
- National organic chemical industri
- Associate Consultants
- IGP Engineers Limited
- S.D.Toorkey
- Toyo engg. India ltd.
- Godrej & Boyce Mfg. Co. Ltd.
- Bharat Petrolium Corp. Ltd.
- Industrial X-Ray& Allied Radiograp
- Underwater Services Company
- Deepak. I. Desai
- M/s Sievert India Pvt. Ltd.
- Chemtrols Engineering Ltd.
- C.S.Doshi
- C.G.Nayak
- A.V.Kulkarni
- Sudhir Menon
- E.B.Devan
- Dr. D. Chandiramani
- ABS Industrial Verification (I) P. L.
- Hemant Dhamorikar
- Mohan Babu
- Chetan R. Raikar
- R.J.Chaudhari
- Meghasonic Industries P. Ltd.
- Bay-Forge Limited
- V.K.Parikh
- M.J.Varde
- Mahindra Intertrade Ltd
- NILESH V. SONAR
- Sabyasachi Dutta
- Microlab
- Chennai Petroleum
- NDT Technologies (P) Ltd.
- Galfan Engineers Pvt. Ltd
- Madras Metallurgical Services
- I.P. Rings Ltd
- Indomet Inspection services
- Kitana Industries
- Naval Aviation
- Choudary Technical Ship ser
- Sri Balamurugan Engineering Works
- Arudra Engineers Pvt. Ltd
- Vikram Mulay (Director- Sales)
- Betz Engineering & Technology Zone
- Subikaar NDT Engineers
- BHARAT S. BIRADAR
- Omega Inspection
- DCMS Engineering Co.
- Electronic & Engg Co(I) Pvt.Ltd
- Olympus Medical Systems India Pvt Ltd
- KUB Quality Services Pvt Ltd
- AMET University
- Empirical Technocrats
- TWI India Pvt.Ltd
- Noble Quality EvaluationPvt Ltd
- Inmar Engineering Services Pvt Ltd
- Intertek India Pvt Ltd
- A-Star Training and Consultancy Pvt Ltd
- Cybertech Engineering
- KIT's College of Engineering,Kolhapur
- Sharad Institute of Technology college of Engineering
- AnnaSaheb Dange College of Engineering & Technology
- Electro Magfield Controls & Services
- L.G.Inspection Services
- Usui Susira International Pvt Ltd
- Ordnance Factory Medak
- Government Polytechnic,Kolhapur
- Roshan Instrumentation
- Advanced Training Institute
- Insight Quality Services
- International Radiography Services
- Saksham Industries
- Rotomatrix Reliability Solutions Pvt Ltd
- Lucid Software Ltd
- Q Tech Inspection Services
- VJ Imaging Technologies Pvt Ltd

LIFE CORPORATE MEMBERS

Our Esteemed Life Corporate Members

- College of Engineering Trivandrum
- NDT International (India) Private Limited
- Enmas O & M Services Private Limited
- Aruntech Industrial Services Pvt Ltd
- Royal NDT Services
- Alco Inspections
- Eagle Industrial Inspection Services
- Vibrant NDT Services Pvt Ltd
- Emerson Process Management Chennai Pvt Ltd
- Lloyd's Register Asia
- Tractor and Farm Equipment(TAFE)
- MM Forgings Limited
- Government Engineering College Barton Hill
- Karmen International Pvt Ltd
- Precision Equipments Chennai Private Limited
- Mohandas College of Engineering & Technology
- Dhanalakshmi College of Engineering
- Callington India Private Limited
- Techcorr India Pvt Ltd
- Chemetall India Pvt. Ltd
- Flora Education Society
- Saveetha School of Engineering
- Hyderabad Institute of Technology and Management
- Fix Fit Fasters Mfg. Pvt Ltd
- Veeyes Foundary Private Limited
- Modsonic Instruments Mfg Co(P) Ltd
- JSW Steel Limited
- ISGEC Hitachi Zosen Ltd
- Icorrpro Projects India Private Limited
- Hi Tech Imaging Private Limited
- Medequip Services
- Geecy Apave Pvt Ltd
- Saiprasad Enterprises
- Government Polytechnic, Pune
- GE Global Research
- Pandit Deendayal Petroleum University
- Electronics Devices Worldwide Pvt Ltd
- Centre For Advanced Systems , DRDO
- Heavy Vehicles Factory
- Advanced Systems Laboratory (ASL)
- Topax NDT Solutions LLP
- ACS Solutions GMBH
- Maarg Technologies
- Eddyfi Technologies
- Vinod Medical Systems Pvt Ltd
- Fujifilm India Pvt Ltd
- Spellman High voltage Electronics Corp
- Incertech
- Innotech Systems Pvt Ltd
- NDTS India (P) Limited
- Arora Technologies (P) Limited
- Kronix NDT Corporation
- Indus University
- Defence Metallurgical Research Lab
- C/ Mos Processors
- MR Chemie India Pvt Ltd
- Zhonke NDT Technology Pvt Ltd
- IRC Engineering Services India P Ltd
- Coimbatore Institute of Technology
- Chir- Ayu Controls Pvt Ltd
- APPLUS INDIA PRIVATE LIMITED
- RiM LaS Private Limited
- Santricals Services India Private Limited,
- QIS College of Engineering and Technology
- TESTING & MEASURING EQUIPMENTS
- QUALITY INSPECTION SERVICES,
- Chadalawada Ramanamma Engineering College-Autonomous,
- ShiKag's Engineering Labs Private Limited
- The Phased Array Company
- TCR ENGINEERING SERVICES PVT LTD
- 3AK CHEMIE PRIVATE LIMITED
- WESTERN INDIA FORGINGS PVT LTD
- RTE Transweigh India Private Limited
- HEM VIJ PLASTUBES
- PRO ENGINEERS
- Maitravaruna Technologies PVT LTD
- ANSA Training & Quality Assurance Pvt. Ltd.
- INDO MIM PRIVITE LIMITED

With best compliments

P-MET HIGH-TECH COMPANY PVT.LTD.

1- 5 / 6, INDUSTRIAL ESTATE, GORWA,
VADODARA - 390 016. GUJARAT. INDIA.

P-MET
High - Tech Co. Pvt. Ltd.

ICS JAS-ANZ

AN ISO 9001 - 2015 CERTIFIED COMPANY

MANUFACTURERS OF " PMC" BRAND

Non-Destructive Testing Chemicals

- "PMC FLAWCHECK" VISIBLE PENETRANTS
- PMC "VISFLUORCHECK" PENETRANTS
- "PMC LUMINCHECK" FLUORESCENT PENETRANTS
- "PMC INSTACHECK" MPI TESTING ITEMS
- PMC STRIPPABLE DEVELOPERS FILM

Non-Ferrous Foundry Fluxes

For Aluminium Alloys

- Cover Flux
- Degassers
- Grain Refiners
- Magnesium Removers

For Copper Alloys

- Bronze Cover
- Bronze Refiner

For Zinc Alloy

- Cover Flux

Agent in india for M/s. Sherwin Inc. USA

- Water Washable Penetrats
- Post Emulsification Fluorescent Penetrant
- Hydrophilic Emulsifler
- Water Soluble Developer
- Dry Developer Powder

STOCKIST AT ALL MAJOR CITIES IN INDIA

TEL.NOS. (91) (265) 2282326 / 2281125 FAX NO (91), (265), 2282937,
E-mail : pmetco@gmail.com, mehtapmet@gmail.com
Website : www.p-met.com

MODSONIC®
(SINCE 1987)
Simplifying NDT

Next Level Conventional Ultrasonic Testing with

ARJUN30 *Plus* THE RECORDABLE Ultrasonic Flaw Detector

Fulfils All The Requirements Of Modern Conventional Ultrasonic Testing Palmtop , Cost-efficient And Highly Reliable



35 years OF FOCUSED LEADERSHIP IN PORTABLE ULTRASONIC TESTING EQUIPMENT

AN ELECON GROUP COMPANY

DESIGNED, DEVELOPED & MANUFACTURED by
MODSONIC INSTRUMENTS MFG. CO. (P) LTD.

FACTORY & REGD. OFFICE : AHMEDABAD , INDIA | +91 (79) 48908054
E-MAIL : modsonic@modsonic.com | | www.modsonic.com

Acoustic Emission-Based Non-Destructive Technique for Integrity Assessment of Heavily Reinforced Typical Trunnion Beam of Spillway Structure

A. Thirumalaiselvi[1], M. Kannusamy[1], Srinivas Voggu[2], Saptarshi Sasmal[2a,]

[1]Senior Scientist, [2]Chief Scientist,
CSIR-Structural Engineering Research Centre, CSIR Campus, Taramani, Chennai – 600013, India;
[a]*Email: saptarshi@serc.res.in; sasmalsap@gmail.com*

Abstract

Owing to the large mass of concrete with heavy reinforcement in dam spillways and the long-expected life of these structures, they are susceptible to degradation mechanisms that can start as minor problems and be present for years. The presence of initial degradation tends to accelerate future problems. For example, the presence of voids/flaws in the trunnion beams lead to greater damage if unattended. However, it is highly impossible to identify the internal voids through visual means. Further, the Ultrasonic Pulse Velocity (UPV) method, which is widely used for condition assessment of concrete structures, may not be effective (sometimes a misleading) here due to the presence of heavily dense reinforcement and prestressing strands in large concrete trunnions.
In view of this, attempts were made to assess the health of a typical trunnion beam of the spillway structure employing the Acoustic Emission (AE) technique. During the investigations, ambient conditions (excitation due to water thrust on the dam), as well as the slow movement of the radial gates, were used. A three-dimensional sensor arrangement was used so that the acoustic source localization inside the massive concrete turions could be carried out. High-speed acquisition of data through multichannel was performed using an integrated and synchronized AE system (with an in-built amplifier). Due to the ambient condition and during gate operation, the noise-generated acoustic signals were carefully discarded. Through intensive signal processing, the AE parameters, such as the number of AE hits, signal amplitude, and signal strength, were considered to assess the existing health of the trunnions. The present study discusses on typical signals, acoustic characteristics and inference from the AE-based NDT, along with the method used for acoustic source localization. The present study, the procedure and the inferences are helpful to the practising NDT engineers to perform the health assessment of concrete structures with a high amount of reinforcement.
Keywords: *Non-destructive testing, Acoustic emission, Health assessment, Prestressed trunnion beam*

1. INTRODUCTION:

Concrete dams have been constructed as significant infrastructure to perform the tasks of power generation, flood control, navigation, etc. However, these concrete structures are prone to face safety issues due to certain reasons, such as the presence of voids/flaws, and slow-developing cracks in the dam interior. Thus, prior monitoring of integrity before putting the structure into service is the most effective safeguard against these dangers. However, visual checking often only reveals problems that have developed into major degradation. Furthermore, some kinds of damage, including voids under a spillway slab or cracks in the interior of the dam, are challenging or impossible to detect visually. This is where non-destructive testing (NDT) techniques come into play. NDT methods use ultrasonic waves, radio waves, and other types of low-level energy to propagate through the concrete [1]. These methods can be used to locate a void under a spillway. Ultrasonic pulse velocity (UPV) testing is the most widely used NDT method towards assessing structural health. However, the presence of heavy reinforcement may influence the UPV measurements as a method of evaluating the concrete's integrity/quality. UPV-quality guidelines are framed on the basis of laboratory plain concrete specimens tested. However, the trunnion beam contains heavy steel reinforcement and pre-stressing strands that

interferes with UPV measurements, thereby resulting in erroneous measurements. This work proposes an alternative NDT technique based on acoustic emission testing as it does not depend on the material characteristics and also it does not involve any input of energy into the materials.

Besides AE and UPV, Impact Echo (IE), the Spectral Analysis of Surface Waves (SASW), Ground Penetrating Radar (GPR), and cross-face sonic tomography, are some of the NDT techniques that could be used for monitoring the health of dam structures [1,2]. The main advantage of these alternatives compared to AE is that skilled labour is required to operate the equipment efficiently and accurately infer the data obtained from AE. The main disadvantage of these alternatives compared to AE is that in all other NDT techniques, external input of energy into the materials is needed, and they may hold limitations for large geometry structures. Acoustic Emission (AE) testing is one such NDT technique that is based on the generation of waves environmental noise. While other tools, such as ultrasonic pulse testing, can also be deployed for this specific application, the present study aims to demonstrate the potential application of AE to characterize the internal condition of such a heavily reinforced trunnion beam.

2. BRIEF ABOUT AE TECHNIQUE:

The basis of the AE technique is the rapid release of energy from various internal sources that results in elastic waves [25]. Appropriate AE sensors capture the emitted acoustic waves and convert them into an electric waveform that can be processed and stored. Different AE parameters can be defined from a typical presentation of acoustic waveform, as illustrated in Fig. 1. The AE waveform's maximum voltage is called amplitude (dB), threshold is the amplitude that the user defines based on the noise level of the surrounding environment, rise time is the period of time between the initial threshold crossing and the maximum amplitude, counts are how many times an AE hit goes over the threshold, the interval between the first and last threshold crossings is known as duration, absolute energy is the integration of the squared voltage signal (V_s) over the duration divided by a reference resistance as expressed below [26]

produced by a sudden redistribution of stress in a material. AE has been used in field testing for various applications: source localization [3–5], crack detection [6-11], corrosion monitoring [12,13], structural integrity assessment [14-16], and health monitoring of cable stays in bridges [17-22]. Very few researchers used AE technique in dam monitoring, during grouting operation [23], post-peak cyclic loading [24]. However, assessing the health of dam structures employing the AE technique is still not explored.

In the present work, AE monitoring was conducted in order to ensure the safety of the dam spillway trunnion beam under construction. Low-frequency AE sensors were employed to detect AE waveforms since the signals with conventional frequencies may attenuate greatly during the propagation in the large-sized concrete structure. When AE-based assessment was conducted, the construction was suspended for a few days to avoid disturbance due to

$$Absolute\ energy = \frac{\sum V_s^2}{reference\ resistance\ (10k\Omega)} \quad (1)$$

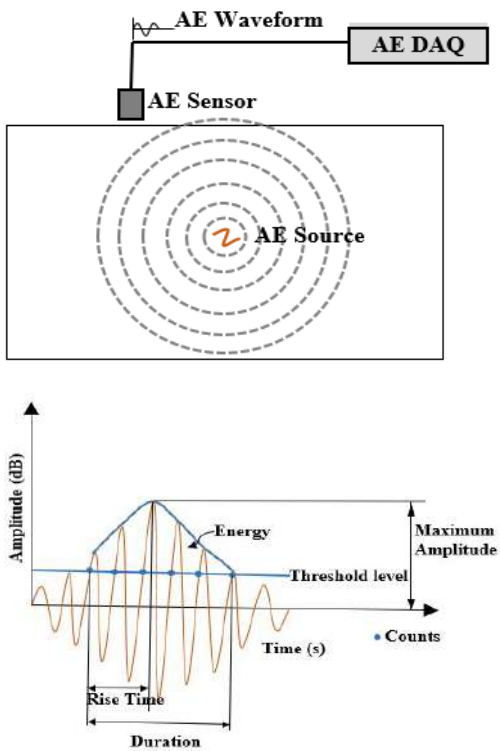

Fig.1 *Acoustic wave formation and a typical waveform*

3. TEST PROCEDURE

3.1 Structure: Trunnion Beam

The spillway under investigation consists of radial gates which are connected with bi-directionally prestressed Trunnion beams (Fig. 2).

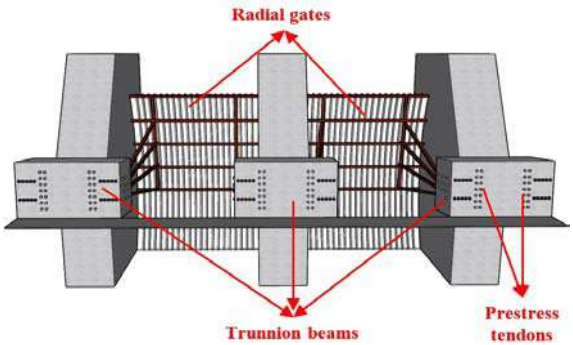

Fig.2 *Schematic view of a typical trunnion beam with radial gates*

A typical prestressed trunnion beam is proposed to be instrumented and tested to investigate on structural integrity. First, a detailed non-destructive evaluation (NDE) using conventional UPV testing is carried out on the prestressed trunnion beams to evaluate the concrete durability and strength. The quality of concrete is assessed by taking UPV responses at different locations, as shown in Fig. 3. UPV measurement is taken by making 5 x 5 grids with dimensions of 300 x 300 mm (see Fig. 3). Commonly used instrument PUNDIT (Portable Ultrasonic Non-destructive Digital Indicating Tester) instrument as shown in Fig. 3(b) is used for UPV testing in indirect /surface transmission mode. It includes a pulse generation circuit, consisting of an electronic circuit for generating pulses and a transducer for transforming electronic pulse into a mechanical pulse having an oscillation frequency in the range of 40 kHz to 50 kHz, and a pulse reception circuit that receives the signal. The following test procedure for determining the ultrasonic pulse velocity as described in IS 13311(Part-I) is adopted:

- Dividing the members into well-defined grid points with spacing of 200 - 300 mm is preferred
- Each grid point is prepared to obtain a smooth surface by thorough cleaning
- Attain good acoustical coupling by applying grease or petroleum jelly
- Transmitting the pulses by placing the transmitter on one end and the receiver at the other end
- Recording the transit time displayed by the instrument - a reliable, steady reading to be recorded (T)
- Measurement of distance between transmitter and receiver (L)
- Calculation of velocity, V = L / T

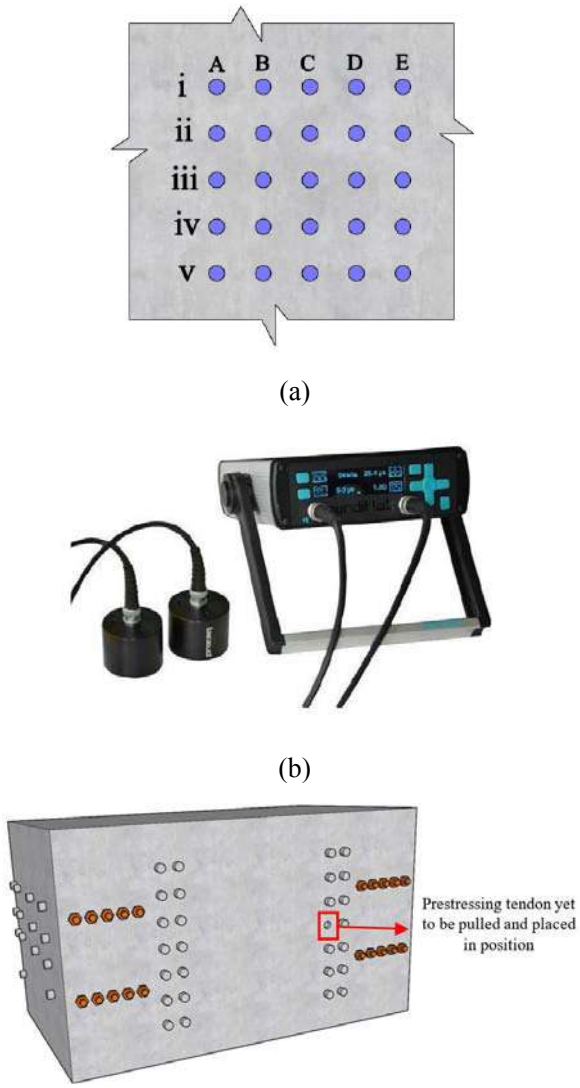

Fig.3 *(a) Experimental setup of UPV measurements; (b) PUNDIT LAB+ UPV Test Equipment and Transducers; (c) View of the front face of prestresses trunnion beam*

UPV value is found to be around 3000 to 5000 m/s, and in many locations, it is above 3500 m/s (see Fig. 4). According to BIS 13311-1:1992 [27], the general guideline is that when the UPV values range

between 3500 m/s and 4500 m/s, the concrete is referred to as good concrete. Thus, the quality of the concrete of trunnion is found to be excellent in terms of its integrity/uniformity checking. However, it is evident from visual inspection that the prevailing situation is not properly reflected through the UPV results. UPV value is influenced by the elastic moduli and the density of the material, which in turn are mainly governed by the number of various phases present. It is mainly due to the fact that the heavy reinforcement, irrespective of the concrete equality, causes high UPV values in the present study, and it can mislead the results [28-30]. Hence it is required to further investigate the homogeneity of prestressed concrete trunnion beams, and, therefore, for assessment of discontinuity exists due to interior cracking/ deterioration/ honeycombing/ variations in mixture proportions. AE testing does not depend on the material characteristics and also it does not involve any input of energy into the materials.

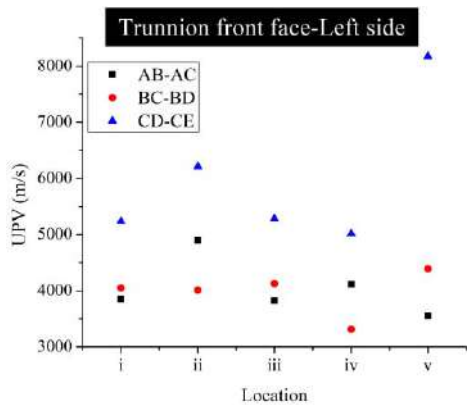

(a)

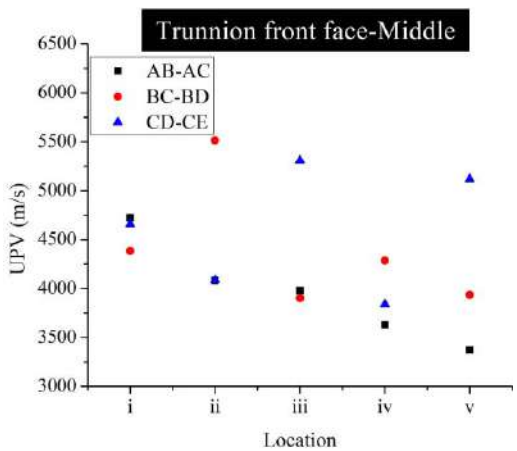

(b)

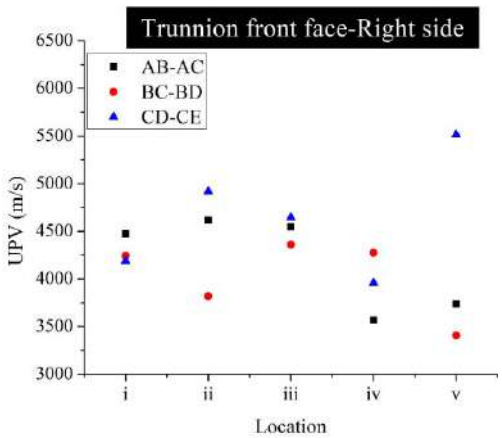

(c)

Fig.4 *UPV testing results on the trunnion beam*

3.2 AE Instrumentation and Test Protocol:

A comprehensive and multi-point AE technique was used to investigate the health of the trunnion beam. The acoustic signals are captured at a very high speed (sampling frequency) so that no signals from minute dislocations are missed out. Accordingly, the signals were captured using the state-of-the-art multichannel AE data acquisition system. Twenty-two low-frequency AE sensors (PAC R15) were employed to detect AE signals in large-sized concrete trunnion. The resonant frequency of the AE sensor is 15 kHz, and the operating frequency range is between 10 kHz and 50 kHz, which is low as compared to the conventional sensor frequency. It is obvious that the attenuation during wave propagation is very high in concrete so the conventional high frequencies are not useful enough to capture AE signals in such a large concrete structure as a dam. The pencil break calibration test was conducted and showed that this frequency range is effective enough to detect meaningful AE signals over a defined threshold.

Data was acquired using 2 MSPS (Mega Samples Per Second). Grease was applied as a coupling agent between AE sensor bottom and the concrete surface. Screw-on type clamping holder was also used to keep the sensors in position during the tests. A threshold limit of 30 dB was chosen, and the signals were amplified using 40 dB in-built pre-amplifier and input into an AE system (SAMOS 48-channel AE system procured from Physical Acoustics) connected with a computer which has AEwin software for further post-processing.

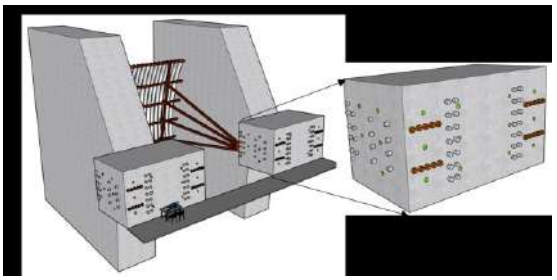

Fig.5 *Schematic representation of trunnion beam along with instrumentation plan for multichannel AE studies*

A schematic representation of the trunnion beam along with the instrumentation plan for multichannel AE studies, is shown in Fig. 5 and the detailed instrumentation plan for the trunnion beam's three faces (front, left and right) adopted is shown in Fig. 6.

The radial gates were planned to be operated to activate the system to generate the acoustic parameters. The followed test protocol for the field investigation is given below:

1. The trunnion will be instrumented with a grid of instruments. Testing of trunnion beam comprises of following three phases.

- Phase 1 - Radial gate movement from water level to spillway bed level
- Phase 2 - Both radial gates are fully closed and kept at rest position
- Phase 3 - Radial gate lifting out up to water level

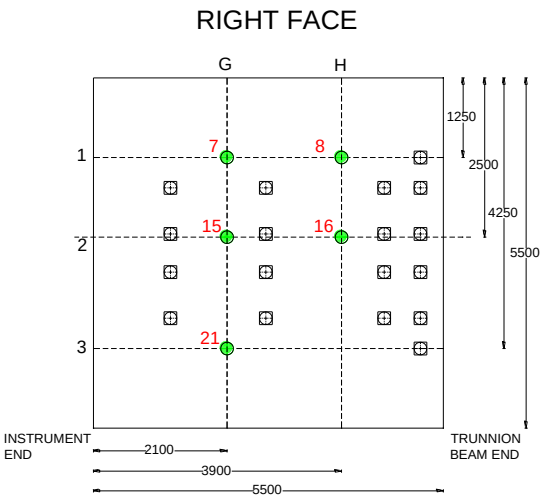

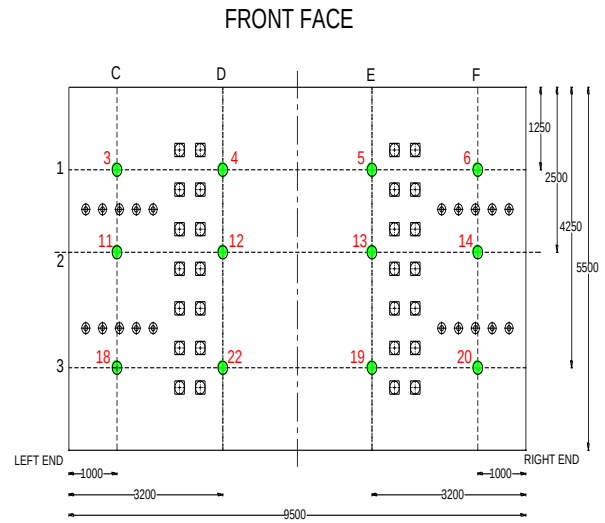

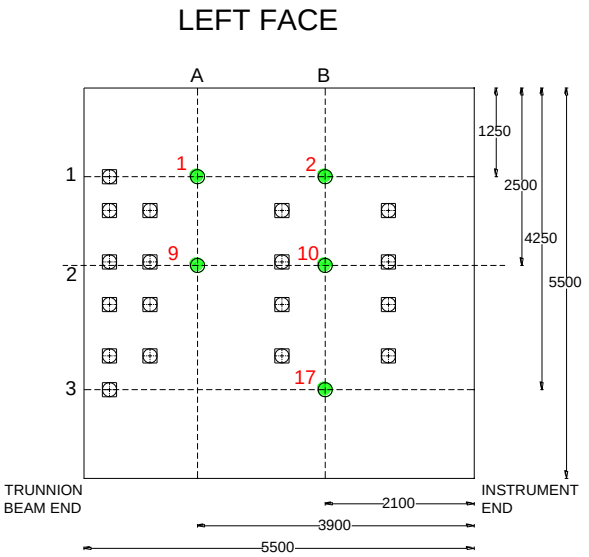

Fig.6 *Detailed instrumentation plan in trunnion beam three faces (green marking represents AE sensor locations)*

2. Each time of testing, both the radial gates will be operated simultaneously
3. During the opening and closing of the radial gates, data will be acquired using multi-channel AE DAQ with a specific frequency
4. It is planned to carry out 5 times gate operations for the trunnion (as mentioned in point #1) to check for consistency

4. AE DATA ANALYSIS AND RESULTS:

AE activity monitored during testing through the acquisition setup is analysed. Detailed and comprehensive data processing of all the AE signals acquired during testing in all 22 channels is done. However, few AE parameters and pertinent information are provided for the trunnion beam in a brief manner. Typical AE signal obtained during the testing is shown in Fig. 7.

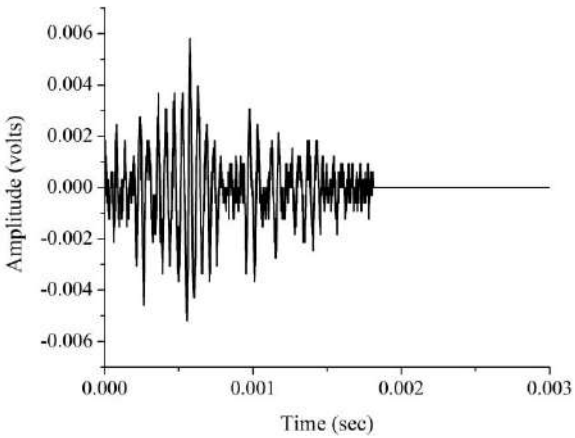

Fig.7 *Typical AE signal recorded during testing*

4.1 AE Signal - Time Domain Analysis

Fig. 8 presents the plots of AE features in the time domain at different phases of testing. Time domain analysis of these signals reveals that the signal amplitude of AE hits is found to be in the range of 30-65dB. In addition, hits are found to be more concentrated in the front face (middle and bottom regions) of the beam. The occurrence of a greater number of such hits may be due to discontinuous regions/internal voids/cavities. Increasing AE hits at the critical location is evidence of AE energy released during the interaction of acoustic waves with internal discontinuity. During field investigations, it was observed that prestressing tendons were yet to be placed in the front face at a similar location where a greater number of hits are recorded (see Fig. 3b). Wall dampness was also noticed in the front face. Though qualitatively, the high AE activities could be attributed to the local discontinuity.

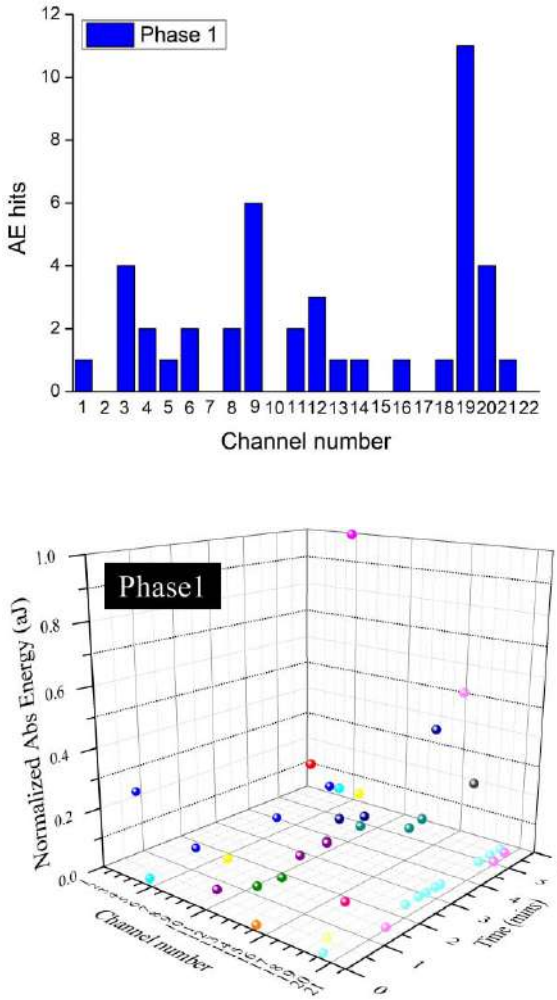

(a)

4.2 AE Signal - Frequency Domain Analysis

Data acquired during experimentation was in the time domain (say function, f(t)), so, Fourier analysis was used to visualize acoustic signals in the frequency domain, F(ω) as expressed in Eq. (2). Fast Fourier Transform (FFT) of a signal is a representation of its frequency versus amplitude. FFT of the acquired acoustic signals is calculated using the in-built algorithm with SAMOS AE system. The typical distribution of the peak frequency of AE signals is shown in Fig. 9. Through the observation, it can be found that the AE signals have several frequency-concentrated bands. Among them, the frequency concentration bands around 50kHz and 350kHz were obvious. These signals may reflect different characteristics of AE sources.

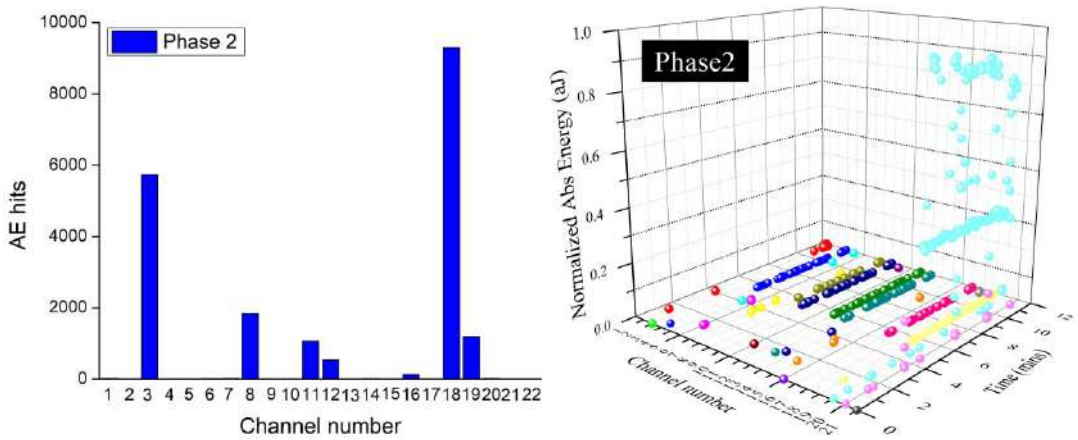

(b)

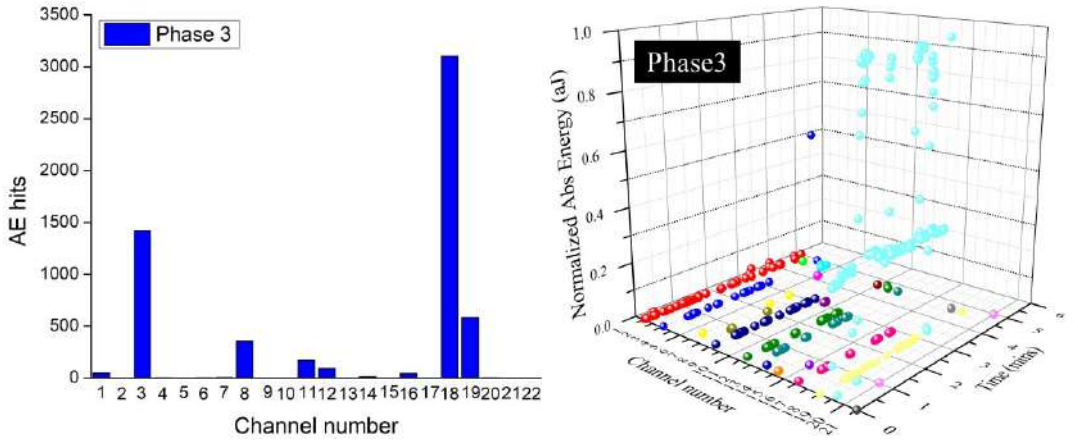

(c)

Fig.8 *AE features in time domain at different phases of testing*

The two frequency bands almost existed and were widely distributed in all phases of testing except in phase 1, where only a frequency band around 50kHz exists. This makes it difficult to find the characteristics of the signals for a source characterization. Further in-depth studies on laboratory scale model specimens are needed to arrive at the correlation between the AE source and the mechanism associated with it.

$$F(\omega) = \int_{-\infty}^{\infty} f(t) e^{-i\omega t}\, dt \qquad (2)$$

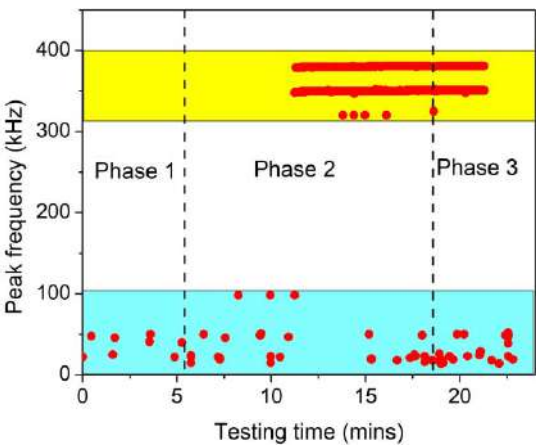

Fig.9 *Typical distribution of the peak frequency of AE signals during testing*

4.3 AE Source Localization:

With the help of multi-point AE technique and with the use of multi-sensors, the relative position of AE sources is determined. The 3D-Location algorithm, which is in-built with the AE-win software is used to locate the source position. The 3D-Location algorithm incorporates a "Smart Location Algorithm" to take advantage of the geometry of sensor placement as well as data from all the sensors that detected the event (up to 8), in calculating an accurate source. A minimum of 4 hits in an event is needed to determine and display a 3D location. The 3D location principle of an AE source assumes an AE source s(x_i, y_i, z_i) to be in some medium, as illustrated in Fig. 10. The AE sensors are mounted on the structure with the coordinates of an arbitrary sensor i(x_i, y_i, z_i). The distance *d* between the AE source *s* and sensor *i* can be expressed by Eq. (3)

$$d(s,i) = \sqrt{((x_s - x_i)^2 + (y_s - y_i)^2 + (z_s - z_i)^2)} \quad (3)$$

This equation provides the basis to obtain the solution of the analytic problems [31]. The 3D localization technique has been shown diagrammatically in Fig. 9. Readers are advised to see references [32-34] for detailed description about the AE source localization employed in the present study.

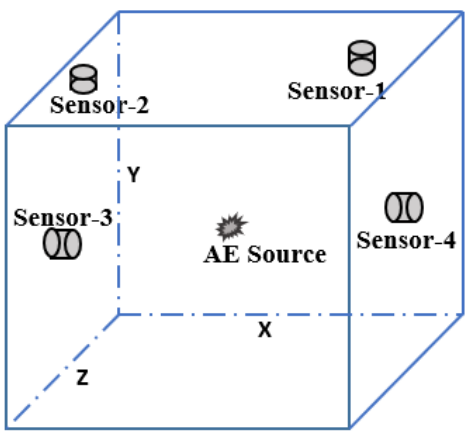

Fig.10 *Localization of AE sources in 3-D structures*

From the determined AE source positions, critical location is arrived/categorised based on the signal strength of AE events. For the investigated trunnion beam, critical locations are obtained and presented in Fig. 11.

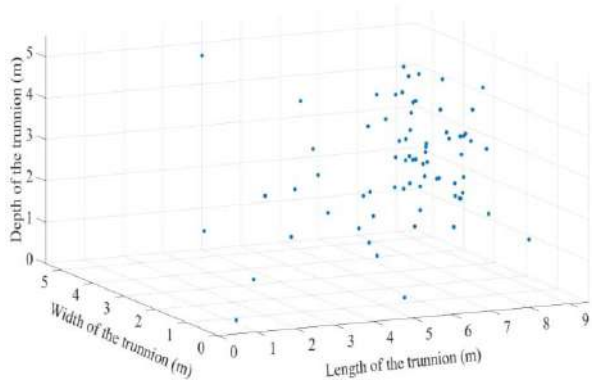

(a) Localized AE sources

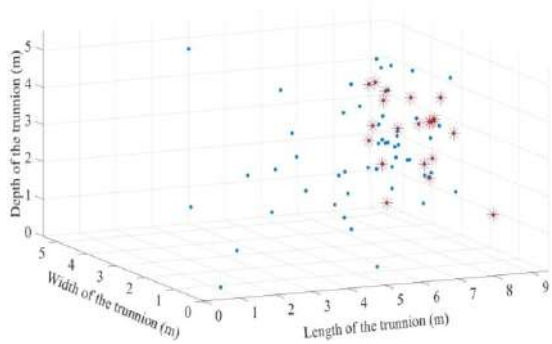

(b) Identified critical locations

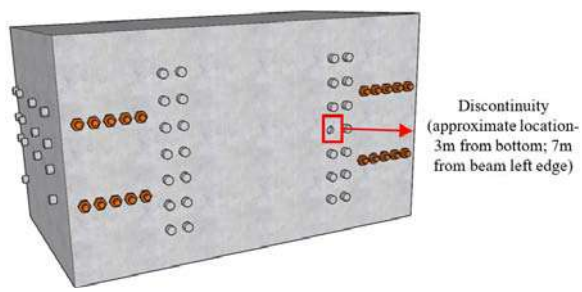

(c) Front face of trunnion beam

Fig.11 *Localization and critical zone mapping in trunnion beam*

The source of significant events is localized and plotted in Fig.11(a). Among these critical sources are highlighted in Fig.11(b). The critical sources, as approximately obtained from the acoustic source locations from the captured signals and acquired data, are based on the acquired acoustic signals (of different acoustic parameters) generated through gate operation/ambient conditions. The acoustic signal strength and acoustic parameters have an influence on structural configuration, gate operation and ambient conditions during field investigations. The information on locations provided here as sources

may be treated as indicative. However, it is to mention here that, the testing being carried out during construction of dam, few prestressing tendons were yet to be placed and the inhomogeneity arises due to absence of prestressing tendons are well captured by the AE critical source localization (see Fig, 11(c)).

5. CONCLUSION:

The present work has demonstrated the possible application of AE technique in assessing the health of heavily reinforced concrete dams. AE activities in the dam spillway pre-stressed concrete trunnion beam under ambient conditions (excitation due to water thrust on the dam), as well as the slow movement of the radial gates, were analysed in order to determine AE features towards assessing its health. The following conclusions may be drawn from this limited research work.

1. AE-based NDT technique presented can provide details on the health of the trunnion beam that a visual inspection alone cannot. Even conventional UPV testing failed to fully capture the discontinuity in a heavily reinforced structure along with prestressing steel tendons.
2. Increasing AE hits at the critical location is evidence of AE energy released during the interaction of acoustic waves with internal discontinuity.
3. From the frequency analysis based on peak frequency, it is observed that the frequency concentration bands around 50kHz and 350kHz are present.
4. The critical sources, as approximately obtained from the acoustic source locations from the captured signals and acquired data, are based on the acquired acoustic signals (of different acoustic parameters) generated through gate operation/ambient conditions.
5. Together, AE activity monitoring and critical source, provide a powerful first-hand tool that dam operators can employ to make sure the structures continue to operate securely.

The potential observations made from the present work are further extended, and extensive experimental works are being carried out to categorically bring out the frequency-based sensitive acoustic parameters that can be helpful to use as a tool to assess the health of heavily reinforced concrete dam structures.

6. ACKNOWLEDGEMENT:

The authors would like to acknowledge the technical and project staff of Special and Multifunctional Structures Laboratory (SMSL), CSIR-Structural Engineering and Research Centre, India, and other stakeholders for their help during the investigations..

7. REFERENCES:

[1] Sack, D.A., Olson, L.D. and Yarbrough, H.A., 2007. Nondestructive techniques for inspecting concrete dams and spillways. HYDRO REVIEW, 26(4), p.42.

[2] Olson, L.D. and Sack, D.A., 1995, May. Nondestructive evaluation of concrete dams and other structures. In Nondestructive evaluation of aging structures and dams (Vol. 2457, pp. 113-124). SPIE.

[3] Pollock, A.A. and Smith, B., 1972. Acoustic emission monitoring of a military bridge. Nondestructive Testing, 5(6), pp.164-186.

[4] Han, Q., Xu, J., Carpinteri, A. and Lacidogna, G., 2015. Localization of acoustic emission sources in structural health monitoring of masonry bridge. Structural Control and Health Monitoring, 22(2), pp.314-329.

[5] ElBatanouny, M.K., Anay, R., Abdelrahman, M.A. and Ziehl, P., 2019. Acoustic emission measurements for load testing. Load Testing of Bridges, pp.169-198.

[6] Bayane, I. and Brühwiler, E., 2019. Acoustic emission and ultrasonic testing for fatigue damage detection in a RC bridge deck slab. In SMAR 2019-5th Conference on Smart Monitoring, Assessment and Rehabilitation of Civil Structures (No. CONF).

[7] Prine, D.W. and Hopwood, T.I.I., 1985. Detection of fatigue cracks in highway bridges with acoustic emission. J. Acoust. Emiss., 4(2).

[8] Watson, J.R., Yuyama, S., Pullin, R. and Ing, M., 2005. Acoustic emission monitoring applications for Civil structures. In Bridge Management 5: Inspection, maintenance, assessment and repair: Proceedings of the 5th International Conference on Bridge Management, organized by the University of Surrey, 11–13 April 2005 (pp. 563-570). Thomas Telford Publishing.

[9] Pullin, R., Holford, K.M., Lark, R.J. and Eaton, M.J., 2008. Acoustic emission monitoring of bridge structures in the field and laboratory. Journal of Acoustic Emission, 26, pp.172-181.

[10] Johnson, M.B., Ozevin, D., Washer, G.A., Ono, K., Gostautas, R.S. and Tamutus, T.A., 2012. Acoustic emission method for real-time detection of steel

fatigue crack in eyebar. Transportation research record, 2313(1), pp.72-79.
[11] De Santis, S. and Tomor, A.K., 2013. Laboratory and field studies on the use of acoustic emission for masonry bridges. Ndt & E International, 55, pp.64-74.
[12] Suma, A.B., Ferraro, R.M., Metrovich, B., Matta, F. and Nanni, A., 2011. Nondestructive evaluation techniques and acoustic emission for damage assessment of concrete bridge in marine environment. Special Publication, 277, pp.109-128.
[13] Ziehl, P. and ElBatanouny, M., 2016. Acoustic emission monitoring for corrosion damage detection and classification. In Corrosion of steel in concrete structures (pp. 193-209). Woodhead Publishing.
[14] Kishi, T., Ohtsu, M. and Yuyama, S., 2000. Acoustic emission-beyond the millennium. Elsevier.
[15] Olaszek, P., Casas, J.R. and Świt, G., 2016, June. On-site assessment of bridges supported by acoustic emission. In Proceedings of the Institution of Civil Engineers-Bridge Engineering (Vol. 169, No. 2, pp. 81-92). Thomas Telford Ltd.
[16] Fukuda, M., Chang, K.C., Nakayama, H., Asaue, H., Nishida, T., Shiotani, T., Miyagawa, T., Watabe, K. and Oshiro, T., 2017. Assessing Deterioration of an In-field RC Bridge Deck by AE Tomography. In Advances in Acoustic Emission Technology: Proceedings of the World Conference on Acoustic Emission–2015 (pp. 289-298). Springer International Publishing.
[17] Rizzo, P. and di Scalea, F.L., 2001, August. Acoustic emission monitoring of CFRP cables for cable-stayed bridges. In Health Monitoring and Management of Civil Infrastructure Systems (Vol. 4337, pp. 129-138). SPIE.
[18] Kretz, T., Brevet, P., Cremona, C., Godart, B. and Paillusseau, P., 2006. Continuous monitoring and structural assessment of the Aquitaine suspension bridge. Bull LPC, pp.13-32.
[19] Zejli, H., Laksimi, A., Tessier, C., Gaillet, L. and Benmedakhene, S., 2006. Detection of the broken wires in the cables' hidden parts (anchorings) by acoustic emission. Advanced materials research, 13, pp.345-350.
[20] Fricker, S. and Vogel, T., 2007. Site installation and testing of a continuous acoustic monitoring. Construction and Building Materials, 21(3), pp.501-510.
[21] Li, D., 2008, April. Acoustic emission monitoring and critical failure identification of bridge cable damage. In Nondestructive Characterization for Composite Materials, Aerospace Engineering, Civil Infrastructure, and Homeland Security 2008 (Vol. 6934, pp. 170-174). SPIE.
[22] Jin, T., Sun, Z. and Sun, L.M., 2008, April. Acoustic emission monitoring of stayed cables based on wavelet analysis. In Sensors and Smart Structures Technologies for Civil, Mechanical, and Aerospace Systems 2008 (Vol. 6932, pp. 951-957). SPIE.
[23] Minemura, O., Sakata, N., Yuyama, S., Okamoto, T. and Maruyama, K., 1998. Acoustic emission evaluation of an arch dam during construction cooling and grouting. Construction and Building Materials, 12(6-7), pp.385-392.
[24] Li, S., Chen, X. and Zhang, J., 2021. Acoustic emission characteristics in deterioration behavior of dam concrete under post-peak cyclic test. Construction and Building Materials, 292, p.123324.
[25] Chaipanich, A., Nochaiya, T., Wongkeo, W. and Torkittikul, P., 2010. Compressive strength and microstructure of carbon nanotubes–fly ash cement composites. Materials Science and Engineering: A, 527(4-5), pp.1063-1067.
[26] Tragazikis, I.K., Dassios, K.G., Exarchos, D.A., Dalla, P.T. and Matikas, T.E., 2016. Acoustic emission investigation of the mechanical performance of carbon nanotube-modified cement-based mortars. Construction and Building Materials, 122, pp.518-524.
[27] BIS: 13311 (Part 1) : 1992 Non-destructive Testing of Concrete – Methods of Test , Part 1 Ultrasonic Pulse Velocity, BIS, New Delhi.
[28] Chung, H.W., 1978. Effects of embedded steel bars upon ultrasonic testing of concrete. Magazine of Concrete Research, 30(102), pp.19-25.
[29] Fodil, N., Chemrouk, M. and Ammar, A., 2019, September. The influence of steel reinforcement on ultrasonic pulse velocity measurements in concrete of different strength ranges. In IOP Conference Series: Materials Science and Engineering (Vol. 603, No. 2, p. 022049). IOP Publishing.
[30] Nanayakkara, O., Najm, H.M. and Sabri, M.M.S., 2022. Effect of using steel bar reinforcement on concrete quality by ultrasonic pulse velocity measurements. Materials, 15(13), p.4565.
[31] Hassan, F., Mahmood, A.K.B., Yahya, N., Saboor, A., Abbas, M.Z., Khan, Z. and Rimsan, M., 2021. State-of-the-art review on the acoustic emission source localization techniques. IEEE Access, 9, pp.101246-101266.
[32] Mao, W., Aoyama, S. and Towhata, I., 2020. A study on particle breakage behavior during pile penetration process using acoustic emission source location. Geoscience Frontiers, 11(2), pp.413-427.
[33] Li, X., Lin, W., Mao, W. and Koseki, J., 2020. Acoustic emission source location of saturated dense coral sand in triaxial compression tests. Japanese Geotechnical Society Special Publication, 8(9), pp.331-334.
[34] Lin, W., Mao, W., Liu, A. and Koseki, J., 2021. Application of an acoustic emission source-tracing method to visualise shear banding in granular materials. Géotechnique, 71(10), pp.925-936.

Enhancing Corrosion Monitoring in Bolted Steel Joints Through Ultrasonic Inspection

Jay Kumar Shah[1], Subhra Majhi[2], and Abhijit Mukherjee[2]
[1] Centre of Advance Infrastructure and Transportation, Rutgers – The State University of New Jersey, NJ, USA
[2] School of Civil and Mechanical Engineering, Curtin University, Perth, WA, Australia

Abstract

Monitoring joint damage in bolted steel structures due to corrosion is a formidable challenge. The formation of rust at joint interfaces leads to significant material loss, profoundly impacting the load-bearing capacity of these structures. Therefore, early detection becomes crucial for implementing effective maintenance strategies. In this state-of-the-art ultrasonic inspection, we report our preliminary findings on joint corrosion inspection using different ultrasonic frequency signals. To study ultrasonic signal transmission across corroding bolted interfaces, we conducted laboratory experiments, employing the electrochemical corrosion technique for controlled and accelerated corrosion. Monitoring the propagation of ultrasonic signals at various corrosion stages provided initial insights into the importance of selecting the optimal inspection frequency in detecting joint corrosion. Two inspection frequencies centred at 300 and 500 kHz have been used in this study. Notably, when monitoring the bolted structure with a 300 kHz ultrasonic signal, we observed relatively insignificant changes in signal transmission energy, even at the advanced stages of corrosion. However, the 500 kHz central frequency excitation exhibited a decrease in signal energy corresponding to various stages of corrosion. This highlights the constraints and subsequent challenges associated with choosing the appropriate inspection frequency. The study concludes with the potential of using pulsed laser-based signal generation for simultaneous monitoring of a wide range of signal frequency components, offering a promising alternative to conventional piezo transducer-based setups.
Keywords: *Bolted joints; corrosion monitoring; piezo ultrasonics; laser ultrasonics.*

1. INTRODUCTION

Bolted infrastructure provides reliable and time-efficient construction, offering the advantage of easy component recycling upon decommissioning, provided proper maintenance during its service life. Maintaining prescribed clamping force between structural components through optimal bolt torque is essential for the structural integrity of these systems. However, joint corrosion presents a significant challenge, causing material loss at joint interfaces and leading to a premature reduction in clamping force. If left undetected during its early stages, joint corrosion can ultimately lead to catastrophic failures in structures, posing a severe threat to human lives and causing substantial economic losses. As such, effective detection and monitoring of corrosion in bolted joints are critical to ensure the safety and longevity of these structures.

Guided wave ultrasonic is a diverse technique to inspect bolted joints in a non-destructive manner, where wave propagation in bolted components is studied to determine joint-specific features correlating to clamping force [1]. Typically, change in the axial strain of the bolt is measured indirectly by measuring ultrasonic signal features such as velocity [2], phase [3], and time of flight [4] under

different bolt preload scenarios. However, such applications are relatively limited in joint corrosion scenarios as bolt damage may not allow the usage of conventional contact-based transducers. In addition, individual bolt inspection is not recommended for multi-joint structures. Many relevant studies also utilize the concept of signal generation on the bolted components instead such as plates in bolted plate joints and then monitor the wave interaction with the bolted interface under inspection [5]. This approach can accommodate the cumulative influence of multiple bolts on the clamping force and does not rely on the inspection of individual bolts, hence is suitable for this study.

Shah et al. [6] have reported the role of initial bolt torque conditions on the influence of joint corrosion by monitoring the energy transmission across the bolted interface. They demonstrated the importance of maintaining sufficient bolt torques to avoid sudden failures of joints subjected to corrosive environments. A similar study was reported by Cui et al. [7] on bolted joints connecting marble plates. Wang [8] extended ultrasonic inspection on multiple joint studies where emphasis had been made on the use of linear and non-linear shape wavelets to isolate corrosion-specific features. The use of advanced methods like the generation of higher-order harmonics and frequency modulations is widely reported for bolt loosening conditions in its incipient stages, however, there is a lack of such studies for corrosion monitoring.

This study aims to investigate the application of guided wave ultrasonic techniques for monitoring joint corrosion, achieved through an accelerated corrosion setup. Our primary approach involved using conventional transducer-based inspection to monitor the influence of joint corrosion on signal transmission across the bolted interface for various signal frequencies. In addition, we introduce a novel element to the study by employing a High energy laser-based signal generation. This innovative approach offers several advantages, including non-contact monitoring and higher signal strength, thereby eliminating the need for a high-power amplifier typically required in conventional transducer-based setups. The findings from this research will contribute to establishing the potential of ultrasonic testing methodologies for monitoring joint corrosion in civil infrastructure.

2. EXPERIMENTAL DESCRIPTION

2.1 Specimen Description

The specimen consists of two steel plates, each measuring 300 mm × 100 mm × 5 mm, bolted together using an M16 fully threaded bolt. The bolt creates an overlapping area of 100 mm × 100 mm. To achieve the maximum clamping force without damaging the bolt thread, a bolt torque of 100 Nm was applied. This approach not only ensured the optimum clamping force but also allowed for a focused study on corrosion-related bolt preload loss while eliminating the potential contributions from lower bolt torque-related features.

2.2 Corrosion Setup

The joint was subject to controlled and accelerated corrosion using an electrochemical corrosion setup, as depicted in Figure 1. This process involved immersing the joint in an electrolytic bath containing 3.5% salt water and the bolt was made the anode of the electrical circuit, promoting oxidation reactions that caused mass loss. To complete the current flow in the circuit, a spare metal served as the cathode, facilitating the reduction reaction that formed hydroxyl ions in the process. To control the corrosion rate, an electric DC power supply was utilized in constant current mode which allowed for precise regulation of the corrosion process. The mass loss at the bolt site was calculated using Faraday's mass loss relation (Equation 1). For more detailed information about the chemical reaction involved, readers can refer to the authors' previous works [6].

$$m = \left(\frac{It}{\mathrm{F}}\right)\frac{M}{z} \qquad (1)$$

Here m is the mass loss in grams, I is the constant current applied for electrolysis, t is the total time for which the current is flowing in the circuit, F is Faraday's constant with a value of 96,500 C/mol, M is the molar mass in grams per mol, and z Represents the valency number of steel.

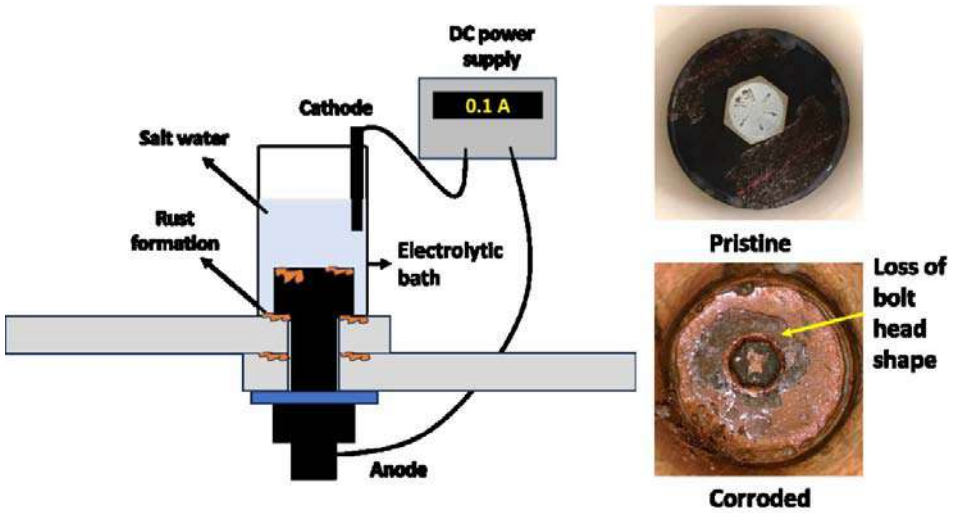

***Fig 1**. Accelerated corrosion setup*

2.3 Experimental Setup

Figure 2 presents the experimental setup designed for the planned investigation where piezoceramic transducers with dimensions of 10 mm in diameter and 0.5 mm in thickness (supplied by Warsash Scientific Pty Ltd) were placed in pitch-catch configuration to investigate the influence of joint corrosion on wave propagation across the interface. The cumulative distance between the two transducers was fixed at 300 mm to ensure adequate wave interaction with the corroding interface. For signal generation, a function generator (RIGOL DG1035) produced the desired signal, which was then amplified using a high-voltage power amplifier (Ciprian HVA 400A) before being transferred to the transmitter. The signal transmission was recorded using an identical transducer and digitized using an oscilloscope and a PC, and no amplification was necessary on the receiving end of this setup.

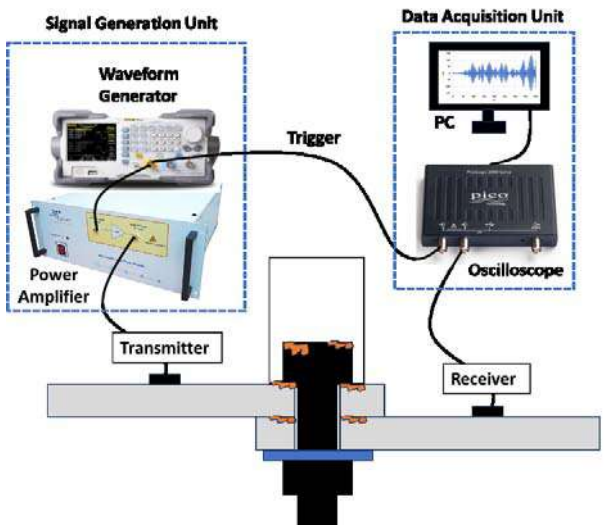

***Fig 2:** Experimental set-up for transducer-based inspection*

2.4 Methodology

To achieve controlled and accelerated corrosion, the DC power supply was operated in constant current mode, maintaining a consistent current of 0.1 A throughout each corrosion stage. Each stage of corrosion lasted for 20 hours, during which ultrasonic measurements were taken at mass loss intervals of 2 grams. Thus a total of 20 grams of mass was lost after an exposure period of 200 hours.

To ensure accurate measurements, the electrolytic bath was emptied and allowed to dry for 24 hours before conducting the ultrasonic assessments. This precautionary step aimed to prevent wave attenuation caused by residual moisture. For each measurement, the electrolytic bath was replenished with fresh salt water, and an average of three A-scans was collected for subsequent analysis. Subsequently, the received A-scans were transformed to a frequency domain using the Discrete-Time- Fourier transform, enabling the

monitoring of frequency components of interest. This frequency domain analysis provided crucial insights into the behaviour of the corroding bolted joints and their impact on ultrasonic signal propagation.

3. RESULTS

The transmission of ultrasonic signals across the bolted interface was studied over several frequencies. The results obtained at a central frequency of 300 kHz and 500 kHz excitation are presented in this section. To optimize the signal generation at the chosen inspection frequency, a 10-cycle Hanning windowed-shaped signal was selected for the investigation, allowing signal generation around the tuned central frequency. Figure 3 shows the A-scans of the transmitted signals showing the transmission of multiple envelopes that can correspond to different guided wave modes in the specimen and multiple reverberations as a result of wave interaction with specimen boundaries.

Since the fundamental evaluation of these envelopes is a complex task, signals were analyzed by converting the A-scans to their frequency domains (Figure 3b and 3d) where it is evident that the majority of the signal's energy is contained around the central frequency of the signal. To monitor the influence of the corrosion process on signal transmission, the transmitted energy of the signal was continuously monitored within a

$$Energy = \sum_{f_{low}}^{f_{high}} W(f).df \qquad (2)$$

where $W(f)$ is the amplitude at each frequency data point, df is the sampling frequency, f_{low} and f_{high} are the upper and lower bounds of the considered bandwidth around the central frequency of the signal. Figure 4 represents the variation in the transmitted energy at different levels of mass loss where all the energies are normalized relative to the energy of the pristine specimen. As depicted in Figure 4a, for the 300 kHz central frequency excitation, no clear correlation was observed between the transmitted energy and the mass lost, where variation was observed about the zero-mass loss. Overall, the observed response remained within a ±20% range of the pristine signal, indicating little change.

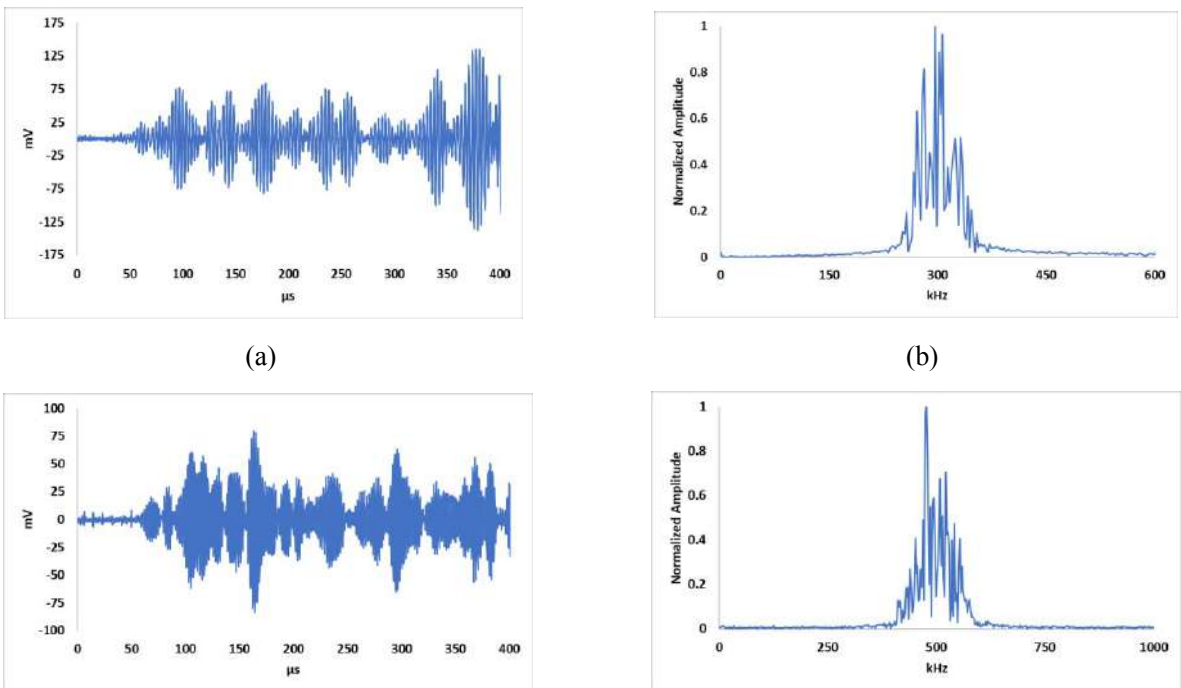

***Fig 3**. A-scan for the transmitted signal and its normalized frequency spectrum at (a, b) 300 kHz and (c, d) 500 kHz*

Thus, the selected excitation frequency is not sensitive to monitor corrosion. Conversely, in the case of the 500 kHz central frequency signal (Figure 4b), a clear declining trend in the transmitted energy was observed with the progression of corrosion. Thus, the 500 kHz central frequency excitation has the potential for applications in corrosion inspections.

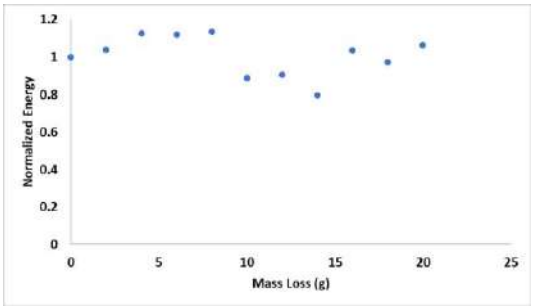

(a)

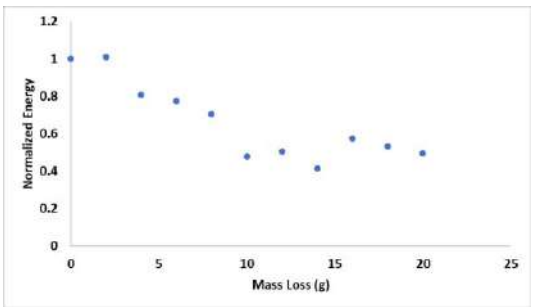

(b)

Fig 4: *Transmitted energy variation with corrosion-induced mass loss in the specimen for (a) 300 kHz and (b) 500 kHz central frequency excitation*

4. DISCUSSION AND CHALLENGES IN INSPECTION

The observations in this study have affirmed the viability of ultrasonic inspection for studying the influence of joint corrosion on clamping force. However, it was notable that the variation in energy transmission for signals with a central frequency of 300 kHz did not demonstrate the required sensitivity to corrosion-induced mass loss at the interface. The 500 kHz signal showed a declining energy trend, thus demonstrating its potential for corrosion inspections. One plausible explanation for the lack of sensitivity at 300 kHz is the signal's limited ability to capture incipient changes in clamping force resulting from corrosion at the joint. Thus, the inspection at 300 kHz may not be suitable for capturing early-stage corrosion effects on the clamping force. It appears that the 500 kHz central frequency component is more sensitive to incipient changes than 300 kHz and can be used for early damage detection.

Despite the initial insights, determining sensitive inspection frequencies remains a challenging task, currently relying on a trial-and-error approach. Another challenging aspect of using conventional transducers is the reduced signal strength at higher frequency signals. This may require designing transducers with specific resonance frequencies or using a high-power amplifier, which adds to the cost of inspection. High-energy laser-based signal generation can offer simultaneous generation of a wide frequency range and can alleviate the challenges of low signal strength for inspecting large specimens.

To explore the potential of laser-based inspection, we have used a high-energy Q-switched Nd: YAG laser as a transmitter and recorded the transmission using a conventional transducer. Using lasers, non-contact delivery of energy towards the excitation of the substrate is possible [9]. Further, no amplification of the received signal is needed. In the present study, at the transmitting end, the laser was able to generate 6 ns optical pulses with an energy output of up to 0.8 Joules. Figure 5 shows the A-scan and the frequency spectrum of the transmitted signal in an identical pristine bolted specimen in the 50 kHz to 1 MHz range. A-scan demonstrates the higher strength of transmitted signal with typical amplitude in volts compared to millivolts in case of transducers. This shows that the laser based excitation can alleviate low transmission energy challenges in relatively big structures. Furthermore, the frequency spectrum demonstrates the simultaneous existence of a wide range of transmitted frequencies, which is a better alternative to conventional transducers that have narrow-banded frequency responses. However, the energy distribution is well spread across various frequencies, thus requiring additional signal processing to decipher information related to corrosion from the signal. This can potentially be undertaken using a suitable windowing function, that would capture the energy variation along frequencies of interest. A study to monitor corrosion using laser-

generated ultrasound will now be undertaken, and the findings will be subsequently reported.

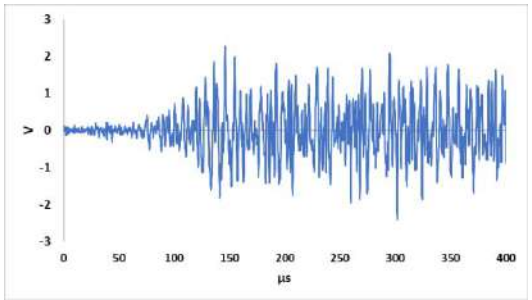

(a)

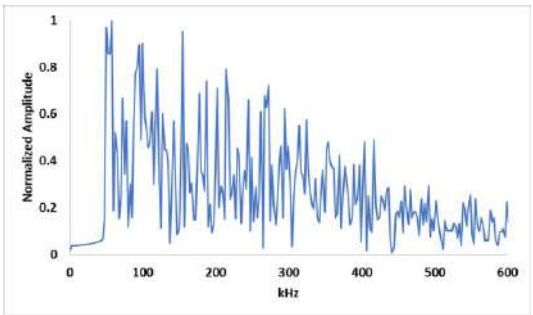

(b)

Fig 5. *(a) A scan of laser based signal generation and (b) frequency spectrum of the transmitted signal*

5. CONCLUSION

The study presented herein showcases the potential of ultrasonic inspection methods for assessing bolted steel joints in corrosive environments. The joint corrosion was simulated using an accelerated electrochemical approach, and the ultrasonic signal transmission was monitored across the bolted joint using a conventional piezo transducer-based setup. This joint was monitored using piezo ultrasonic signals of central frequencies of 300 kHz and 500 kHz. It was observed that the 300 kHz central frequency excitation signals are not sensitive to joint corrosion as a relatively insignificant change was observed in the transmitted signal energy. However, a gradual decline in the transmitted energy for a 500 kHz central frequency signal was noted, which highlights the importance of selecting the optimal inspection frequency for corrosion-related investigations. The trial-and-error underlying the selection of excitation frequency in the piezo transducer-based setup requires alleviation. The broad-banded-multiple frequency excitations in the case of a pulsed Laser thus offers a viable potential in monitoring over piezo-based systems. Our preliminary investigation highlights the potential of conducting the non-contact laser-based inspection of corroding bolted joints.

6. FUNDING STATEMENT

The authors gratefully acknowledge Australian Research Council for funding this investigation through grant LP150100475.

7. REFERENCES

[1] Jhang, K.-Y., et al., Estimation of clamping force in high-tension bolts through ultrasonic velocity measurement. Ultrasonics, 2006. **44**: p. e1339-e1342.
[2] Nassar, S.A. and A.B. Veeram, Ultrasonic control of fastener tightening using varying wave speed. 2006.
[3] Pan, Q., et al., Research review of principles and methods for ultrasonic measurement of axial stress in bolts. Chinese Journal of Mechanical Engineering, 2020. **33**(1): p. 1-16.
[4] Lee, E.-S., S.W. Choi, and L.-H. Kang, Estimation of the ultrasonic time-of-flight for evaluating the axial force acting on bolt/nut assemblies under various mechanical and thermal conditions. Structural Health Monitoring, 2023. **22**(4): p. 2481-2495.
[5] Amerini, F. and M. Meo, Structural health monitoring of bolted joints using linear and nonlinear acoustic/ultrasound methods. Structural health monitoring, 2011. **10**(6): p. 659-672.
[6] Shah, J.K., et al., Ultrasonic monitoring of corroding bolted joints. Engineering Failure Analysis, 2019. **102**: p. 7-19.
[7] Cui, E., et al., Monitoring of corrosion-induced damage to bolted joints using an active sensing method with piezoceramic transducers. Journal of Civil Structural Health Monitoring, 2021. **11**: p. 411-420.
[8] Wang, F., Identification of multi-bolt head corrosion using linear and nonlinear shapelet-based acousto-ultrasonic methods. Smart Materials and Structures, 2021. **30**(8): p. 085031.
[9] Majhi, S., et al., Corrosion monitoring in steel bars using Laser ultrasonic guided waves and advanced signal processing. Mechanical Systems and Signal Processing, 2021. **149**: p. 107176.

Monitoring Stress Concentration Using Ultrasonic Signals

Saurabh Agarwal[1], Surendra Beniwal[2], Debdutta Ghosh[3]
[1]*Research Scholar,* [2]*Indian Institute of Technology, Jammu, India*
[2]*Assistant Professor, Indian Institute of Technology, Jammu, India*
[3]*Senior Scientist, CSIR-CBRI, Roorkee, India*

[a]*Email: 2019rce0021@iitjammu.ac.in*

Abstract

This research focuses on the ultrasonic wave propagation in rails when subjected to a rolling load. Most of the simulations performed for wave propagation on a medium are when the simulated medium is unstressed, but in the physical state most of the time, no medium is in under unstressed condition. This makes it essential to understand the signals when the medium is stressed and unstressed and to understand the changes in signal under a stressed medium. This study investigates the influence of a rolling load on wave propagation in rails. When a load is applied to the rails, they undergo displacements. Consequently, the signals received by sensors, strategically placed along the rail section, undergo changes due to the presence of stress concentration as the force exerted by the wheel and subsequent displacement in the medium. To delve deeper into this phenomenon, a simulation approach is employed to calculate the rail displacements and subsequent signal variations. Numerical models are utilized to simulate the dynamic response of the rails under the rolling load. By integrating these models with ultrasonic wave propagation, the changes in signal characteristics caused by displacements in the medium are recorded, analyzed, and stress concentration is localized on the rail section by analyzing the signals and Gabor features. The study shows that the signal variations correlate with the level and location of stress induced by the rolling load. Ultimately, this research aims to contribute to the advancement of nondestructive testing methodologies for railways. A better understanding of ultrasonic wave propagation and its correlation with deformations under rolling load conditions with stress localization will enable more effective detection, ultimately improving the safety and reliability of railway systems.
Keywords: *Numerical Modeling, Spectral Element Method (SEM), Wave Propagation, Gabor Atoms*

1. INTRODUCTION

Railway transportation plays a vital role in modern society, providing efficient and reliable means for the movement of passengers and freight. Ensuring railway tracks' safety, integrity, and reliability is of utmost importance for maintaining operational efficiency and preventing potential accidents or failures [1,2]. Structural Health Monitoring (SHM) techniques, such as ultrasonic techniques [3,4], have proven to be valuable tools for assessing the condition of rail infrastructure [5–7].

Ultrasonic techniques have been extensively studied for their effectiveness in detecting and characterizing defects [8,9] in the rail section. However, most simulations and studies of wave propagation focus on unstressed mediums [6,10–12], which do not accurately represent real-world conditions. Railway tracks experience significant stress and displacement due to rolling loads. Understanding the effects of these displacements on ultrasonic wave propagation is crucial for developing reliable and accurate SHM techniques.

As with the removal of load, the medium should regain its original geometry, and no change in geometry should be observed, but if the medium does not regain its original position after the removal of load, then this shows that the medium is yielded [13] from its original geometry and needs to be checked. This research focuses on investigating the behavior of ultrasonic wave propagation in rails when subjected to rolling loads and localizing the area of the stress concentration. The objective is to explore the influence of rolling load-induced displacements on the signals received by sensors strategically placed along the rail section. A spectral element method (SEM) [14] based simulation tool was adopted to propagate the wave on the linearly elastic deformed rail medium. Numerical models are employed to simulate the dynamic response of the rails under the rolling load, considering various factors such as load magnitude, interaction of wheel with rail, and speed. By integrating these models with ultrasonic wave propagation, the signal characteristics resulting from geometric changes due to generated displacements are recorded and analyzed. The signal can be analyzed by extracting parameters or converting the signal from one domain to another using many transforms like Fourier transform, Laplace transform, Z transform, Wavelet transform, Gabor Atoms. Gabor atoms are complex-valued functions that are obtained by modulating a Gaussian function with a sinusoidal wave [15–17]. Gabor atoms have some unique properties that make them useful in various applications [18]. They are localized both in time and frequency domains. Gabor atoms can be highly effective for analyzing time-domain ultrasonic signals due to their ability to capture both time and frequency localization properties.

The findings of this study are expected to provide the region of stress concentration when rolling load-induced on the rail, and corresponding variations in ultrasonic signals are observed respectively. A comprehensive understanding of this relationship will contribute to the advancement of SHM techniques for railways, enabling more accurate defect detection and condition assessment techniques. By detecting and addressing potential issues at an early stage, the safety and reliability of railway systems can be significantly improved, leading to enhanced operational efficiency and reduced maintenance costs. In this paper, the methodology employed for simulating ultrasonic wave propagation in stressed rails is discussed, and present the results of analysis regarding the changes in signal characteristics.

2. METHODOLOGY

A rail section with a length of 1 meter is adopted for this study, which conforms to the UIC 60 Kg/m standard, a widely used rail profile in railway tracks worldwide. For simulating the loading conditions encountered in railway tracks, a moving wheel with a maximum axle load of 22 tonnes, adhering to the guidelines set by the Indian Roads Congress (IRC) is introduced, as shown in Fig. 1. This loading configuration was crucial to replicate the actual stresses and deformations experienced by the rail under the influence of a passing train. The dynamic explicit simulation was adopted to capture the dynamic response of the rail during the passage of the moving wheel. In the simulation, the wheel is considered rigid, as the rail section is of interest. Using this technique, the interaction between the rail and the rolling load was analyzed. The explicit formulation allowed us to calculate the stress and displacements over time, which was essential for understanding ultrasonic wave propagation behavior under rolling load conditions.

A friction surface interface considering the Lagrange Multiplier Friction formulation with a friction coefficient value of 0.1 was incorporated into the simulation model to consider the interactions between the moving wheel and the rail. For the analysis of ultrasonic wave propagation, the 2D middle longitudinal plane of the rail is specifically focused. The displacement data from the middle longitudinal plane nodes are extracted from the simulation results. This involved calculating the displacements at these nodes due to the applied rolling load. These node displacements were incorporated as the initial displacement field for the 2D longitudinal plane for the shear horizontal (SH) wave propagation using spectral element method (SEM) based numerical tool [19] considering the input signal of 50 kHz with 2 cycle hanning modulated sine wave propagated on the medium as shown in Fig. 2.

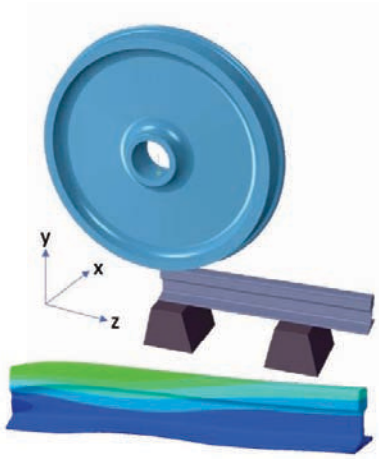

Fig. 1: *Rail section with moving wheel (top) and its upscaled deformed shape (below)*

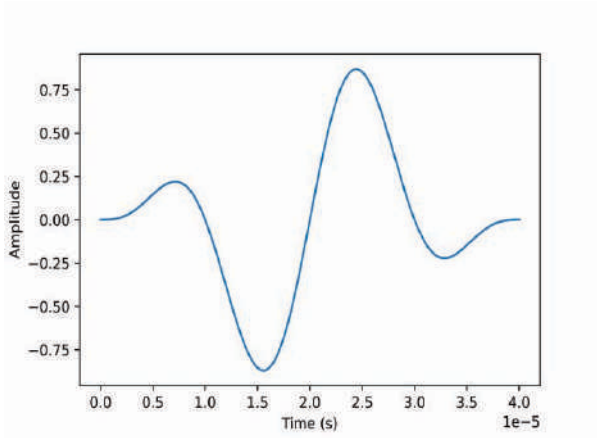

Fig. 2: *Input Signal*

The transducers were placed at every 100 mm from one end to another, and the change in the signal was analyzed as the wheel was moved through the length of the rail. This study focuses on Shear Horizontal (SH) wave propagation in the rail medium.

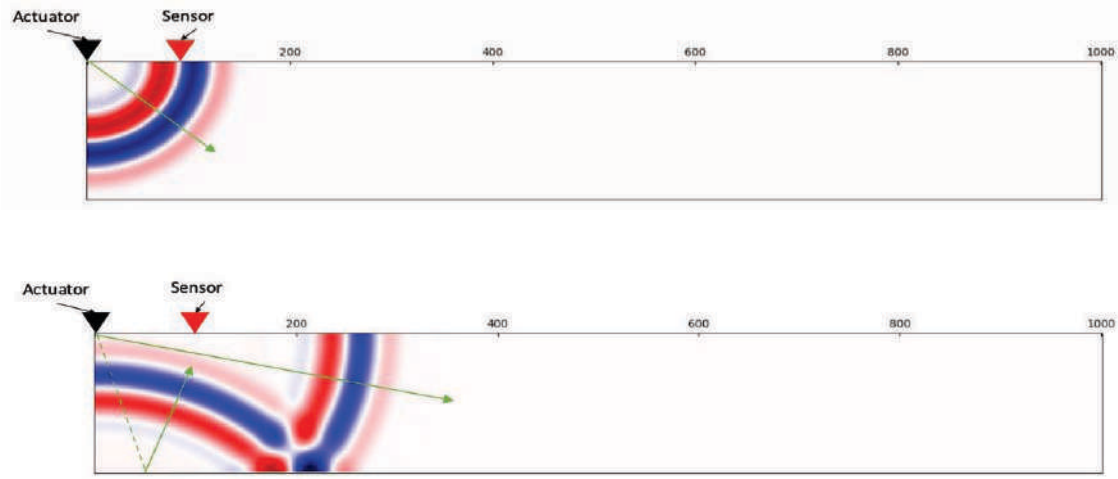

Fig. 3: *Wavefield at the longitudinal plane of the rail at (a) 50 μs (b) 100 μs*

To assess the behavior of SH waves along the rail section, transducers are strategically positioned at regular intervals of 100 mm, spanning from one end of the rail to the other. Wave propagation in the rail is shown in Fig. 3. These transducers served as actuators and receivers, detecting and actuating the ultrasonic signals as the wheel moved through the length of the rail. By placing the transducers at these specific locations, the changes in the ultrasonic signals induced by the rolling load and the ensuing rail displacements are captured. The process involved continuous monitoring of the signals received by the transducers as the moving wheel progressed along the rail. This allowed us to observe how the passage of the wheel influenced the propagation characteristics of SH waves and the subsequent changes in the received signals. Analyzing the signal variations at each transducer location can provide insights into the effects of the rolling load-induced displacements on wave

behavior. Throughout the simulation process, signal changes are recorded and analyzed at each transducer location, correlating them with the dynamic response of the rail under the rolling load. This correlation was crucial for deciphering the intricate relationship between the deformation of the rail and the corresponding changes in SH wave behavior. Using two approaches, the stress concentration has been localized on the length of the rail section.

a. Dissimilarity Index (DI)

The stressed state signal is compared with the baseline signal (unstressed signal), and the Dissimilarity Index between the signals is calculated using Eq. 1.

$$DI = \sum_{i=1}^{N} \frac{(A_s[i]-A_o[i])^2}{A_o[i]^2} \quad (1)$$

Where A_0 is the signal of unstressed condition and $A_s$is the signal of stressed condition for the N time points in the signal.

b. Gabor Features

Gabor atoms have excellent time and frequency localization properties. In ultrasonic signals, different phenomena may occur at specific time intervals and correspond to specific frequencies. Gabor atoms can be used to detect and represent these localized features accurately. The Gabor transform can decompose an ultrasonic signal into a set of time-frequency atoms as shown in Fig. 4.

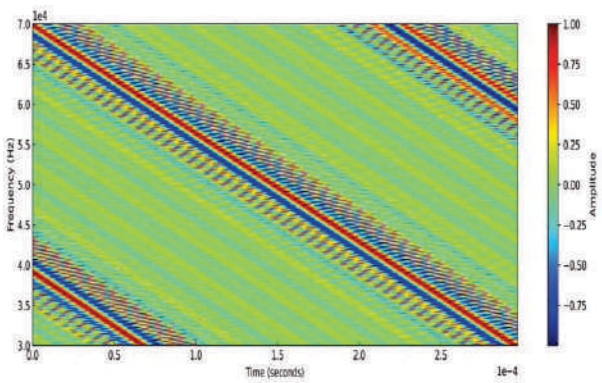

Fig. 4: *Gabor atoms*

This approach to calculated Gabor atoms considering $\Delta f \Delta t > 1$, using Eq. 2.

$$\phi_{jk}(t) = e^{-\pi(t-j\Delta t)^2} e^{i2\pi k\Delta f(t-j\Delta t)} \quad (2)$$

Where Δf is the nominal bandwidth, Δt is the nominal duration of the signal, j is the cell's independent quantum number, and k is the frequency band quantum number [17]. Eq. 2. provides the Gabor atoms in complex numbers from which real values are considered and convoluted with the stressed and unstressed state signals. The Gabor transform was performed on the convoluted data. Then Euclidean distance was calculated between the transforms of each stressed state signal and the unstressed state signal obtained from the sensor placed on the rail at every position.

3. RESULTS AND DISCUSSION

In simulations, the time domain signals received from the sensor, which was strategically positioned at a distance of 100 mm from the left end of the rail are closely monitored. Additionally, to gain deeper insights into the signal characteristics, signals from the time domain into the frequency domain are also transformed, as depicted in the figures of Fig. 5. Upon observation, it was evident that as the wheel progressed along the rail due to the displacements as shown in Fig. 5. top, significant changes were observed in the time domain signals, like change in the time of flight (TOF), frequencies, amplitude.

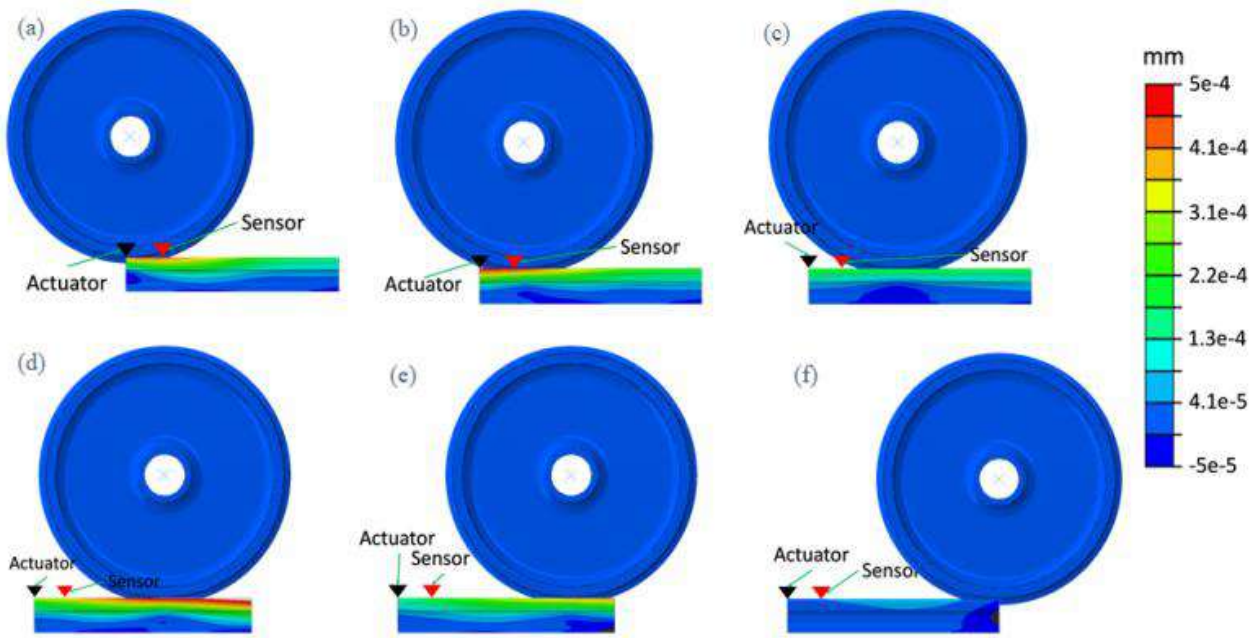

(i). Displacement in rail section due to the movement of wheel position at (a) 20, (b) 200, (c) 400, (d) 600, (e) 800, and (f) 1000 mm from the left end

(a)

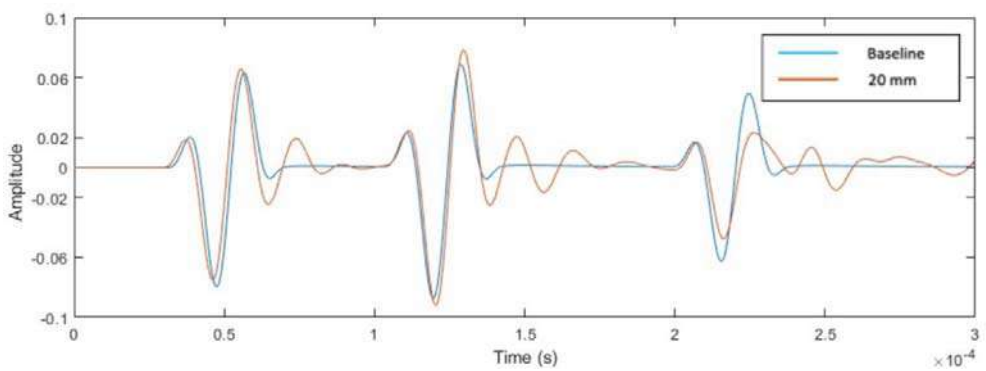

(b)

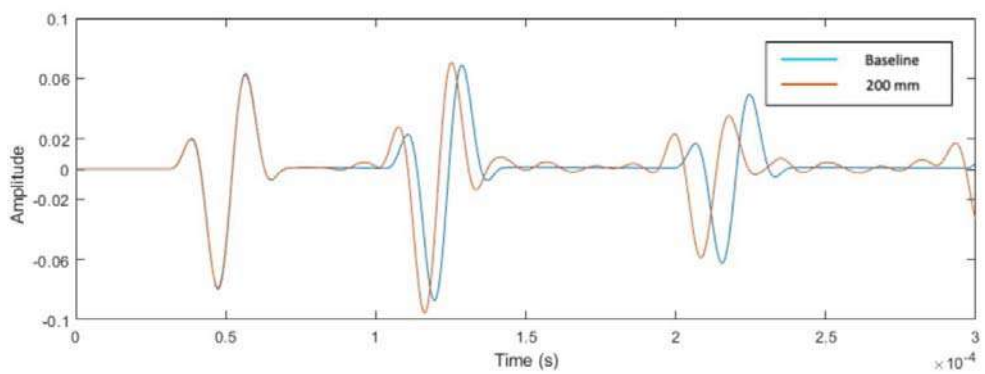

(c)

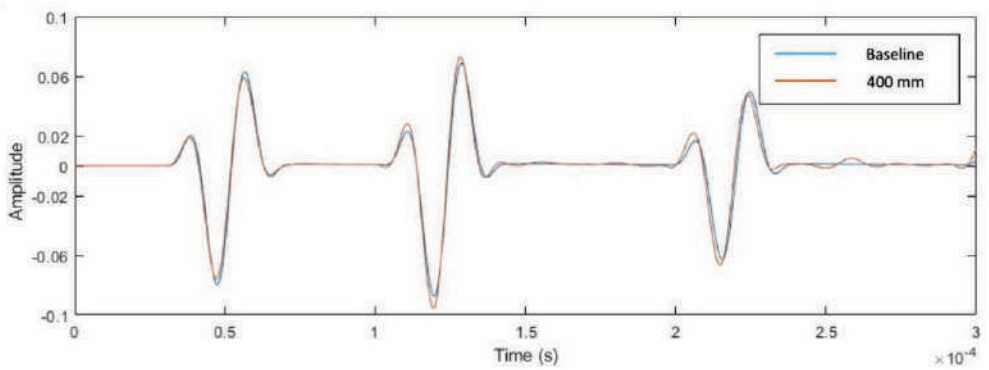

(d)

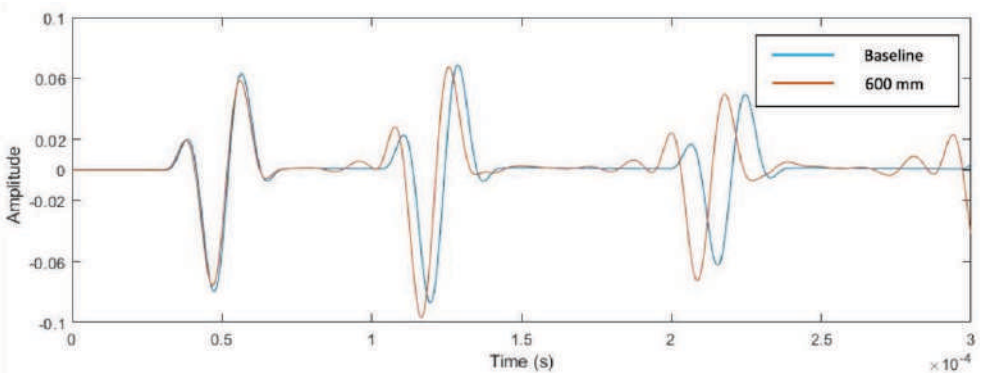

(e)

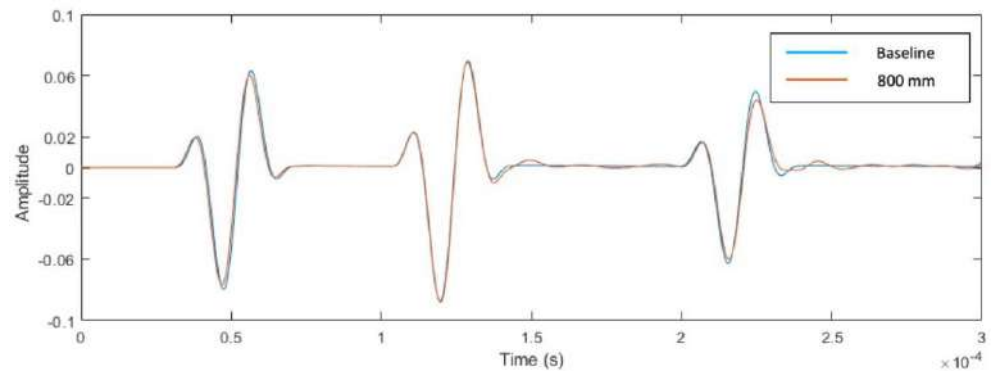

(f)

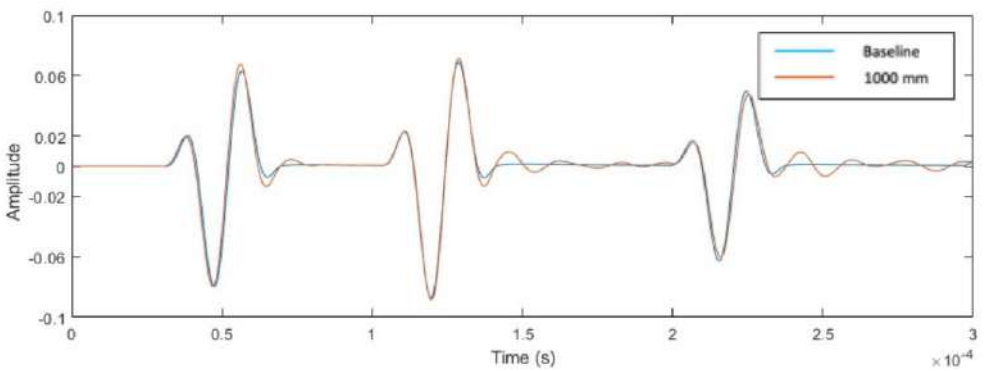

(ii). Time Domain signal at (a) 20, (b) 200, (c) 400, (d) 600, (e) 800, and (f) 1000 mm from the left end

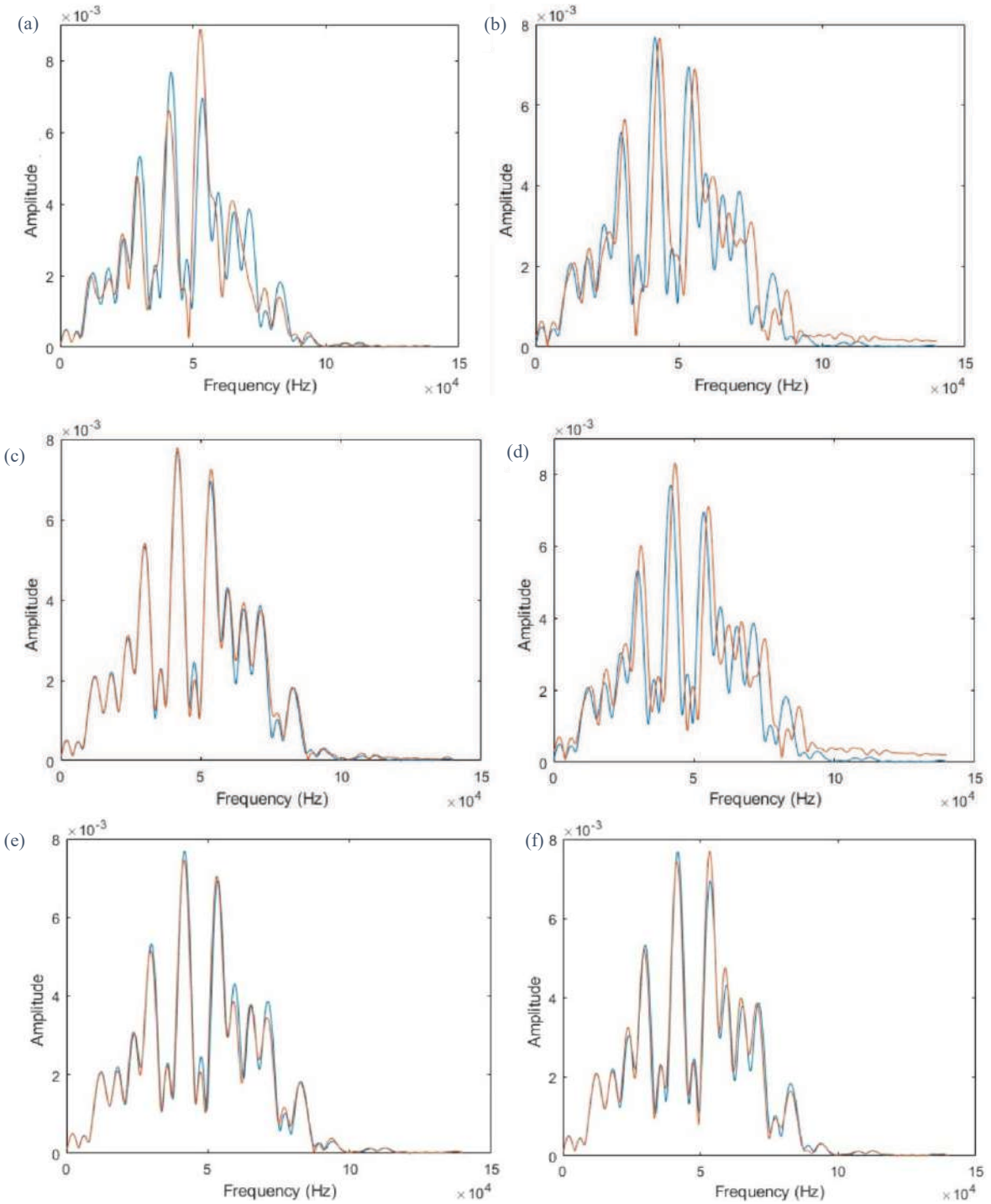

(iii). Frequency transform of the signal at (a) 20, (b) 200, (c) 400, (d) 600, (e) 800, and (f) 1000 mm from the left end

Fig: 5: *Wheel positions with Time domain signals and their frequency domains when the wheel is at different positions*

These changes were a direct consequence of the rolling load-induced deformation experienced by the rail. As the wheel moved further away from the left end of the rail, the deformed geometry near the left end side began to regain its original position. Consequently, the signal variations in both the time and frequency domains tend to align closer to the baseline signals. When the wheel at 400 mm, smaller displacements in the rail section are observed comparatively, leading to a convergence of the signal towards the baseline. The reduced magnitude of displacements resulted in minor changes in the signal, pushing it closer to its original state. However, at the wheel location of 600 mm, higher displacements are causing more significant changes in the received signal.

Additionally, as the wheel crosses the 800 mm location, the magnitude of the displacements near the sensor position continuously decreases, allowing the signal to converge further toward the baseline. This convergence indicated that the rail's geometry near the left end had attained a state of relative stability as the wheel moved away from it. At this point, the dynamic response of the rail to the rolling load exhibited reduced sensitivity to changes in the wave propagation, resulting in signals that more closely resembled those observed in an unstressed state.

Table. 1: *Euclidean Distance of Gabor transform of stressed signal with Gabor transform of the unstressed signal at different positions of the wheel at rail*

S. No.	Position on Rail (mm)	Euclidian Distance at position on rail section			
		20 mm	200 mm	400 mm	600 mm
1	0	22851.27	41210.46	5011.782	35977.94
2	100	51918.08	19859.17	12669.95	32134.66
3	200	24555.05	24015.5	10851.93	16203.2
4	300	36451.29	18370.4	23730.22	17575.36
5	400	22634.43	22718.18	26359.61	19698.99
6	500	14927.4	21393.15	30865	30535.48
7	600	27203.95	24974.29	33278.69	37808.22
8	700	28876.14	27966.01	29796.23	59974.71
9	800	20433.46	21555.06	19694.14	19247.59

For stress localization, In Fig. 6, at the top of the figure, the contour plot depicting the equivalent stress in the rail caused by the movement of the wheel is shown. To further analyze the effects of the rolling load-induced displacements on the received signals, the dissimilarity in signal between stress conditions at various lengths along the rail with the signal under an unstressed condition is examined. For this purpose, specific locations at lengths of 20 mm, 200 mm, 400 mm, and 600 mm from the starting point are selected, and compared the respective received signals at the position of the sensor to that of the signal obtained under an unstressed state at every sensor position placed at the interval of 100 mm using the Eq. 1. By comparing the signal dissimilarity index under stressed and unstressed conditions, regions are localized of the rail where the stress concentrations were most prominent. The peaks in the dissimilarity index at a particular location indicate a higher level of stress concentration.

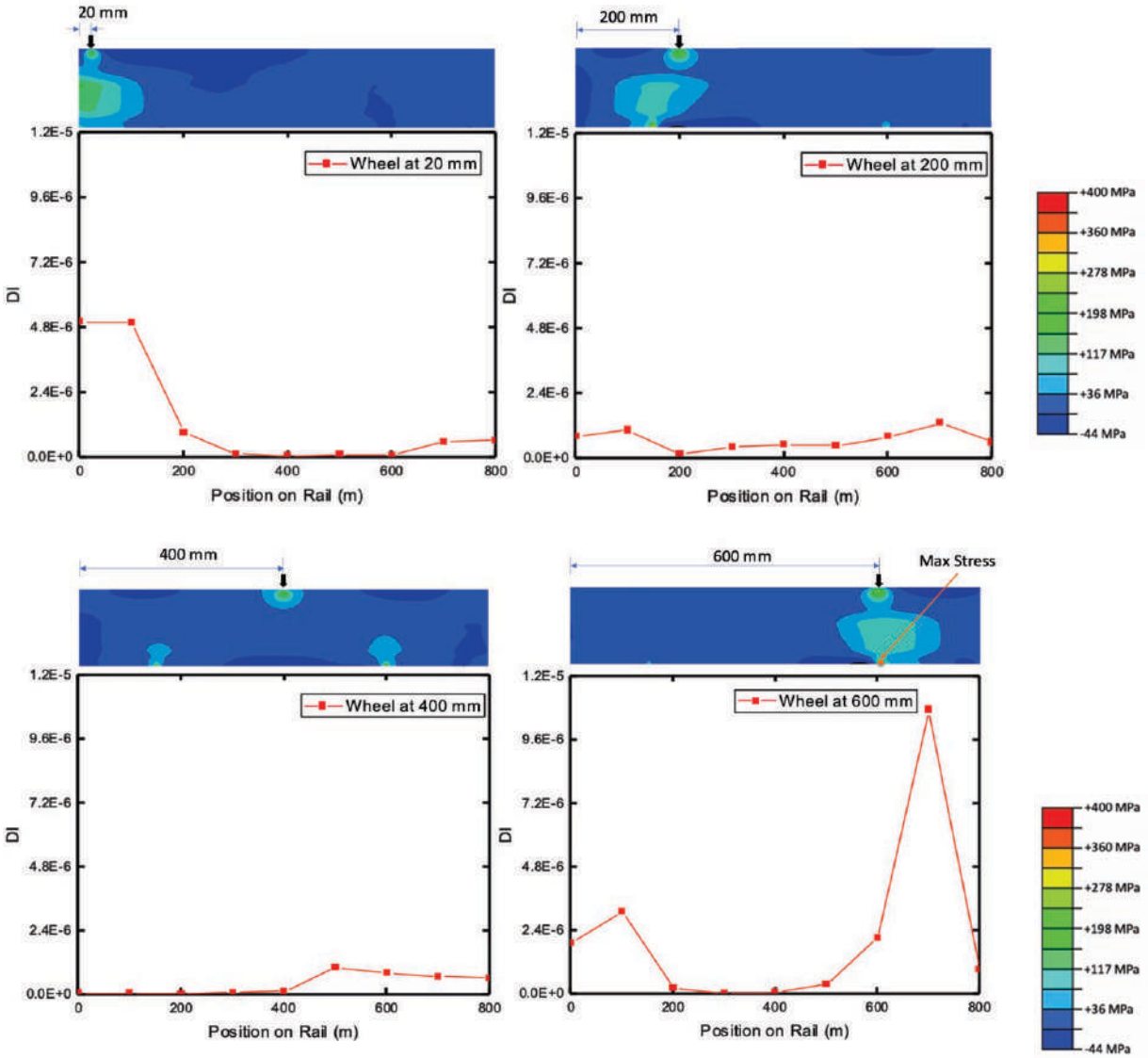

Fig. 7: *Euclidean Distance of stress signal to baseline signal w.r.t the position of the wheel on the rail*

For the next analysis, the Gabor features of the stressed signal with the Gabor features of the unstressed signal are calculated using Eq. 2, Euclidean distance between the Gabor transform of unstressed signals with the Gabor transform of the stressed signal was calculated, and it shows better results in localizing the concentration of the stress with the movement of the wheel on the rail as shown in Fig. 7. These concentration localization helped us to locate the critical areas that were more susceptible to yield early and experienced the most significant changes in wave behavior due to the rolling load. This can also be seen in Table 1, as the wheel moves, the Euclidean distance at the sensors nearby the wheel shows higher values due to an increase in the magnitude of stress in that region. Table 2 shows the position of maximum stress shown by the peaks coming in the vicinity of the peak positions, but the peak values do not provide a linear variation with the change in the stress values. Especially in the case of the wheel at 200 mm position, the peaks of DI show very small values than those at other wheel positions.

***Table. 2**: Comparison of Position and values of stress generated due to wheel movement with Peak positions and the value of the peak*

S.No	Position of wheel	Due to Wheel Load		DI		Euclidean Distance	
		Position of stress	Stress Value	Peak Position	Value at peak position	Peak Position	Value at peak position
1	20	22	175	0	5.00E-06	100	51918.08
2	200	150	346	100	1.00E-06	0	41210.46
						200	24015.5
3	200	600	100	700	1.30E-06	700	27966.01
4	400	600	285	500	9.90E-07	600	33278.69
5	600	152	76	100	3.11E-06	0	35977.94
						100	32134.66
6	600	600	380	700	1.07E-05	700	59974.71

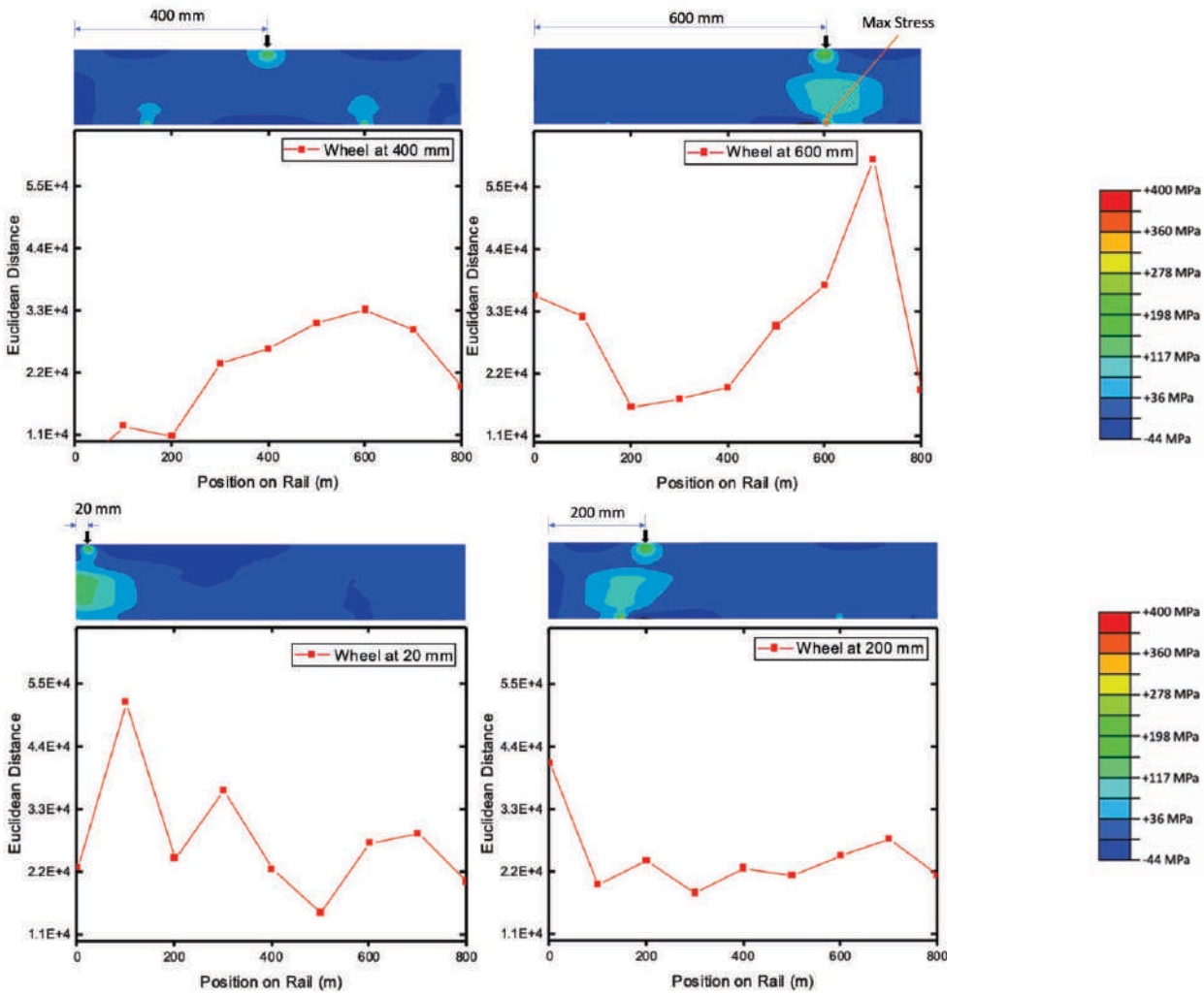

***Fig. 7:** Euclidean Distance of stress signal to baseline signal w.r.t the position of the wheel on the rail*

4. CONCLUSION

In this research, an investigation was conducted to check the behavior of ultrasonic wave propagation in the rail of 1m under the influence of rolling loads, with a specific focus on understanding the localization of the developed stress concentration. The one-meter rail section analyzed in this study reflects a typical rail section considering support conditions provided by sleepers. The result obtained through this section will be applicable to the other sections. The examination of time domain signals, and frequency domain transformations, provided essential insights into the changes in wave characteristics as the wheel advanced through the rail section. The continuous monitoring of signals at regular intervals allowed us to understand the rail's dynamic response to the rolling load. Through the analysis of the signal to localize the stress concentration at specific locations along the rail, Gabor atoms can be used as they identify regions better. These crucial regions indicated where the rail experienced significant changes due to the rolling load, serving as key locations for further inspection and maintenance considerations.

The observed convergence of signals towards baseline levels as the wheel moved away from the left end demonstrated the stabilization of the rail's deformation. This important finding revealed that certain areas along the rail cross-section gradually regained their original positions, reducing the sensitivity of signals generated through the propagation of SH wave. The correlations established between stress concentration locations and changes in SH wave signals highlighted the dynamic nature of wave propagation in stressed rails. This understanding is of paramount importance for the development of non-destructive testing methodologies in railway track inspection. It enables the identification of critical regions that are more susceptible to deform early, leading to the development of targeted inspection and maintenance strategies that ensure the safety and reliability of railway systems.

Ultimately, findings contribute to the enhancement of railway infrastructure maintenance practices, fostering improved performance, and operational reliability. The knowledge gained from this study will serve as a stepping stone for further advancements in non-destructive testing methodologies, ultimately elevating the safety and efficiency of railway systems worldwide.

5. REFERENCE

[1] W. Cao, Structural Health Monitoring of High-speed Railway Tracks Using Diffuse Ultrasonic Wave-based Condition Contrast: Theory and Validation Fatigue damage identification in FRP-reinforced steel plates View project, Smart Struct Syst. 26 (2020) 227–239. https://doi.org/10.12989/sss.2020.26.2.227.

[2] M. Masmoudi, S. Yaacoubi, M. Koabaz, M. Akrout, A. Skaiky, On the use of ultrasonic guided waves for the health monitoring of rails, Proc Inst Mech Eng F J Rail Rapid Transit. 236 (2022) 469–489. https://doi.org/10.1177/09544097211025898/ASSET/IMAGES/LARGE/10.1177_09544097211025898-FIG18.JPEG.

[3] A. Ganguli, S. Beniwal, Cross Correlation based Synthetic Aperture Focusing technique applied to Imaging of Rebars in Cement Mortar, in: Conference: 6th International Conference of the Asian Concrete Federation (ACF 2014), Seoul, South Korea, 2014, 2014.

[4] S. Beniwal, A. Ganguli, Defect detection around rebars in concrete using focused ultrasound and reverse time migration, Ultrasonics. 62 (2015) 112–125. https://doi.org/10.1016/j.ultras.2015.05.008.

[5] K. Wang, W. Cao, L. Xu, X. Yang, Z. Su, X. Zhang, L. Chen, Diffuse ultrasonic wave-based structural health monitoring for railway turnouts, Ultrasonics. 101 (2020) 106031. https://doi.org/10.1016/J.ULTRAS.2019.106031.

[6] A. Pantano, D.C.-A.P. A, undefined 2010, Simulation of laser-generated ultrasonic wave propagation in solid media and air with application to NDE, SpringerA Pantano, D CernigliaApplied Physics A, 2010•Springer. 98 (2010) 327–336. https://doi.org/10.1007/s00339-009-5402-0.

[7] Y. Jiang, H. Wang, S. Chen, G. Tian, Visual quantitative detection of rail surface crack based on laser ultrasonic technology, Optik (Stuttg). 237 (2021) 166732. https://doi.org/10.1016/J.IJLEO.2021.166732.

[8] S. Beniwal, A. Ganguli, A. Mukherjee, SIMULATION OF ULTRASONIC RAYLEIGH WAVE BASED DAMAGE DETECTION IN CONCRETE STRUCTURES, (n.d.). https://www.researchgate.net/publication/331974869.

[9] D. Ghosh, S. Beniwal, A. Ganguli, Detection of defect in concrete slab using Rayleigh waves, in: 2015 IEEE International Ultrasonics Symposium (IUS), IEEE, 2015: pp. 1–4. https://doi.org/10.1109/ULTSYM.2015.0338.

[10] D. Ramatlo, C. Long, P. Loveday, D.W.-Ultrasonics, undefined 2020, A modelling

framework for simulation of ultrasonic guided wave-based inspection of welded rail tracks, Elsevier. (n.d.). https://www.sciencedirect.com/science/article/pii/S0041624X20301542 (accessed July 19, 2023).

[11] D.A. Ramatlo, C.S. Long, P.W. Loveday, D.N. Wilke, Physics-based modelling and simulation of reverberating reflections in ultrasonic guided wave inspections applied to welded rail tracks, J Sound Vib. 530 (2022)116914. https://doi.org/10.1016/j.jsv.2022.116914.

[12] S. Rodriguez, V. Gayoux, E. Ducasse, M. Castaings, N. Patteeuw, Ultrasonic imaging of buried defects in rails, NDT&E International. 133 (2023) 102737. https://doi.org/10.1016/j.ndteint.2022.102737.

[13] Theory of Elasticity. By S. Timoshenko. 1934, (n.d.). https://scholar.google.com/scholar?hl=en&as_sdt=0%2C5&q=Theory+of+Elasticity.+By+S.+Timoshenko.+1934&btnG= (accessed July 26, 2023).

[14] A.T. Patera, A Spectral Element Method for Fluid Dynamics: Laminar Flow in a Channel Expansion, J Comput Phys. 54 (1984) 468488.

[15] B. Wu, W. Zhou, Ultrasonic defect detection in noisy signals by a nonconvex sparse regularization approach, Applied Acoustics. 210 (2023) 109461. https://doi.org/10.1016/J.APACOUST.2023.109461.

[16] Z. Lu, C. Yang, D. Qin, Y. Luo, Estimating the parameters of ultrasonic echo signal in the Gabor transform domain and its resolution analysis, (2015). https://doi.org/10.1016/j.sigpro.2015.10.006.

[17] Gabor Analysis and Algorithms, Gabor Analysis and Algorithms. (1998). https://doi.org/10.1007/978-1-4612-2016-9.

[18] G. Ayalew, Q.U. Zaman, A.W. Schumann, D.C. Percival, Y.K. Chang, An investigation into the potential of Gabor wavelet features for scene classification in wild blueberry fields, (2021). https://doi.org/10.1016/j.aiia.2021.03.001.

[19] S. 'Agarwal, S. 'Beniwal, SEM Based Model for 2D SH Wave Propagation in Heterogeneous Medium, in: NDE 2022, 2022

Assessment of Residual Compressive Strength of Geopolymer Concrete Exposed to Elevated Temperature Using Artificial Neural Network Approach

Kishor S. Kulkarni[1], Sana D. Sayyad[2], M. Reyazur Rahman [3]
[1]*Senior Scientist,* [2]*Intern Student, Architecture Planning and Energy Efficiency,*
[3]*Senior Scientist, Advanced Concrete, Steel and Composites (ACSC)*
CSIR-Central Building Research Institute, Roorkee, India,

[a]*Email: kishorsk@cbri.res.in, sanasayyad0126@gmail.com, reyaz@cbri.res.in*

Abstract

The population growth and industrial activities nowadays creates a considerable volume of rubbish, producing disposal challenges and major environmental hazards. The cement industry is a major generator of greenhouse gases like carbon dioxide. The use of waste resources, which avoids disposal worries while lowering greenhouse gases emissions into the atmosphere. This is a key factor in the development of cement-free Geopolymer Concrete (GPC). In the present work, GPC was made using a 75:25 proportions of fly ash (FA) and ground granulated blast furnace slag (GGFBS). The cube specimens were exposed to various temperatures ranging from 200 °C, 400°C, 600°C and 800 °C. The mechanical characteristics were then assessed. The compressive strength of GPC exposed to elevated temperatures is predicted using an Artificial Neural Network (ANN) technique in this study. The assessment of the residual compressive strength of GPC exposed to elevated temperatures was also done using non-destructive tests (NDT), such as the Rebound Hammer (RH) and Ultrasonic Pulse Velocity (UPV). In this study, the 255 experimental data from the other studies are also used for the ANN model's training, testing, and verification. The results of the study validate the use of ANN models to estimate the concrete's residual compressive strength in a manner that is quite similar to experimental data. The results show that the average prediction error for an unknown set of data was about 3.5 MPa.

Keywords: *Geopolymer concrete, elevated temperature, compressive strength, artificial neural network*

1. INTRODUCTION:

The population is growing at an exponential rate, which is driving up infrastructure demand. Because of its widespread usage adjacent to water, this need is negatively reflected in construction materials, notably Ordinary Portland Cement (OPC) [1]. The rise of urbanization and the global population increase have resulted in a 12% increase in global cement output in 2019, which is expected to quadruple by 2050. China, which produces 2.4 Bt of cement annually and accounts for half of the world's cement consumption, leads the cement sector globally, followed by India, which produces 290 Mt. One tonne of cement may produce 0.6 to 1.0 tonne of CO_2 depending on the production process used, accounting for 59% of worldwide CO_2 emissions [2] The environmental impact of cement on our ecosystem is quite severe, and it is hazardous to both human health and animals. It wastes natural resources and takes more energy to produce, in addition to emitting CO_2. From an environmental standpoint, it has been determined that OPC utilization in the construction area has restrictions. As a result, finding a replacement binder from industrial by-products to complement OPC in concrete manufacture is crucial.

Over the past few decades, many researchers have undertaken in-depth studies on environmentally friendly and energy-efficient building materials. Davidovits proposed the Geopolymer Concrete theory in 1978 [3], which states that unique binders may be integrated by a polymeric reaction of geologically formed silicon and aluminium base

material, which comprises kaolin clay and alkaline liquids. Geopolymers are tetrahedral mixtures of $[AlO_4]^{-5}$ and $[SiO_4]^{-4}$ that are three-dimensional semi-crystalline frameworks. Lower content, greater content, and moderate content calcium alkali-activated binders are the three varieties available. By activating alkali materials based on aluminium silicates such GGBFS, fly ash (FA), metakaolin (MK), and others, alkali activated binders are produced [4].

Geopolymers, as opposed to OPC, are produced utilizing aluminosilicate-rich natural materials and industrial wastes as the primary raw materials, instead of calcium carbonate calcination ($CaCO_3$) [5]. $CaCO_3$ is the primary contributor to carbon dioxide emissions during the production of OPC. Geopolymer usage can thereby reduce greenhouse gas emissions by 73% while using 43% less energy. It is reasonable to draw the conclusion that geopolymer binders will be a potentially viable substitute for OPC in the production of concrete [6].

Geopolymers are mostly made from geological materials with high strength and specialized characteristics. When compared to Portland cement (PC) binders, geopolymer binders perform similarly to cement binders [7]. Geopolymer exhibits significant mechanical performance and stability when exposed to high temperatures [6]. Due to their ability to withstand fire, geopolymers have attracted the greatest interest in recent years [8]. This is because they enable a variety of uses, including concrete that can store heat energy and fire-resistant materials [8]. However, the development for in-situ applications is severely restricted by the energy-intensive high-curing procedure and insufficient starting strength [9]. In order to get over these restrictions, researchers are focusing on blended alkali-activated fly ash/GGFBS binders (AAFS), which combine an aluminosilicate source (fly ash or metakaolin) with calcium additions. [10].

Geopolymer concrete (GPC) is referred to as a potential eco-friendly building material [11]. By-products of polymerization procedures that employ aluminosilicate-rich substrates and alkali activators include geopolymers [12]. Fly ash (FA), GGBFS, metakaolin and the activators such as sodium silicate (SS) (Na_2SiO_3), and sodium hydroxide (SH) (NaOH) are basic materials of GPC [13]. Geopolymer concrete offers the benefit of using industrial waste in place of cement. Industrial leftovers could be used as raw materials by the GPC, thus drastically enhancing sustainability [14]. The inorganic geopolymer binder is created by polymerizing aluminosilicate minerals in a potent alkaline solution [15]. There are two phases to the polymerization process. Al and Si atoms from the raw material dissolve by the action of hydroxide ions in stage I to form geopolymer precursor ions (monomers). In Stage II when the precursor ions (monomers) polymerize to create the three-dimensional geopolymer structure [16].

Although buildings can absorb considerable fire damage, it is always important to protect people and valuables. Despite technological advancements and fire-control initiatives, there is still a potential that a fire will start. Ordinary concrete loses structural integrity when exposed to high temperatures because to dehydration, the dissolution of crystallised hydrates, and C-S-H gel. Due to their inorganic structure, geopolymeric materials are naturally fire resistant and heat resistant, unlike organic polymers [4]. Concrete generally has excellent fire-resistance qualities. However, the strength qualities of OPC concrete following a fire between 800°C and 1000°C are frequently less than 20% due to dehydration and destruction of C-S-H and other crystalline hydrates, aggregate types, permeability, and other variables [17]. Due to the significant temperature difference caused by fire, the hot exterior layer of the body has the propensity to separate from the colder interior layer. On the other hand, geopolymers have exceptional fire resistance at high temperatures because of their widely dispersed nano-pores in their ceramic-like microstructure, which allow physically and chemically linked water to pass through them and evaporate without causing damage the aluminosilicate network. [17].

Evaluating the residual strength properties of concrete exposed to high temperatures is difficult since concrete structures are typically composite. Physical inspection, in-situ laboratory testing, non-destructive experimentation, and partially destructive experimentation are all involved in assessing concrete after exposure to high temperatures. There is no single assessment method that is superior to others. Multiple approaches may be necessary, and results must be carefully monitored at consistent residual strength levels. Traditional test methods that are utilized under normal circumstances, such destructive testing on

core specimens, frequently fail to take into consideration the non-uniformity of concrete after a fire. The main goal of NDT is to find internal flaws in concrete members to aid in later suitability evaluation or to quickly offer a value of in-place concrete strength to be utilised in structural capacity assessment. The two Non-Destructive Testing (NDT) techniques that are most frequently used to evaluate the characteristics of concrete are the rebound hammer test and ultrasonic pulse velocity (UPV). Interior cracks, voids, and other faults can also be identified using the ultrasonic pulse velocity method. The ultrasonic pulse velocity method was used to evaluate the structural integrity of high-temperature-heated concrete. Combining multiple NDT methodologies would result in a reasonable evaluation.

In this study, an Artificial Neural Network (ANN) technique is used to assess the residual compressive strength of geopolymer concrete subjected to elevated temperatures. For the purpose of assessing the residual compressive strength of GPC concrete, a supervised learning model built on the ANN approach was developed. With nine input parameters and one output, the ANN model's structure was created in MATLAB. The experimental test results of the specimens have been compared with the developed ANN model.

2. EXPERIMENTAL METHODOLOGY

2.1 Experimental Programme

A total of thirty Geopolymer concrete specimens were cast, ambient cured, exposed to the elevated temperatures and tested for the destructive and non-destructives residual physical and mechanical properties. The Geopolymer concrete is prepared by using fly ash, GGBFS, fine and coarse aggregates and alkaline solutions.

2.2 Materials and Mix Proportions

The starting material for this experiment was low-calcium (Class F) dry fly ash obtained f rom a nearby power plant. It contains less than 3 % calcium (CaO) and more than 70% silica, alu mina, and iron oxide. Steel and Iron industry was te GGBFS is used which contains contains calciu m oxide, silica, alumina, and magnesia. The natu ral sand with a particle size of less than 4.75 mm was used as fine aggregate. The coarse aggregate of size 12.5 mm and 20 mm was used. For geopolymer ization, sodium hydroxide (NaOH) and sodium silic ate (Na_2SiO_3) were utilised as alkaline solutions. Ma sterglenium 51 a new generation based on modified polycarboxylic ether superplasticizer used (2% of Bi nder). For geopolymer concrete, there is no standard mix design available. Geopolymer concrete mix pro portions for M25 grade were finalized by trial and er ror method. Table 1 illustrates the component mix p roportions required.

Table 1. *Mix proportion of GPC*

FA (kg/m3)	GGBS (kg/m3)	NaOH (Solution) (kg/m3)	(Solution) Na_2SiO_3
310	**102**	**55**	**135**

Water (kg/m3)	Fine aggregate (kg/m3)	Coarse aggregate (kg/m3)	
		20mm	**12.5mm**
41	750	570	570

2.3 Specimen Preparation and Exposure To Temperatures

The sodium hydroxide solution with the 12 molarity was kept ready for 24 hours prior to mixing to prepare the alkaline solution. This much time is necessary for the full breakdown of sodium hydroxide pellets in water as well as the liberation of heat from the created solution since the dissolving process is an exothermic reaction. In a ratio of 2.5, sodium hydroxide and sodium silicate were combined to create an alkaline solution. The mixing started with the thoroughly mixing of fly ash and GGBFS with fine and coarse aggregates. Then alkaline solution and superplasticizer were then gradually added in to the dry mix, then mixed for approximately 4-5 minutes. Following the completion of the mixing, the concrete specimens of size 150 mm cubes were cast and cured for 28 days in ambient condition. After the 28 days of curing the specimens were exposed to 200°C, 400°C, 600°C, and 800°C in the muffle furnace (Fig. 1) and retained for 2 hrs. Three samples were

subjected in the muffle furnace at each indicated exposure temperature. The electric furnace used in the studies had a 2°C/min average heating rate. The specimens were cooled in the furnace to ambient temperature following exposure to the higher temperature.



Fig. 1. *Muffle furnace*

2.4 Testing of Specimens

After the temperature exposure the specimens were tested physically and then through the non-destructive and destructive testing. the colour change and surface cracks were observed physically. The specimens were taken for the Ultrasonic Pulse Velocity (UPV) test using Proceq Tico ultrasonic instrument. The instrument measures the propagation time of ultrasonic pulses in a sample with an accuracy of 0.1 µs and a range of 0.1-9999.9 µs. The transducers utilized had a diameter of 50 mm and a maximum resonance frequency of 54kHz. For appropriate transducer connection, concrete surface prepped, and grease was applied. The pulse velocity of the samples was determined using IS 13311 (Part 1). Further, rebound hammer (RH) test is carried out to determine the strength of concrete. Type N Schmidt test hammer has an impact energy of 2.207 Nm was used. The rebound hammer test was done in line with IS13311 (Part 2).

2.5 Artificial Neural Network Modelling

In the present study, ANN is used to estimate the compression strength of concrete. Many researchers are adopting ANN method to predict the desired outcome in other engineering fields. An artificial neural network is a sort of knowledge processing technology that is created by replicating the thinking and operating abilities of the human brain. A model of a real brain network is an artificial neural network. As a consequence, an artificial system that replicates the functioning of a biological neural systems will be built. The artificial neural network was made up of three parts: neurons, connection, and weights. ANN can learn, recall, and generalize from the dependent and independent variables of a data set, and it can be re-trained with new data on a continuous basis.

In the present study, exposure temperature, fly ash, GGBS, fine aggregate, coarse aggregate, sodium silicate (SS), sodium hydroxide (SH), SH/SS ratio, molarity of alkaline solution parameters was considered as input variables and compressive strength is considered as an output parameter. The total 255 specimen's data includes the present experimental data were considered for the development of ANN models [2, 4-7, 10-11, 17-20]. Out of which, 70%, assigned to training step, 15% assigned to validation and 15% assigned to testing. The Levenberg Marquardt (LM) backpropagation training algorithms was used in ANN model preparation. The Levenberg-Marquardt backpropagation is typically the fastest available backpropagation algorithm and is strongly recommended as a first-choice supervised approach. The ANN model was also tested with the experimental data produced in the present study. The details of ANN model are presented in the Table 2. The performance of the ANN model was assessed using coefficient of regression (R).

Table 2*. Details of ANN model*

Input layer Neurons	9
Hidden layer Neurons	11
Output layer Neurons	1
Training method	backpropagation
Learning algorithm	trainlm
Activation function	sigmoid

3. RESULTS AND DISCUSSION

3.1 Physical Observation

Fig. 2 shows the geopolymer concrete specimens after exposure to various heated temperatures. Normal at 27°C, light grey at 200°C, and grey shade at 400°C were observed. At 600°C and 800°C, the colour of the geopolymer concrete changed from pink to reddish and also observed fissures on the concrete surface. This may be due to the thermal incompatibility between the aggregate and the matrix. Dehydration and breakdown of hybrid gel have a major influence on the matrix in the case of

geopolymer concrete. This is due to the fact that, with the addition of slag, the sodium in N-A-S-H gel can be replaced by calcium to create N-C-A-S-H gel, reducing its heat stability [10].

The weight loss of geopolymer concrete subjected to high temperatures was also measured. As the exposure temperature increases the weight loss also increases. The weight loss of 4.15%, 5.34%, 5.70% and 6.20% was observed for the exposure temperature of 200°C, 400°C, 600°C and 800°C respectively. At 200°C, the weight loss mostly due to absorbed water, free water, and capillary water loss. The weight loss between 200°C and 600°C may be blamed for further geopolymerization and the disintegration of a tiny amount of $CaCO_3$ with varying crystallinity [21]. Furthermore, the breakdown of $CaCO_3$ is a major factor influencing weight loss between 600°C and 800°C [21].

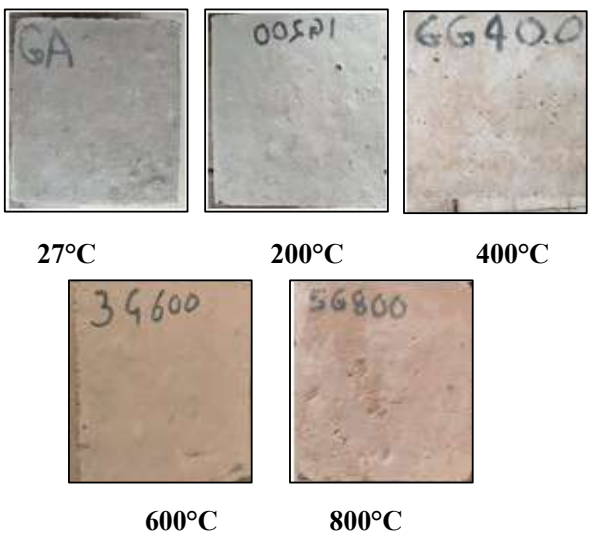

Fig. 2: *Physical appearance of geopolymer concrete at different exposure temperatures*

3.2 Ultrasonic Pulse Velocity (Upv) and Rebound Hammer (Rh) Test

The average relative Ultrasonic Pulse Velocity (UPV) and relative rebound number of three test samples of geopolymer concrete after subjected to elevated temperature is shown in Fig. 3. The UPV of concrete is affected drastically when subjected to elevated temperature. The UPV measurements shown no significant change in the temperature range up to 200°C. The UPV drops by 35% at 400°C and then to 68% at 600°C temperature exposure. The UPV reduction, which is probably due to great amount of porosity and cracks in the concrete when subjected to elevated temperature [22].

In the temperature range up to 400°C, the rebound hammer test readings show no significant changes. They have even shown a little rise. The rebound values are influenced mainly by the surface condition of concrete. Since temperature increases to 200°C causes drying and hardening of the surface layer, rebound measurements present a small increase [23]. Rebound number drops by 40% from 400°C to 800°C. At higher temperature, intensive cracking of the surface layer become more significant.

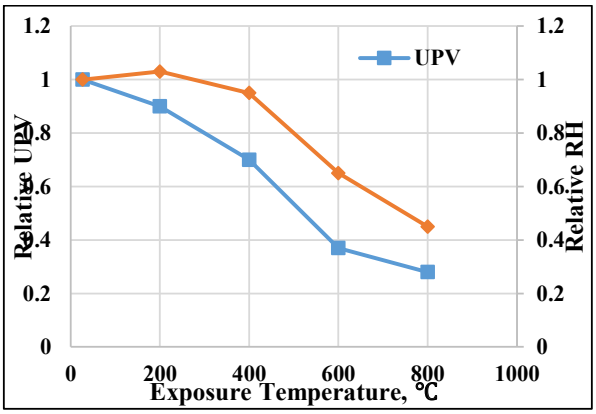

Fig. 3. *Variation in Relative UPV and RH at different elevated temperature*

3.3 Compressive Strength

Figure 4 indicates the average relative compressive strength of three test samples of geopolymer concrete at varied temperature exposures. From 27°C to 200°C, compressive strength increases, then progressively decrease at higher temperature exposures. The compressive strength increases by 20% after exposure to 200°C. The increase in strength at 200°C was attributed due to unreacted particles continuing to participate in the geopolymerization process, which normally happened below 300°C. From 200°C to 800°C, the compressive strength of geopolymer was reduced by 80%. The decrease in strength at temperatures over 200°C was caused by dehydration, which generated fractures, density loss, and pores in the concrete.

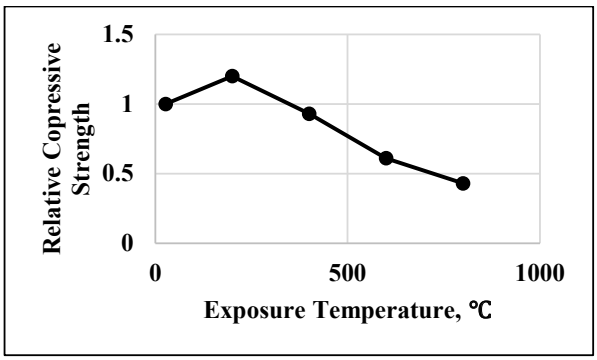

Fig. 4. *Relative compressive strength at different elevated temperature*

3.4 ANN Model

Figure 5 & 6 shows the performance of the developed model. The horizontal axis in these graphs represents the actual value, while the vertical axis represents the anticipated values of the proposed ANN model. The samples on the diagonal lines represent an optimal forecast of the model. The performance of the ANN model is evaluated by regression coefficient (R). The coefficient of regression for the developed model is more than 0.9. Figure 7 depicts an error histogram of the proposed ANN model's. The error was the difference between the ANN model's predicted and actual values. Figure 7 shows the vertical axis represents the number of samples from a dataset, while the horizontal axis represents the inaccuracy associated with the bins. The zero-line displays the zero inaccuracy of the horizontal axis. From Fig. 7 it can be observed that the majority of samples has errors ranging from -6.65 MPa to 10.80 MPa. The negative errors indicated that the anticipated value of the ANN model was smaller than the experimental value.

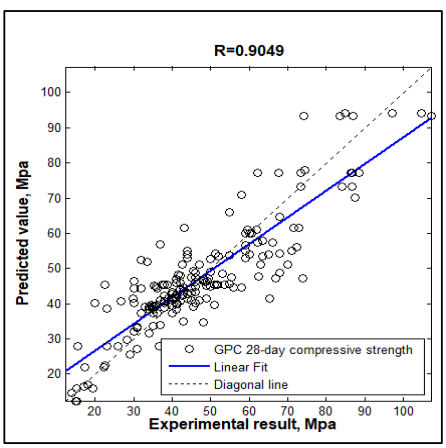

(a) Training

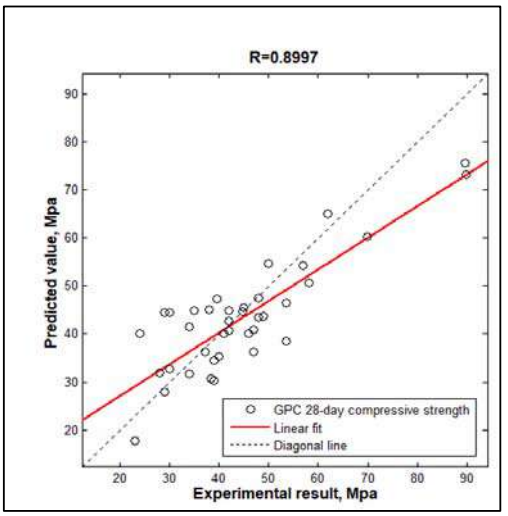

(b) Testing

Fig. 5 *Training and Testing of developed ANN model*

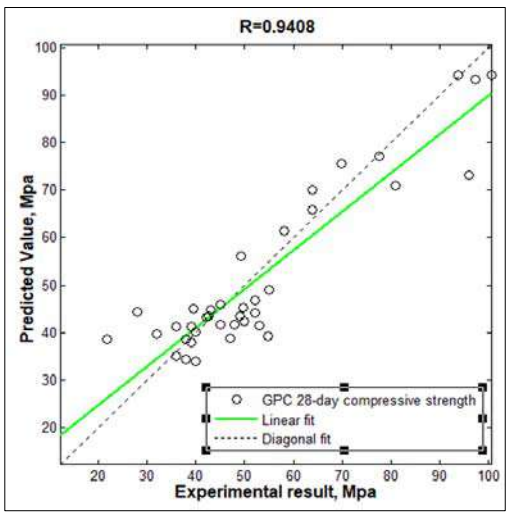

(a) Validation

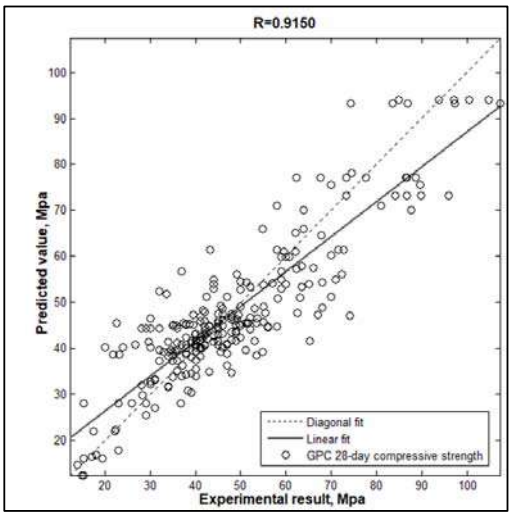

(b) Overall

Fig. 6 *Validation and Overall performance of developed ANN model*

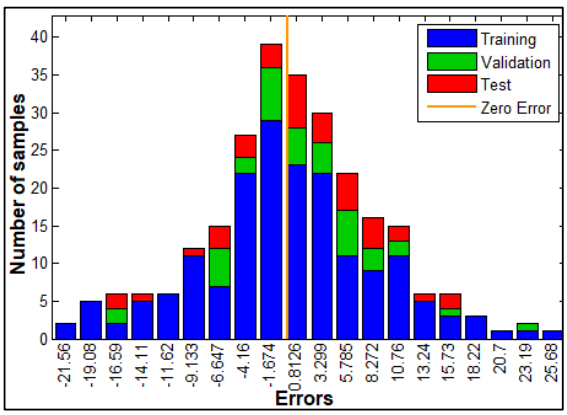

Fig. 7 *Error assessment for the developed ANN model*

3.5 Testing Developed ANN Model With Experimental Data

The developed ANN model was also tested by using the experimental data of the present study. Figure 8 shows the comparison between experimental and the ANN predicted compressive strength. The developed ANN model performed admirably on the experimental dataset, with an average error of 3.5 MPa and maximum of 20% error.

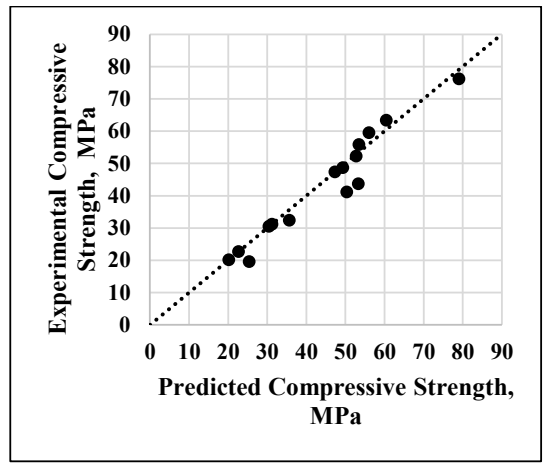

Fig. 8 Experimental vs ANN model predicted Compressive strength

4. CONCLUSIONS

The following conclusions are drawn from this study:

- The weight loss, colour change and surface cracking is noticeable within exposure temperature.
- GPC showed a 20% increase in compressive strength at 200°C, followed by a 7%, 39%, and 57% strength loss at 400°C, 600°C, and 800°C exposure temperatures.
- GPC showed strength losses after being exposed to temperatures ranging from 200-800°C due to thermal non-compliant between the geopolymer matrix and the aggregates, leading to debonding and internal cracks.
- ANN based model have been developed for predicting the residual compressive strength of GPC subjected to elevated temperature exposure.
- The proposed ANN model shown coefficient of regression (R) more than 0.90 and consistently good correlation.
- The findings of this study might contribute to the development of a solid soft computing tool for precisely and quickly estimating the compressive strength of GPC.

4. ACKNOWLEDGEMENTS

The author is grateful to the Director, CSIR-CBRI, Roorkee for giving permission to publish this work. The author is also grateful to CSIR, New Delhi, Government of India for the financial support.

5. REFERENCES

[1] Sasi Rekha, M., & Sumathy, S. R. (2021). A study on cement-free geopolymer concrete incorporated with industrial waste cured at open environment for different molarities of sodium hydroxide. Global NEST Journal, 23 (2), 265-274.

[2] Gunasekara, C., Atzarakis, P., Lokuge, W., Law, D. W., & Setunge, S. (2021). Novel analytical method for mix design and performance prediction of high calcium fly ash geopolymer concrete. Polymers, 13(6), 900.

[3] Rajamane, N. P., Nataraja, M. C., & Lakshmanan, N. (2011). An introduction to geopolymer concrete. Indian Concr J, 85(11), 25-28.

[4] Yasaswini, K., & Rao, A. V. (2020). Behaviour of geopolymer concrete at elevated temperature. Materials Today: Proceedings, 33, 239-244.

[5] Ahmad, A., Ahmad, W., Chaiyasarn, K., Ostrowski, K. A., Aslam, F., Zajdel, P., & Joyklad, P. (2021). Prediction of geopolymer concrete compressive strength using novel machine learning algorithms. Polymers, 13(19), 3389.

[6] Cong, P., & Cheng, Y. (2021). Advances in geopolymer materials: A comprehensive review. Journal of Traffic and Transportation Engineering, 8(3), 283-314.

[7] Amin, M., Elsakhawy, Y., Abu el-hassan, K., & Abdelsalam, B. A. (2022). Behavior evaluation of sustainable high strength geopolymer concrete based on fly ash, metakaolin, and slag. Case Studies in Construction Materials, 16, e00976.

[8] Almutairi, A. L., Tayeh, B. A., Adesina, A., Isleem, H. F., & Zeyad, A. M. (2021). Potential applications of geopolymer concrete in construction: A review. Case Studies in Construction Materials, 15, e00733.

[9] Nuruddin, M. F., Malkawi, A. B., Fauzi, A., Mohammed, B. S., & Almattarneh, H. M. (2016, June). Geopolymer concrete for structural use: Recent findings and limitations. In IOP conference series: materials science and engineering (Vol. 133, No. 1, p. 012021). IOP Publishing.

[10] Luo, Y., Li, S. H., Klima, K. M., Brouwers, H. J. H., & Yu, Q. (2022). Degradation mechanism of hybrid fly ash/slag based geopolymers exposed to elevated temperatures. Cement and Concrete Research, 151, 106649.

[11] Verma, M., Dev, N., Rahman, I., Nigam, M., Ahmed, M., & Mallick, J. (2022). Geopolymer concrete: a material for sustainable development in Indian construction industries. Crystals, 12(4), 514.

[12] de Oliveira, L. B., de Azevedo, A. R., Marvila, M. T., Pereira, E. C., Fediuk, R., & Vieira, C. M. F. (2022). Durability of geopolymers with industrial waste. Case Studies in Construction Materials, 16, e00839.

[13] Çelikten, S., Sarıdemir, M., & Deneme, İ. Ö. (2019). Mechanical and microstructural properties of alkali-activated slag and slag+ fly ash mortars exposed to high temperature. Construction and Building Materials, 217, 50-61.

[14] Alaneme, G. U., Olonade, K. A., & Esenogho, E. (2023). Eco-friendly agro-waste based geopolymer-concrete: a systematic review. Discover Materials, 3(1), 14.

[15] Sharma, R., Pei, J., Miah, M. J., & Jang, J. G. (2023). Effect of sillimanite sand on the mechanical property and thermal resistance of alkali-activated slag mortar. Construction and Building Materials, 370, 130654.

[16] Cao, V. D., Pilehvar, S., Salas-Bringas, C., Szczotok, A. M., Do, N. B. D., Le, H. T., ... & Kjøniksen, A. L. (2018). Influence of microcapsule size and shell polarity on the time-dependent viscosity of geopolymer paste. Industrial & Engineering Chemistry Research, 57(29), 9457-9464.

[17] Singh, B., Ishwarya, G., Gupta, M., & Bhattacharyya, S. K. (2015). Geopolymer concrete: A review of some recent developments. Construction and building materials, 85, 78-90.

[18] Ahmad, A., Ahmad, W., Chaiyasarn, K., Ostrowski, K. A., Aslam, F., Zajdel, P., & Joyklad, P. (2021), "Prediction of geopolymer concrete compressive strength using novel machine learning algorithms." Polymers, 13(19), 3389.

[19] Krishna, A. S., & Rao, V. R. (2019), "Strength prediction of geopolymer concrete using ANN." International Journal of Recent Technology and Engineering, 7, 661-667.

[20] Toufigh, V., & Jafari, A. (2021), "Developing a comprehensive prediction model for compressive strength of fly ash-based geopolymer concrete (FAGC)." Construction and Building Materials, 277, 122241.

[21] Su, H., Xu, J., & Ren, W. (2016). Mechanical properties of geopolymer concrete exposed to

dynamic compression under elevated temperatures. Ceramics International, 42(3), 3888-3898.

[22] De Oliveira Dias, A. R., Amancio, F. A., de Carvalho Rafael, M. F., & Cabral, A. E. B. (2018). Study of propagation of ultrasonic pulses in concrete exposed at high temperatures. Procedia Structural Integrity, 11, 84-90.

[23] Savva, A., Manita, P., & Sideris, K. K. (2005). Influence of elevated temperatures on the mechanical properties of blended cement concretes prepared with limestone and siliceous aggregates. Cement and Concrete Composites, 27(2), 239-248.

Robotic Ultrasonic Pulse Velocimetry for Submerged Concrete Assets

[1]Susheel Patil, [1]Ashish Antony Jacob, [1, (a)]Vineet Upadhyay, [1]Tanuj Jhunjhunwala, [2]Prabhu Rajagopal, [2]Krishnan Balasubramanian

[1]Planys Technologies Pvt. Ltd., No. 5, Balaji Nagar Main Road, Puzhuthivakam, Chennai, India.
[2]Centre for Nondestructive Evaluation, Machine Design Section, Indian Institute of Technology, Madras, Chennai, India
[a]Email:vineet@planystech.com

Abstract

Concrete structures play a vital role in civil, commercial, and industrial projects. Periodic inspections are mandatory to ensure the safety and reliability of the asset throughout their lifespan. Recently, advancements in inspection technology have allowed for rapid and accurate assessment. Techniques ranging from ground penetrating radar to phased array ultrasonic tomography have made it possible to rapidly analyse the interior of concrete structures. Conventionally, inspecting concrete structures underwater is done visually by manned diving teams. Internal defects are often undetected in visual inspection. Furthermore, manual inspection underwater is often challenging owing to limited visibility, water currents, and debris, making it risky for divers to conduct inspections manually. However, as of date, there are no commercially available quantitative non-destructive techniques (NDT) to inspect submerged concrete assets. We have also observed no research adopting existing techniques for underwater applications. To address this need, this paper proposes the use of remotely operated underwater vehicles (ROVs) to adopt conventional ultrasonic pulse velocity (UPV) technique for underwater applications. ROV-UPV can identify zones of inhomogeneity within the concrete structure. The paper further discusses how factors like water saturation, marine growth, and the inspection surface affect the pulse velocity. Experimental studies conducted in the laboratory and in the field are discussed. Limitations of ROV UPV in practical scenarios are briefly discussed. This work will be of relevance to waterways managers, dam or reservoir engineers, and bridge management authorities.

Keywords: *remote operated vehicles, non-destructive testing, ultrasonic pulse velocimetry, concrete, water saturation, marine growth, asset management*

1. INTRODUCTION:

Civil structures are essential components of our society, serving a wide range of purposes and providing numerous benefits. These structures form the backbone of our infrastructure and play a crucial role in various aspects of our daily lives. They are designed to withstand various loads and forces, ensuring structural integrity, and minimizing the risk of failures. Regular inspections, maintenance, and adherence to safety standards are crucial to guarantee the safety of these structures and prevent potential disasters. This becomes more crucial as the age of infrastructure increases [1].

Inspection and condition assessment of concrete for above water-line structures can be accomplished by a plethora of methods such as audio-visual, stress-wave and electromagnetic test. Audio-visual methods include techniques such as visual inspection, chain drag and coin tap. Stress wave method include techniques such as acoustic emission, impact echo and ultrasonic pulse velocity (UPV). Electromagnetic methods include techniques such as ground penetrating radar, conductivity measurements and half-cell potential [2].

In recent years, there have been remarkable advancements in the tools and technologies used for (in-air) concrete inspections. Ultrasonic phased array devices, such as the ACS 1020 Mira Lite [3], have revolutionized the process by employing full matrix capture and total focusing method to generate precise 3D scans of concrete specimens, to enable rapid defect characterization. Similarly, radar-based tomography like the Proceq instruments GPR8000

[4] have demonstrated their ability to detect a wide range of defects through efficient scanning techniques. Sample images of the devices mentioned above are shown in Fig 1. These advancements have greatly enhanced the efficiency and accuracy of concrete inspections. Furthermore, the integration of AI and machine learning algorithms with non-



(a)



(b)

Fig 1*. (a) ACS A1020 MIRA-Lite ultrasonic phased array system and (b) Proceq GP8000 ground penetrating radar.*

destructive testing (NDT) data has become a significant area of research, promising to further improve defect detection and identification in concrete structures. As technology continues to advance, the field of in-air concrete inspections will undoubtedly witness even more sophisticated techniques and tools, contributing to the overall safety and durability of concrete infrastructure.

In contrast, there is no commercially available non-destructive testing technology to quantitatively inspect the condition of the concrete below the waterline. There are several challenges for inspecting concrete structures underwater including varying tidal conditions, temperature, marine growth, visibility, and accessibility and hence the complexity in inspection. Conventionally, underwater inspection of concrete structures is done by professional diving teams performing visual inspection. Visual inspection primarily focuses on documenting surface defects and is limited in its ability to detect and monitor internal issues. Visual inspection relies on qualitative observations, making it challenging to assess the *true* internal condition of the structure. Furthermore, diver-based inspection methods have limitations in terms of operating depths, inherent risks in restricted or confined spaces, and are susceptible to factors such as water visibility, currents, and debris. Manned inspections often mandate asset shutdowns, impacting productivity and efficiency. Therefore, alternative inspection methods are necessary to complement visual inspection and provide more comprehensive and quantitative insights into the integrity of underwater concrete.

To mitigate the above-mentioned limitations, an alternative solution is explored in this paper – employing a compact and lightweight remotely operated (robotic) vehicle (ROV). Remotely operated vehicles offer several significant advantages over manned diving teams in various underwater operations such as inspection of oil rigs and its components, online inspection of storage tanks and pipelines. The advantages of ROVs are firstly, ROVs provide enhanced safety for operators, as they eliminate the need for humans to physically enter hostile underwater environments. Secondly, ROVs offer increased manoeuvrability and access to confined spaces/deeper depths that may be challenging or impossible for human divers to reach. ROVs with their compact size and versatile robotic arms can navigate intricate underwater structures. Thirdly, ROVs provide extended operational endurance compared to human divers. Lastly, multiple missions can be planned, thereby reducing operational expenses, increasing efficiency over time, higher repeatability, and bringing down the overall cost [5].

The development of an NDT technique for underwater inspection has numerous challenges. Surface preparation: clearing marine growth and transducer alignment over irregular surfaces, marinizing the transducer and the electronics, are among the primary challenges to be addressed. Following evaluation of various constraints from perspectives including operation in water currents, and compatibility on a remote drone for different NDT techniques, the ultrasonic pulse velocity technique was chosen. The technique is widely accepted in the industry. The advantages and limitations of its usage are well understood [6]. However, interpreting the UPV data obtained from an underwater concrete surface to assess the

condition of the concrete presents' significant challenges. This is primarily due to the additional factors that affect measurements underwater, including poor underwater visibility for the ROV operator, water saturation for the material of interest, and the presence of marine growth in the inspection zone. The impact of water saturation and presence of light marine growth on the UPV results are studied. The work presented in this paper aims to provide a comprehensive understanding of the condition of the structure underwater.

This paper is structured in the following manner. It begins with an introduction that highlights the importance of periodic inspection frameworks for civil structures, providing an overview of the current state of conventional inspections as well as underwater inspections employing both divers and remotely operated vehicles. The methodology of inspection using ROVs is then detailed, including the key specifications of the robot. Laboratory tests and field inspections are, then, presented. Highlights from results in both laboratory and field inspection are discussed. Finally, the paper concludes and highlights the key limitations of the technique.

2. METHODOLOGY

2.1 Ultrasonic Pulse Velocimetry

Bulk waves in a specimen are typically either longitudinal waves, or shear waves. The velocity at which sound waves travel through materials is determined by the material's properties, such as density, Young's modulus, and Poisson's ratio. Ultrasonic pulse velocimetry is a technique that utilizes velocity to attempt to infer the condition of a material. When there are discontinuities present in the material, there is an increase or decrease in time of flight of sound waves from the transmitting transducer to the receiving transducer. By measuring the time of flight between the transducers (t) and knowing the distance between them (d), the pulse velocity (V) can be calculated by the relation,

$$V = d/t.$$

The UPV test equipment consists of two piezoelectric transducers, a pulser-receiver, and a data acquisition (DAQ) system. The transducers generate and receive the sound waves, while the pulser-receiver controls the timing and energy to the transducers. The DAQ system captures and processes the received signals. The test can be conducted in three different arrangements: direct, semi-direct, and indirect methods as shown in *Fig 2*. In the direct method, the transducers are placed on opposite surfaces of the specimen, while in the semi-direct method, they are placed on adjacent surfaces. In an indirect method, the transducers are placed on the same surface. The indirect method is employed when access to the structure is limited to only one surface. It provides limited characterization of the interior of the structure, typically within one wavelength from the surface of interest.

The surface condition of the specimen can significantly impact the effectiveness of the method. The pulse velocity obtained through this method can be correlated with the quality of the concrete it traverses. It is influenced by properties, including aggregate size, water content, reinforcement, and others. This makes UPV an ideal technique for identifying non-uniformities in a structure, and it can serve as a preliminary inspection methodology. Due to the non-homogeneous nature of concrete, the use of low frequency transducers is necessary to achieve adequate penetration into the coarse grains of the concrete.

The pulse velocity is affected by the uneven surfaces and structural anomalies, marine growth, surface finish and potential disruptions from nearby reinforcement elements in structures with small or corroded cover thickness. The technique UPV is best used to identify zones of non-uniformity and not a method to estimate overall structural strength [7]. Furthermore, when the indirect method of the

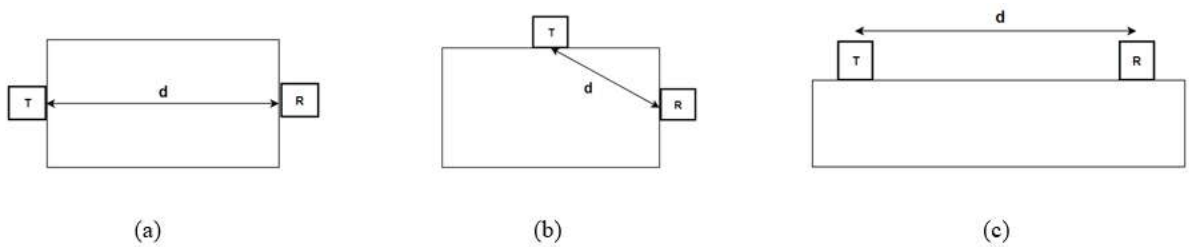

***Fig 2**. Different configurations of UPV inspection (a) direct method, (b) semi-direct method and (c) indirect method*

technique is used, material up to one wavelength of the wave from the surface can be inspected.

2.2 ROV UPV

ROV Beluga, developed by Planys Technologies Pvt Ltd, an incubated startup from IIT Madras. ROV Beluga, depicted in *Fig 3*, is a versatile and adaptable underwater inspection system. It is designed to carry out a wide range of inspections in underwater environments and adheres to high standards of quality and performance.

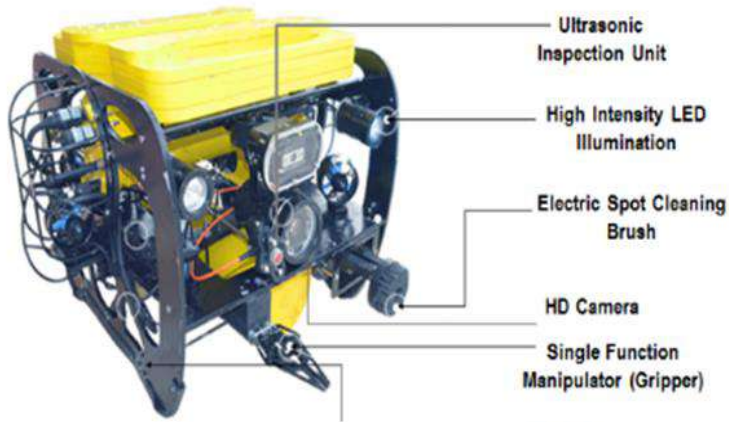

***Fig 3**. A photograph of ROV Beluga highlighting its key features.*

ROV Beluga is operated from a command module, with a tether providing a mechanical connection as well as power and communication channel. The pilot can control, navigate, and perform remote NDT using the feedback on the command module. Photographs of the same are depicted in Fig *4*.



***Fig 4**. In-field operational setup for ROV Beluga (pictured in Fig 3) showing (a) the command module, and (b) the tether and winch.*

The UPV module, designed for the ROV Beluga, features two piezoelectric transducers, one acts as transmitter (T) and the other, as receiver (R), a combined pulser-receiver, and a data acquisition system with necessary adjustable parameters. The waveform of the received signal can be observed on the computer display. The indirect configuration of inspection is incorporated into the ROV based NDT system due to the inaccessibility of opposite faces of the structure and the nature of working with an ROV in underwater environments. Key specifications of ROV and ROV UPV are tabulated in Table 1.

***Table1**: Key specifications of ROV and ROV UPV system*

ROV specifications	
Dimensions	730 x 820 x 600 mm
Depth range	200 m
Weight in-air	53 kg
Maximum payload	10 – 15 kg
Power rating	3000 W (max)
Control system	Auto-depth, auto-heading
Depth sensing	0.01% full-scale error
ROV UPV specifications	
UPV transducer frequency	54 kHz
DAQ sampling rate	250,000 samples/sec
Probe spacing	10 – 45 cm
Peak power	20

2.3 Laboratory Tests of Concrete Specimens

Concrete specimens were cast into cubes and cuboids with varying aggregate size and water content. Two sets of specimens of dimensions 15 x 15 x 15 cm and 15 x 15 x 30 cm (L x B x H) were cast. The specimens were cast with water to cement

ratio varying from 0.35 to 0.45 and aggregate size ranging from 6 to 20 mm. Direct method was used for testing the 15 cm cube specimen, and both direct and indirect methods were used to test the cuboid 15 x 30 cm specimen. In all these experiments, the same batch of marinized transducers were used. Efforts were taken to apply equal load on the transducers.

2.3.1 In-air tests

At first, the in-air tests were performed. The results obtained are the basis to study saturation effects and marine growth on the same set of specimens. Calibration was carried out using a calibration rod made of acrylic of 25 microseconds time of flight. Multiple tests were performed on each of the specimens, and the average pulse velocities were recorded.

2.3.2 Underwater tests

After performing in-air tests, the specimens were submerged in a water tank. Pulse velocities were recorded periodically while the specimen was left submerged in water. Subsequently, light marine growth was introduced. A short period of time was provided for the growth to develop, after which, pulse velocity measurements continued. Testing conditions and duration are tabulated in Table 2. Photographs from the testing phase are attached in Fig 5.

***Table 1**. Testing environment and duration*

Environment	Couplant	Test duration
In-air	Silicone grease	7 days
Underwater	Water	108 days
Underwater with marine growth	Water with marine condition	70 days



***Fig 5.** Photographs during the testing phase (a) in-air, (b) underwater immersion, (c) underwater immersion with marine growth*

2.4 Field Inspection

2.4.1 Hydroelectric dam

Highlights from a ROV based UPV inspection of a hydroelectric dam (Fig 6) are presented in this section. The dam had dimensions of approximately 150 meters in length and an average depth of 20 meters. The structure exhibited a significant amount of silt both underwater and on its surface. The visibility of the water was about 0.5 metres. In this site, ROV UPV was conducted along with visual inspection. To ensure systematic coverage of recording pulse velocities, the area of the dam was divided into separate parts, as presented in section 0. This approach allowed for a comprehensive assessment of the dam's condition, combining visual observations with UPV measurements, providing valuable insights into the structural integrity of the dam.



***Fig 6**. A sample photograph of the ROV-UPV inspection site at the hydroelectric dam*

2.4.2 Division of an asset and inspection procedure

To ensure consistency and facilitate the inspection process, the asset under examination was divided into distinct sections or units, each assigned a standardized nomenclature. This approach aided in organizing the inspection effort and allowed inspectors to easily identify and refer to specific areas or components of the asset. By implementing a uniform nomenclature system, inspectors could effectively communicate and document their findings, enabling clear and concise reporting. Sample sketches of the divisions are shown in Fig 7.

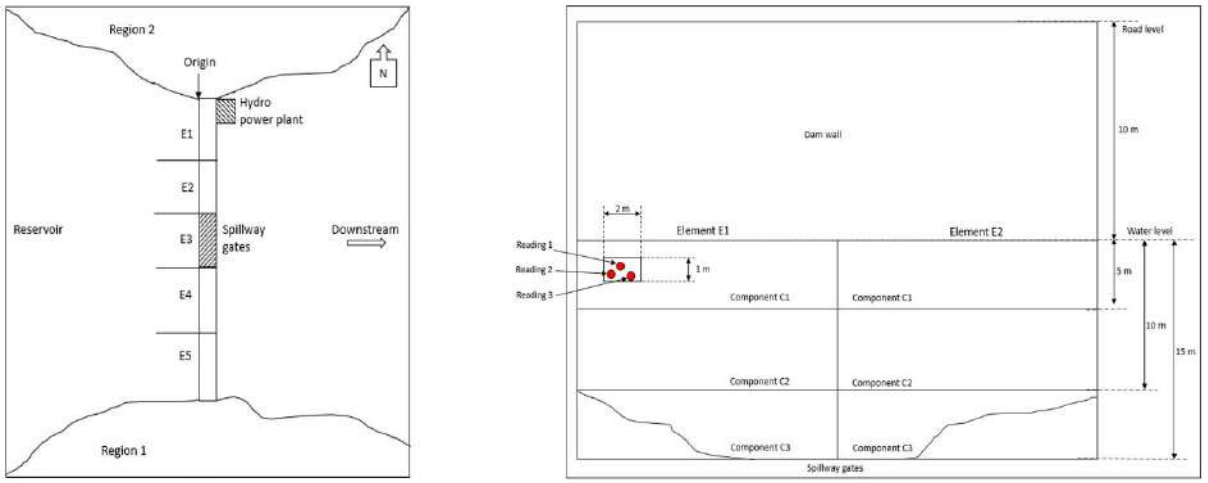

Fig 7*. Divisions in a dam for inspection (a) top view and (b) side view.*

Table 2. *Marine growth severity levels.*

Marine growth intensity	Description	Examples
1	Minimal	Clear surface or barely visible marine growth
2	Soft growth	Algae, sea weeds and sponges
3	Hard growth	Barnacles, oysters, and mussels

2.4.3 Influence of surface condition

Marine growth and surface finish are the major factors which affect the pulse velocities recorded. Clear surface or barely visible marine growth (level 1) were the preferred areas of inspection. A table with the description of the intensity of marine rowth is described in Table ***2*** 3. In the case of hard growth (level 3) as shown in , readings were taken from an alternate region that lies nearby, with no or lesser marine growth. If there was significant marine growth in alternate regions as well, then cleaning was performed, and the measurements recorded. Marine cleaning can be performed by ROV Beluga using high-pressure water jets. A photograph of this cleaning in action is shown in *Fig 9*.

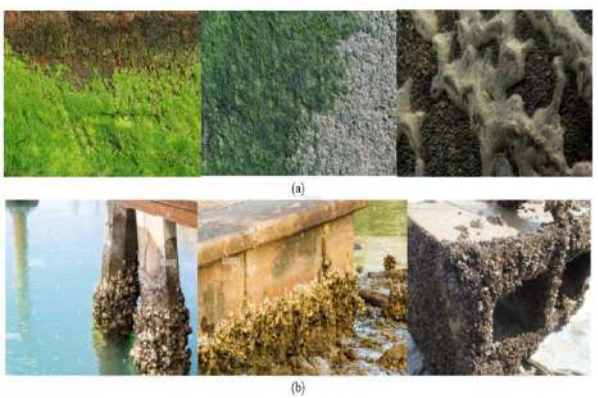

Fig 8 (a) Level 2 marine growth and (b) level 3 marine growth.



Fig 9 *View from the ROV's front camera during a cleaning operation; lighter regions indicate the cleaned regions in the photograph.*

Table 3*. Surface finish levels*

Surface finish level	Description
1	Highly polished surface
2	Semi-polished surface
3	Rough surface
4	Very rough surface

If the area of interest had poor surface finish, measurements were taken from an adjacent region with a better surface finish within the grid. Level 3 and level 4 regions were avoided. The different levels of surface finish are listed in .

3. RESULTS AND DISCUSSION

3.1 Laboratory Tests

The pulse velocities were recorded and plotted against duration in days, as shown in Fig 10. Initially, as the concrete absorbs water, higher velocities are observed for the same input parameters. This observation aligns with existing literature which explains how the pores in the concrete are filled with water, reducing the travel time for stress waves [8] [9]. As water absorption progresses, the concrete specimens reach a point where they have absorbed the maximum amount of water. At this stage, the velocity values reach saturation and do not increase further, as seen from Fig 10.

From the placement of concrete specimens underwater for up to 25 days, there is a substantial increase of the pulse velocity values for indirect testing as seen in Fig 11.This behaviour is expected and is in agreement with findings in literature which states that there is a possibility that only the physical processes evolving in the upper layers of material generate the sudden changes in the UPV by indirect transmission. This feature is not observed in direct transmission [10].

Uneven marine growth in the region of inspection causes significant variations in coupling the transducers to concrete surface and transmission path of ultrasonic waves. These factors influence the time of flight considerably, leading to higher standard deviation of velocity values. In this experimental study, we observed that the standard deviation for indirect configuration is approximately 682 m/s with marine growth as compared to 454 m/s without marine growth. We observed that the

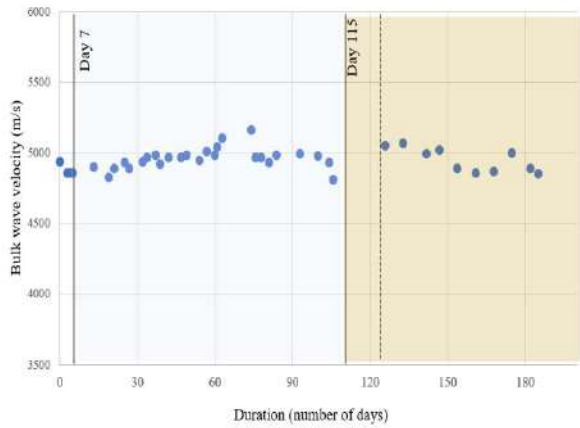

Fig 10 *Plot showing variation of bulk velocity variation as a function of duration in days for direct configuration of inspection. Day 7: specimen placed underwater and day 115: marine growth introduced.*

average weight of the 15 cm x 30 cm cuboid ahead of submergence or dry state was 14.6 kg and at the end ~180 days including marine growth, the weight was 16.3 kg.

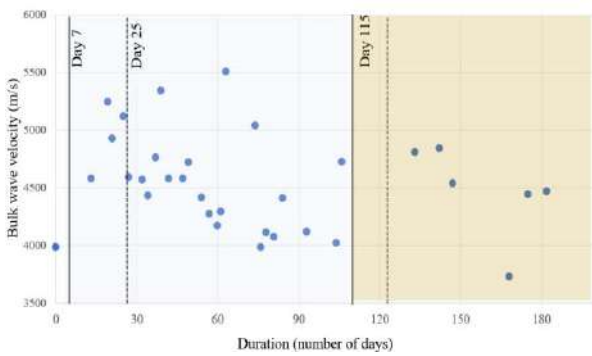

Fig 11. *Plot showing variation of bulk velocity variation as a function of duration in days for indirect configuration of inspection. Day 7: specimen placed underwater, day 25: duration up to which there is*

substantial increase in velocity values after placing specimen underwater, day 115: marine growth introduced.

The increase in pulse velocity values is around 14% for the water saturated concrete specimen as compared to dry state during indirect transmission and only a marginal increase of less than 1% for direct configuration. This is in line with the literature that made similar observations [10].

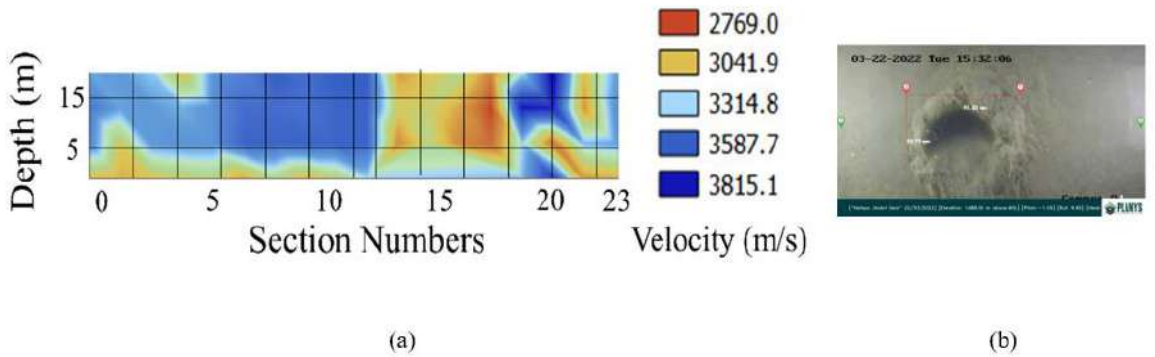

Fig 12. *(a) Velocity map from dam surface and (b) cavity found in section 18, ~5 m depth during visual inspection*

For underwater tests, the mean velocity values in the indirect configuration are approximately 8.5% lower than those in the direct configuration. Additionally, the standard deviation for the indirect configuration is approximately 454 m/s, whereas it is 88 m/s for the direct configuration. These findings are consistent with the literature, which discusses that there is a drop of 5 to 20 % in velocity values for indirect configuration and that this testing configuration has uncertainties regarding the exact length of the transmission path because of the significant size of the areas of contact between the transducers and the concrete [6].

3.2 Field Inspection

The inspection results of the hydroelectric dam are presented in Fig 12(a). The generated velocity map visually displays the velocity measurements taken across the surface of the inspected dam. The plot is structured with the depth of the dam represented on the Y-axis, and the length of the dam divided into sections on the X-axis. The velocity values are depicted using a colour code, allowing for a clear understanding of the variations in velocity throughout the dam's surface.

When interpreting the UPV data, one of the main challenges is determining the underlying cause of a low velocity reading. The variations in velocities are not only influenced by inhomogeneities in the structure but also by other factors such as the extent of marine growth present and surface finish in the region of inspection. To mitigate this challenge, UPV data was interpreted in juncture with visual inspection. By correlating the findings from both methods, the confidence level in the assessment was increased. This combined approach proved valuable in identifying specific issues such as the presence of cavities, as illustrated in Fig 12 (b). The concurrent use of UPV technique and visual inspection allowed for a more comprehensive understanding of the dam's condition, enabling the detection of hidden defects that may have otherwise gone unnoticed.

4. CONCLUSION

Conventionally, submerged concrete inspection is performed by manned diving teams performing visual inspection. The paper discusses an alternative remote inspection technique using remote operated vehicles. Considering several constraints, the widely accepted UPV technique has been adopted for performing inspection of underwater concrete. Laboratory tests were then conducted in-air, underwater, underwater with marine growth on concrete specimens to understand the variation in pulse velocities of concrete under different conditions.

The key results from the laboratory tests indicate that there is a significant increase in pulse velocities for the indirect method by 14% when comparing underwater measurements with in-air measurements. However, there is only a marginal increase of less than 1% for the direct method in the same scenario. We also observed that the increase in pulse velocity values is more pronounced in the indirect transmission method immediately after placing the concrete underwater, while no such effect is observed in the direct transmission method.

Planys' ROV was modified to append the developed underwater UPV system. The ROV-UPV inspection system was deployed on a hydroelectric dam to study local inhomogeneities in the concrete retaining wall. With the integration of the underwater UPV technique and ROV-visual inspection, a comprehensive analysis of the dam's concrete condition could be generated, linking the observed velocity variations to visible anomalies. This provided valuable insights into potential structural issues. The ROV-UPV results quantitatively highlight the variations in the concrete condition and assist in identifying potential areas that may require further investigation or targeted repairs. This allows asset managers to confidently rely on data-driven insights when determining the maintenance needs of concrete structures.

5. LIMITATIONS

- The performance of the ROV-UPV technique is impacted by reduced underwater visibility. Murky or turbid waters are common in several parts of the country. This poses challenges in aligning the transducers to the surface of interest.
- Strong water currents create instability in positioning the ROV.
- Marine growth and uneven or broken surfaces are quite common for submerged concrete. Marine growth needs to be cleaned before ROV-UPV inspection can be done.
- Curved structures, for example, columns or piers, with diameter less than 200 mm cannot be inspected using this methodology.

6. REFERENCES

[1] A. M. Alani, M. Aboutalebi and Kilic, "NDT & E International Integrated health assessment strategy using NDT for reinforced concrete bridges," NDT E Int., vol. 61, pp. 80-94, 2014

[2] S. K. U. Rehman, Z. Ibrahim, S. A. Memon and M. Jameel, "Nondestructive test methods for concrete bridges: A review," Construction and Building Materials vol. 107, pp. 58-60, 2016.

[3] "A1020 MIRA LITE," 2023. [Online]. Available: https://dev.acs-international.com/product/a1020-mira-lite/.

[4] "Portable Ground Penetrating Radar - Proceq GP8000," 2023. [Online]. Available: https://www.screeningeagle.com/en/products/proceq-gp8000.

[5] U. Vineet, G. Sanchit and A. Pulkit, "Multi-functional Remotely Operated Submersible Vehicle (ROV) System". India Patent 201741022485, 2016.

[6] Guidebook on non-destructive testing of concrete structures, Vienna: Industrial Applications and Chemistry Section, International Atomic Energy Agency, 2002.

[7] J. H. Bungey, "The validity of ultrasonic pulse velocity testing of in-place concrete for strength," NDT Int, vol. 13, p. 296–300, 1980.

[8] H. Güneyli, S. Karahan, A. Güneyli and N. Yapıcı, "Water Content and Temperature Effect on Ultrasonic Pulse Velocity of Concrete," Russian Journal of Nondestructive Testing vol. 53, pp. 159-166, 2017.

[9] ASTM C597 – 16: Standard Test Method for Pulse Velocity Through Concrete.

[10] U. Lencis, A. Udris and A. Korjakins, "Moisture Effect on the Ultrasonic Pulse Velocity in Concrete Cured under Normal Conditions and at Elevated Temperature," Construction Science 14, 2013

Ultrasonic Imaging for Detection and Mapping of Complex Pattern of Subsurface Cracks in Concrete

Suhaib Ul Reyaz, Surendra Beniwal
Indian Institute of Technology Jammu

Abstract

The cracks developed within the subsurface of the concrete need to be detected on time before their progression affects the structural performance and durability. However, these cracks have a complex geometry comprised of multiple segments of various lengths and orientation. Ultrasonic reflection-based imaging algorithms like TFM in concrete render images with low contrast and hence poor mapping of the reflectors. In this study instead of conventional imaging algorithms, plane wave imaging algorithm is used for reconstruction of subsurface images. The plane wave images have high contrast images and better mapped reflectors making it feasible for their geometrical quantification. The present study is aimed towards using plane wave ultrasonic imaging for detection and mapping of complex geometry of the subsurface reflectors embedded in the concrete experimentally. Two concrete blocks with their top having complex geometry and wrapped with polyethene sheets are placed in mould and whole specimen is cast with these embedded reflectors. The ultrasonic measurements are obtained using the ultrasonic array under each aperture. For smaller reflector 1 only one measurement is sufficient to map the whole geometry. However, for larger reflector 2, measurements are acquired at three different positions, the reconstructed images stitched together to achieve the complete geometry. The error in quantification of the geometrical properties remains contained within 6%. The study demonstrates the feasibility and effectiveness of imaging of complex geometry of subsurface cracks in the concrete using plane wave imaging.

Keywords: *Subsurface cracks, damage evaluation, ultrasound, plane wave imaging*

1. INTRODUCTION:

Damages in reinforced concrete structures exist in the form of cracks, delamination's, rebar debonding, rebar corrosion, spalling, honeycombing. The presence of these damages either at surface or within subsurface of the structure have the tendency to affect the structural performance and durability. It therefore becomes necessary to evaluate the damages such that timely action for repair and retrofitting can be undertaken. The cracks that develop within subsurface keep on growing until they reach the surface and can be visually detected. The subsurface cracks may develop in fresh concrete due to shrinkage [1], or in hardened concrete cracks start to develop due to corrosion of embedded rebars [2], structure subjected to high stresses [3] etc.

The damages within subsurface need to be evaluated using non-destructive techniques (NDT) as destructive techniques will affect the structural integrity of the concrete structures. Various non-destructive techniques that are employed for damage evaluation in concrete are half-cell potential (HCP), ground penetrating radar (GPR), infrared thermography (IRT), electromagnetic induction (EMI), acoustic emission (AE), impact-echo, ultrasound.

HCP is an electrochemical based technique used to detect the severity of the rebar corrosion [4]. GPR uses electromagnetic wave to inspect the subsurface and due very high contrast in dielectric constant of concrete and metals, the embedded metals like rebars, pipes can be detected and located effectively [5,6]. IRT is used to detect near to surface defects, moisture however it fails to detect deeper surface defects and at the same time difficulty in providing the location of the detected subsurface feature [7,8]. EMI technique is used just to detect and locate the embedded metallic features like rebars, pipes etc [9]. AE technique is an active NDT which records the energy emanates from the developed defect like cracks [10,11]. Impact-echo uses the stress waves

that are generated by the impact of hammer to inspect the medium. It has been used in concrete to detect the delamination and subsurface cracks [12]. Another non-destructive technique employed for inspecting the concrete structures is ultrasound which uses ultrasonic waves for inspecting the medium [13].

In ultrasound a piezoelectric transducer is voltage excited to generate wave energy of ultrasonic frequency (>20 kHz) which propagates within the medium. Another piezoelectric transducer is placed on the surface to record signals. When the source and receiver are placed on opposite faces or adjacent faces this configuration of data acquisition is known as through transmission and indirect transmission. As the path length between source and receiver is known and the arrival time of wave energy from source to receiver is obtained from the recorded signals, the wave velocity can be determined. This wave velocity is then used to evaluate the subsurface of structure [14]. When the data at multiple positions in through and indirect transmission is obtained, the subsurface image can be reconstructed using various transmission tomography algorithms like algebraic reconstruction technique (ART), multiplicative algebraic reconstruction technique (MART), simultaneous iterations reconstruction technique (SIRT). The pixel values in subsurface image represent the slowness of the wave [15] . If the source and receiver transducers are placed on the same side, this mode of data acquisition is known as pitch-catch. Wherever there is a contrast in acoustic impedance the waves reflect at the interface which are recorded by the receiver. If for each possible combination of source and receiver data is acquired, its known as full matrix capture (FMC) data [16]. Using various imaging algorithms like synthetic aperture focussing technique (SAFT) [17], total focussing method (TFM) [18], plane wave imaging (PWI) [19], reverse time migration (RTM) [20–22], the subsurface can be reconstructed wherein the aperture facing geometry of reflectors is imaged. To increase the inspection speed commercial ultrasonic equipment's, use an array of transducer instead of pair of transducers [23]. The reflection tomography requires access to only one side of the structure while at same time being faster to execute compared to through transmission tomography. In this present study reflection tomography will be referred as ultrasonic imaging unless specified.

Ultrasonic imaging has been used to image subsurface and detect tendon defects in the concrete members. To differentiate between a health and debonded rebars embedded in the concrete, ultrasonic imaging has been used effectively [22,24]. Detection and localization of rebars is also reported using ultrasonic imaging [25]. Ultrasonic imaging can detect materials of higher acoustic impedance than concrete like metals as well as the materials of lesser acoustic impedance like Styrofoam, PVC pipes, air filled cavities etc., whereas the GPR is effective in only detecting materials of higher dielectric constants compared to concrete like metals. This property makes ultrasound much favourable to detect the metallic embedment's like rebars as well as cracks. Detection of horizontal and inclined cracks is also reported using the ultrasonic imaging [19,26,27].

The subsurface cracks developed in concrete usually are neither horizontal nor inclined but have complex geometry like multiple segments of horizontal and inclined cracks placed together. With the conventional imaging algorithms, the reconstructed images usually have higher background noise and hence lesser contrast. This makes the detection and tracking such reflectors less feasible. The authors have previously developed plane wave imaging algorithm (PWI) for use in concrete [19], wherein the reconstructed images possess less background noise, hence improved contrast, and well mapped reflector features. In this study PWI algorithm is used for reconstruction of the subsurface images. The present study is one effort towards detection and mapping of complex geometry of the cracks present in the subsurface of concrete. A proper experimental setup is developed to incorporate branched reflectors within the subsurface of concrete. Using the ultrasonic array, the FMC data is acquired from the specimen, which is used to reconstruct the subsurface using PWI algorithm. The embedded reflectors are images in the PW images following which their geometrical parameters *viz.* length and inclination are estimated. The rest of the paper is organized as: Section 2 introduces the experimental setup for the placement of subsurface reflectors, and the process of ultrasonic measurement. The acquired data at each aperture is processed to reconstruct the

subsurface under that aperture the results of which are presented in Section 3. The conclusion of the present study is summarized in the Section 4.

2. EXPERIMENTAL SETUP AND DATA ACQUISITION

To incorporate the branched crack like reflectors in the concrete specimen, two moulds were prepared with top side having geometry as shown in the

Fig. **1**(a). Concrete mix of $M30$ grade was prepared and poured in both the moulds, compacted well, and were left to set. Within 24 hours the moulds were removed to extract the concrete samples. The top of these two samples were wrapped with thin polythene sheet as its acoustic impedance is very less and hence simulates the air-filled interface. These were then placed in main beam mould at their respective positions as shown in the

Fig. **1**(b). The specimen mould was filled with the concrete of the same M30 mix and cured for next 28 days. The top surface of the specimen after 28 days was grinded with the carborundum stone to get rid of any projections and hence reduce the undulations.
For data acquisition, first the boundaries and middle part of each reflector were demarcated on the top surface of the specimen. A shear wave dry-point contact based ultrasonic array with a central frequency of $50\,kHz$ is used for ultrasonic measurements. The length of the array is $175\,mm$ and all the ultrasonic measurements are acquired at along the middle of the specimen. The cast specimen with the ultrasonic array placed on the top surface is shown in the

2. For reflector 1 the middle of the array was aligned with the middle of array to acquire the FMC data. Since the length of the reflector 2 compares to the length of array hence for its complete mapping FMC was acquired at three places: (i) at left boundary of reflector, (ii) at middle of the reflector, and (iii) right boundary of the reflector 2.



Fig. 1: *(a) Pictorial view of the reflector mould.*

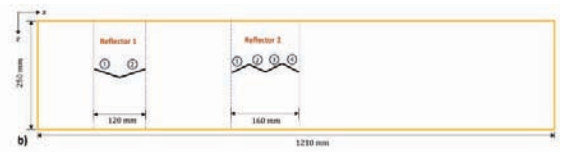

Fig. 2: *(b) Schematic diagram of the cross-sectional view of the concrete specimen with embedded reflectors.*

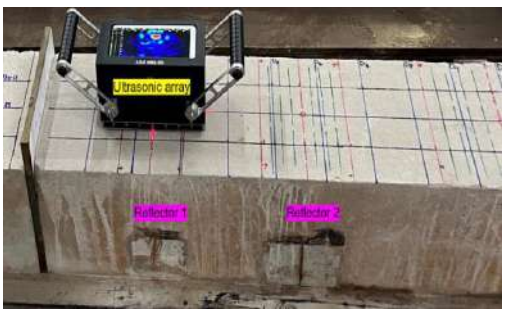

Fig. 3: *Ultrasonic measurement on the concrete specimen using ultrasonic array placed on the top surface.*

3. IMAGE RECONSTRUCTION RESULTS

The FMC at each measurement aperture is extracted such that the subsurface is reconstructed using PWI algorithm. Each FMC consists of 56 A-scans and one such A-scan is shown in the Fig. **3**3(a) and Fig. **3**3(b) is a B-scan when the 1st channel of the array is a source. The sampling interval of recording the signals is 1 µs

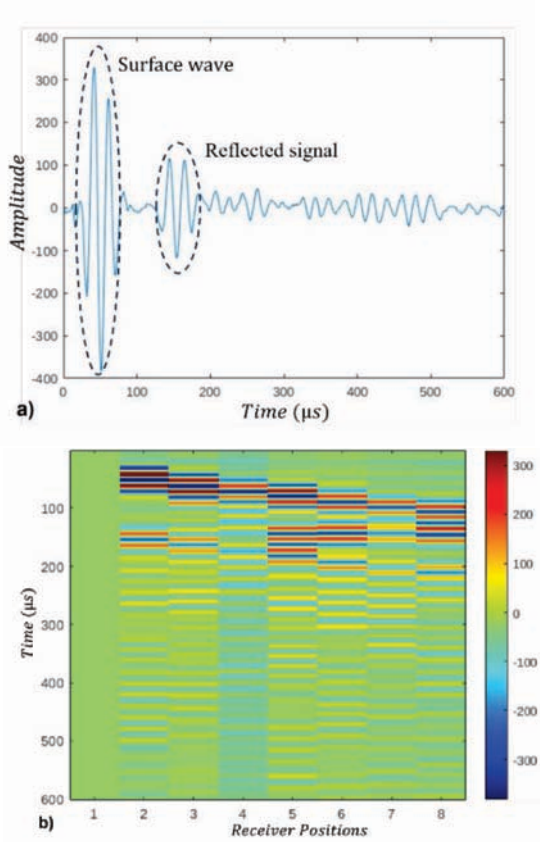

***Fig. 3**: Ultrasonic measurements acquired when the aperture is above reflector 1; (a) A-scan when 1st channel is a source and 2nd channel records, (b) B-scan corresponding to 1st channel.*

From the recorded data it can be observed that its unlikely to detect and map the reflector. However, using this FMC data the subsurface of the medium can be reconstructed with the reconstruction algorithms. The algorithm used for reconstruction of the subsurface in the present study is TFM. It is expected that the aperture facing geometry of the reflector will be mapped since this is a reflection tomography.

3.1 Imaging of Reflector 1

For reflector 1 the centre of the array is aligned with the middle of the reflector to acquire the FMC data. Due to significant amplitude of the surface waves they tend to mask the subsurface reflectors and hence in the first step the surface waves are removed from all the signals. Removal of surface wave from the received time domain signal $f(t)$ is achieved by multiplying it with the time delayed Heaviside function as given in the Eq.1 below:

$$f^S(t) = f(t) \times H(t - t_s - t_w) \quad (1)$$

Where,

$f^S(t)$ is the signal with removed surface wave,
$H(t - t_s - t_w)$ is the time delayed Heavside function,
t_s is the surface wave arrival time,
t_w is the temporal width of surface wave packet.

These post-processed signals are then used to reconstruct the subsurface under the aperture. Fig **4**(a) is the subsurface image reconstructed using TFM algorithm, while as Fig. 4(b) is the image reconstructed using PWI algorithm. Comparing both the images visually, a considerable noise is appearing in the TFM image whereas in the PW image the reflector spot appears prominently and the background noise very low. The same can be observed qualitatively on comparing the surface

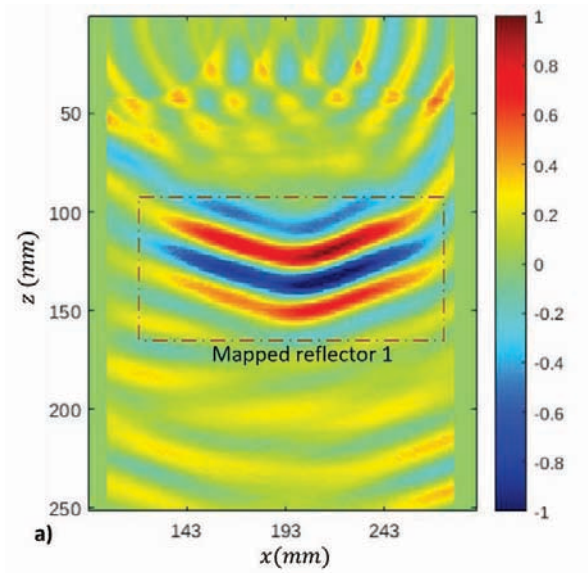

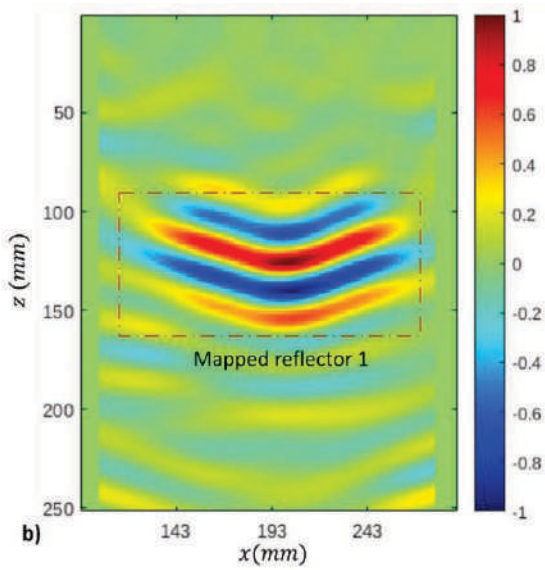

Fig 4: *Imaging results for reflector 1 reconstructed using, (a)TFM, (b) PWI algorithm.*

plots of TFM image shown in 5(a), and PW image as shown in Fig. 5(b). For further qualitative image analysis, lateral profile above the reflector spot at a depth of 60 *mm*, and within the reflector spot at a depth of 118 *mm* are presented in Fig.(a), and Fig. 6(b) respectively. Above the reflector spot the pixels have a significant intensity in TFM image while as for PW image the pixels above the reflector spot are of very small intensity. At 118 *mm* there is a considerable difference between peaks of segment 1 and 2 of TFM image, whereas in PW image the peaks are of similar intensity which is also expected since both the segments have same inclination angle. Along the depth profiles of both the reconstructed images at a length of 143 *mm* and 193 *mm* are shown in Fig7(a) and Fig. 7(b) respectively. Along the depth of the image, these profiles indicate existence of considerable noise in the background of TFM image while as for PW image the pixel values are of low amplitude compared to the reflector pixels.

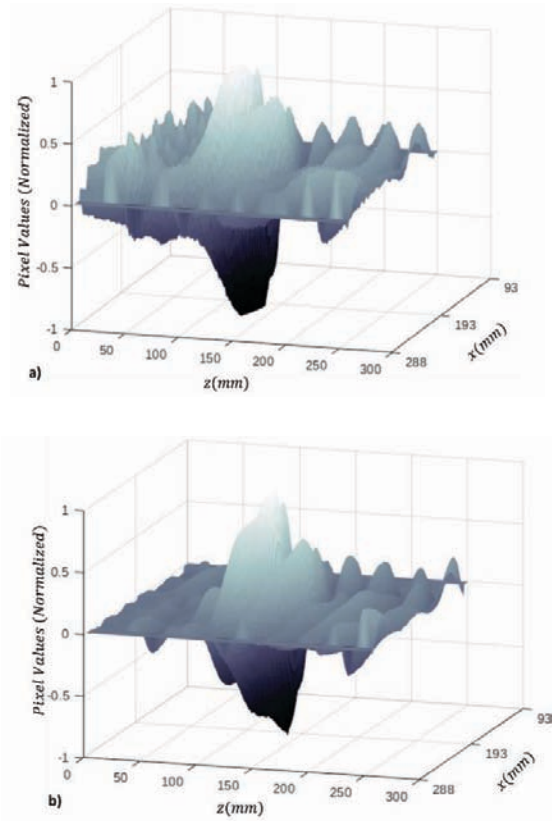

Fig 5*: Surface plots of: (a) TFM image, (b) PW image.*

The contrast to noise ratio (CNR) which is also one of the images qualitative analyses parameters and given in Eq.2 below [28]

$$CNR = 20\log_{10}\left(\frac{|\mu_{ROI} - \mu_{BG}|}{\sqrt{(\sigma_{ROI}^2 + \sigma_{BG}^2)/2}}\right) \qquad (2)$$

where, μ_{ROI}, μ_{BG} are means of pixel intensity in region of interest and background, and σ_{ROI}^2, σ_{BG}^2 are variances. The CNR calculated for the TFM image is 3.145, while as for PW image the CNR value is 4.04 which clearly indicated the improvement in contrast of the PW image over TFM image. Based on lateral and depth profiles and CNR value it can be deduced that compared to TFM image, PW image has lesser background noise and better mapped reflector features.

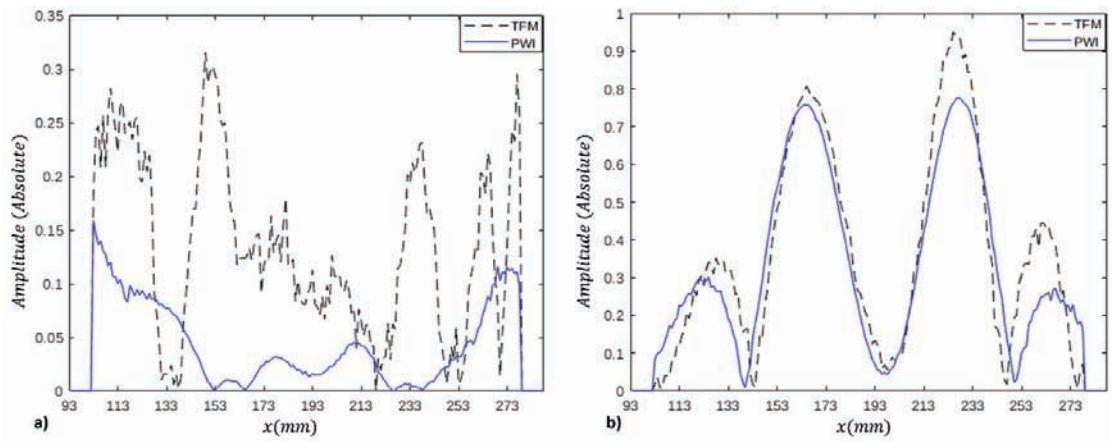

Fig.6: *Lateral profile of reconstructed images of reflector 1 at depth (a)* 60 *mm, (b)* 118 *mm.*

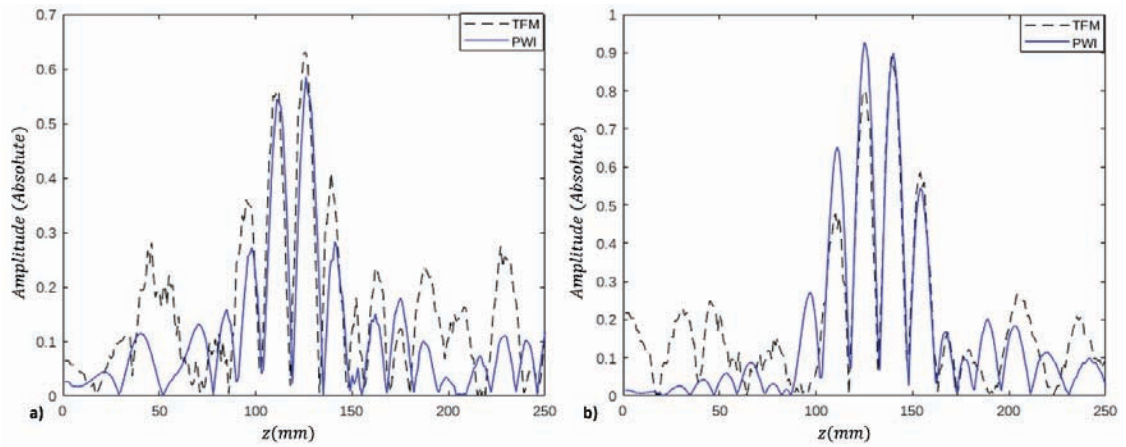

Fig 7: *Depth profile of reconstructed images of reflector 1 at a length of (a)* 143 *mm, (b)* 193 *mm.*

The input signal possesses a definite temporal width and when the reconstruction is done the temporal width of the signal is mapped in the spatial domain. This leads to imaging of reflector spot with definite thickness even though it only represent the aperture facing top geometry of reflector.

Though the whole geometry of the reflector is imaged and estimating the geometrical properties *viz.* length and inclination from images is challenging since reflector spots lack well defined boundaries as well as having definite thickness. Therefore, amplitude-based quantification is performed instead of image- based quantification . The rotation angle at which the maximum width at $-6\ dB$ level is estimated is the inclination angle and the length respectively. The reflector spot has two segments and therefore each segments geometrical parameters are estimated separately. The amplitude plot for segment 1 at rotation angle of 18.2° is shown in the Fig. **8**(a), wherein the estimated length is $63\ mm$. For segment 2, the maximum width at $-6\ dB$ level is $64\ mm$ corresponding to the rotation angle of 18.4° and the amplitude plot is shown in Fig. 6(b). The estimated geometrical parameters and associated errors are presented in the Table 1.

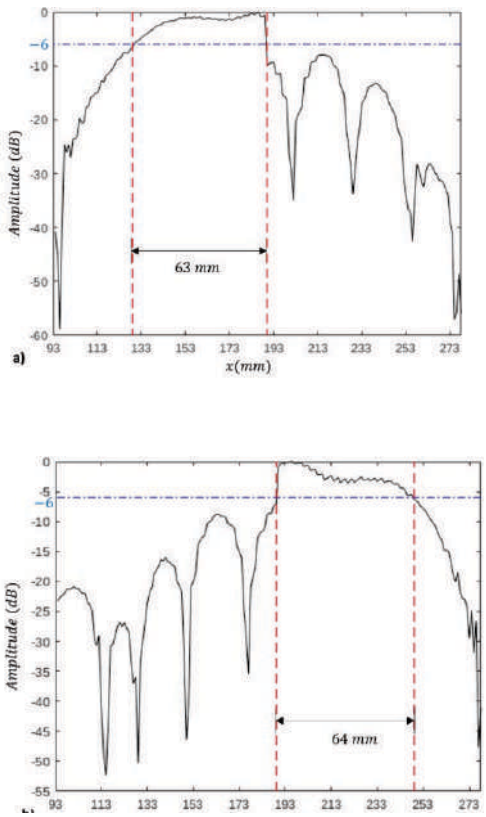

Fig. 8: *Amplitude plots of reflector 1 for (a) segment 1, (b) segment 2.*

Table 1: *Estimated geometrical parameters of reflector 1.*

Parameters		*Length (mm)*	*Angle(°)*
Actual value in medium		62	18
Segment 1	Estimated value	63	18.2
	Error (%)	1.6	1.1
Segment 2	Estimated value	64	18.4
	Error (%)	3.2	2.2

For both segments geometrical parameters are estimated as above and based on this information the trace of the reflector 1 is plotted as shown in Fig9.

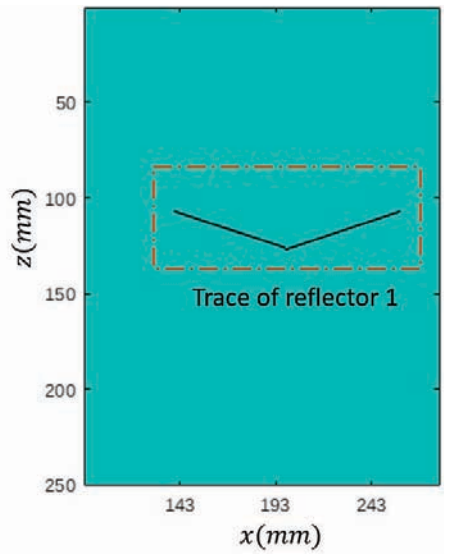

Fig. 9: *Reflector 1 traced based on the estimated geometrical parameters.*

3.2 Imaging of Reflector 2

The horizontal length of the reflector is 160 mm while as the length of aperture is 175 mm. To image the complete top geometry, ultrasonic measurements are required to be obtained at different positions. The ultrasonic measurements are obtained by placing the centre of the array at left edge, middle, and right edge of the reflector 2 as shown in Fig. 100(a). Under each aperture the subsurface image is reconstructed using the PWI algorithm and corresponding to the middle aperture the subsurface PW image is shown in Fig. 100(b).

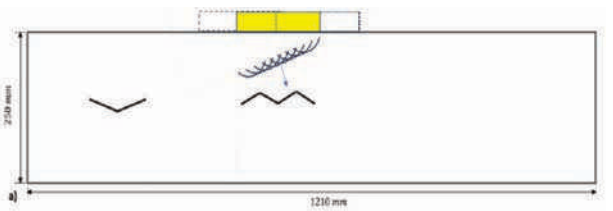

(a)

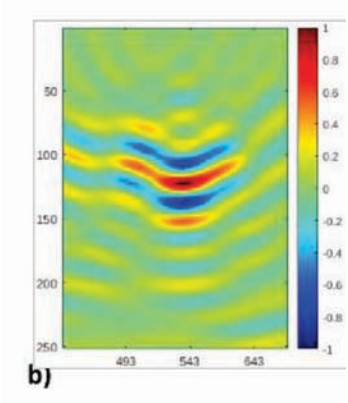

Fig. 10: *(a)Beam steering to generate plane wave at the mid-position of reflector 2, (b) Subsurface PW image reconstructed when the aperture is at the mid-position of reflector 2.*

The reconstructed PW subsurface image under left edge aperture is shown in Fig.1(a), where a part of the reflector is mapped.here is a V-shaped geometry of the reflector and the same is imaged under the middle aperture as shown in Fig.11(b). Fig.11(c) is subsurface PW image corresponding to right edge where only the right inclined part of the reflector is imaged. Under each aperture, only a part of the reflector is mapped in the subsurface images and to realise the actual geometry of the reflector, the images need to be stitched together according to the aperture position. All these reconstructed images are stitched together as shown in the Fig 12(a), where the complete aperture facing geometry of the reflector 2 is mapped. For each segment the inclination and length are estimated using the amplitude-based quantification technique, the results of which are tabulated in Table 2. Once the geometrical parameters are estimated the information is used to plot the trace of the reflector as shown in Fig. 9(b). The error in estimation of the geometrical parameters of each segment of the reflector remains contained within 6%.

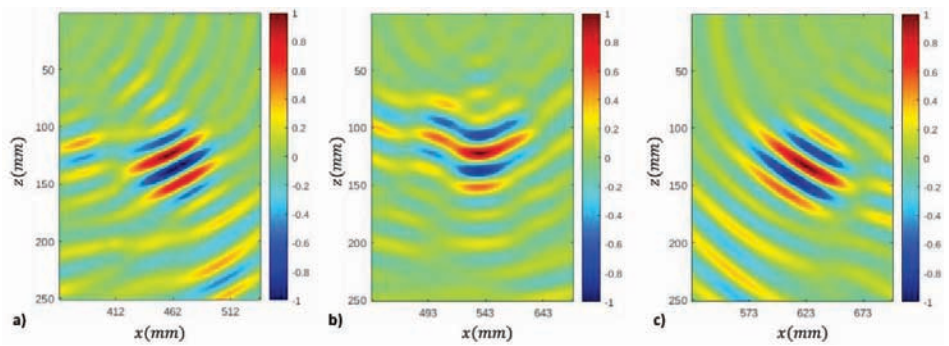

Fig.11: *Reconstructed images under aperture, (a) left edge, (b) middle, (c) right edge.*

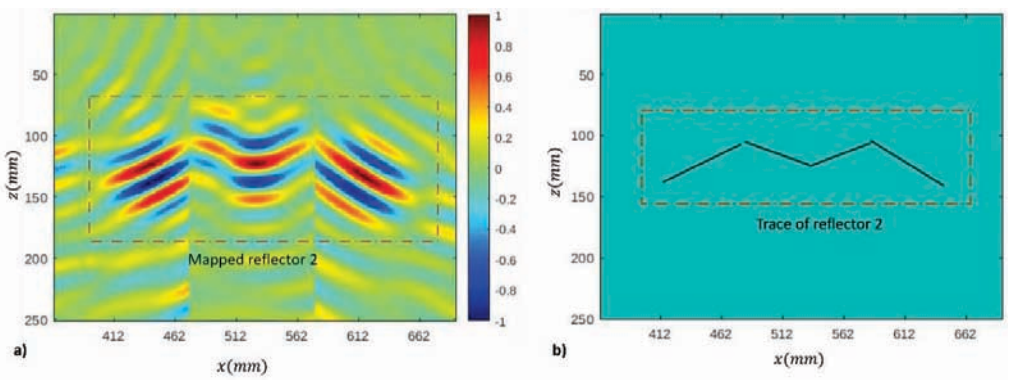

Fig. 12: *(a) Combined image obtained after stitching together the PW images under aperture: left edge, middle and right edge. (b) Trace of the reflector 2 from combined image.*

Table 2: *Geometrical parameters of all the segments of reflector 2.*

$Segments$	$Length\ (mm)$		$Error\ \%$	$Angle\ (°)$		$Error\ \%$
	$Actual$	$Estimated$		$Actual$	$Estimated$	
1	60	62	1.66	26	26.5	1.9
2	52	54.4	4.6	22	21.4	−2.7
3	52	53.5	2.8	22	22.2	0.9
4	66	70	6.0	30	31.6	5.3

4. CONCLUSION

Detection and mapping of complex patterned reflectors like subsurface cracks in the concrete using ultrasound reflection-based imaging is a challenging task. The heterogenous nature of concrete means considerable signal to noise ratio of recorded signals, while as the limited application frequency means lesser resolution. Both these combined with wrong mapping of reflectors as well as presence of grating lobes lead to low contrast of the reconstructed images with the state of art TFM algorithm. To improve the contrast and mapping of the subsurface reflectors, authors have previous developed PWI algorithm. In this study the same algorithm is used for imaging of such complex patterned reflectors in the experimental investigations. The reconstructed PW images have higher contrast and hence better mapped subsurface features compared to the TFM images. The accuracy in estimation of the geometrical parameters of the complex patterned reflectors is close to 94% and above in our experimental investigations. Based on this study it is concluded that plane wave imaging is able to effectively image and trace the subsurface reflectors of complex geometry, like cracks which usually do exist with complex patterns at subsurface of concrete. There are few limitations associated with the geometrical quantification and tracing technique. The amplitude-based quantification technique used in this study needs to be applied one-by-one to each segment of the reflector. This increases the post-processing time and hence in the future study's authors intend to develop quantification technique that will effectively trace and quantify all the reflectors in an image simultaneously.

5. REFERENCES

[1] A. Borosnyói, G.L. Balázs, Models for flexural cracking in concrete: the state of the art, Structural Concrete. 6 (2005) 53–62. https://doi.org/10.1680/stco.2005.6.2.53.

[2] C. Andrade, C. Alonso, F.J. Molina, Cover cracking as a function of bar corrosion: Part I-Experimental test, Mater Struct. 26 (1993) 453–464. https://doi.org/10.1007/BF02472805.

[3] M. Zomorodian, G. Yang, A. Belarbi, A. Ayoub, Cracking behavior and crack width predictions of FRP strengthened RC members under tension, Eng Struct. 125 (2016) 313–324. https://doi.org/10.1016/j.engstruct.2016.06.042.

[4] Y.Y. Kim, J.M. Kim, J.W. Bang, S.J. Kwon, Effect of cover depth, w/c ratio, and crack width on half cell potential in cracked concrete exposed to salt sprayed condition, Constr Build Mater. 54 (2014) 636–645. https://doi.org/10.1016/j.conbuildmat.2014.01.009.

[5] C.W. Chang, C.H. Lin, H.S. Lien, Measurement radius of reinforcing steel bar in concrete using digital image GPR, Constr Build Mater. 23 (2009) 1057–1063. https://doi.org/10.1016/j.conbuildmat.2008.05.018.

[6] X. Zhou, Q. Chen, S. Lyu, H. Chen, Estimating the Direction and Radius of Pipe from GPR Image by Ellipse Inversion Model, (2022).

[7] S. Hiasa, R. Birgul, F. Necati Catbas, A data processing methodology for infrared thermography images of concrete bridges, Comput Struct. 190 (2017) 205–218. https://doi.org/10.1016/j.compstruc.2017.05.011.

[8] T. Omar, M.L. Nehdi, T. Zayed, Infrared thermography model for automated detection of delamination in RC bridge decks, Constr Build Mater. 168 (2018) 313–327.

https://doi.org/10.1016/j.conbuildmat.2018.02.126.

[9] H. Ma, J. Qiu, The Application of Electromagnetic Induction Method in the Detection of Steel Bars Position in Reinforced Concrete Structure, in: 2020 11th International Conference on Prognostics and System Health Management (PHM-2020 Jinan), IEEE, 2020: pp. 490–493. https://doi.org/10.1109/PHM-Jinan48558.2020.00095.

[10] F. Zhang, L. Pahlavan, Y. Yang, Evaluation of acoustic emission source localization accuracy in concrete structures, Struct Health Monit. 19 (2020) 2063–2074. https://doi.org/10.1177/1475921720915625.

[11] D. Wells, An acoustic apparatus to record emissions from concrete under strain, Nuclear Engineering and Design. 12 (1970) 80–88. https://doi.org/10.1016/0029-5493(70)90135-4.

[12] C. Hsiao, C.-C. Cheng, T. Liou, Y. Juang, Detecting flaws in concrete blocks using the impact-echo method, NDT & E International. 41 (2008) 98–107. https://doi.org/10.1016/j.ndteint.2007.08.008.

[13] K.F. Graff, Wave_Motion_in_Elastic_Solids, n.d.

[14] S. Ashok Kumar, M. Santhanam, Detection of Concrete Damage Using Ultrasonic Pulse Velocity Method, in: Proc. National Seminar on Non-Destructive Evaluation , 2006: pp. 301–308.

[15] K. Soetomo, T.F. Rahma, E. Juliastuti, D. Kurniadi, Ultrasonic tomography for reinforced concrete inspection using algebraic reconstruction technique with Iterative Kaczmarz method, in: 2016 International Conference on Instrumentation, Control and Automation (ICA), IEEE, 2016: pp. 16–21. https://doi.org/10.1109/ICA.2016.7811468.

[16] C. Holmes, B.W. Drinkwater, P.D. Wilcox, Post-processing of the full matrix of ultrasonic transmit–receive array data for non-destructive evaluation, NDT & E International. 38 (2005) 701–711. https://doi.org/10.1016/j.ndteint.2005.04.002.

[17] S. Beniwal, A. Ganguli, Localized Condition Monitoring Around Rebars using Focused Ultrasonic Field and SAFT, Research in Nondestructive Evaluation. 27 (2016) 48–67. https://doi.org/10.1080/09349847.2015.1052168.

[18] J. Zhang, B.W. Drinkwater, P.D. Wilcox, A.J. Hunter, Defect detection using ultrasonic arrays: The multi-mode total focusing method, NDT & E International. 43 (2010) 123–133. https://doi.org/10.1016/j.ndteint.2009.10.001.

[19] S.U. Reyaz, S. Beniwal, Plane Wave Imaging of Concrete Using Phased Array Ultrasonic Technique - A Numerical Study, in: 2021 IEEE International Ultrasonics Symposium (IUS), IEEE, 2021: pp. 1–4. https://doi.org/10.1109/IUS52206.2021.9593436.

[20] S. Müller, E. Niederleithinger, T. Bohlen, Reverse Time Migration: A Seismic Imaging Technique Applied to Synthetic Ultrasonic Data, International Journal of Geophysics. 2012 (2012) 1–7. https://doi.org/10.1155/2012/128465.

[21] M. Grohmann, S. Müller, E. Niederleithinger, S. Sieber, Reverse time migration: introducing a new imaging technique for ultrasonic measurements in civil engineering, Near Surface Geophysics. 15 (2017) 242–258. https://doi.org/10.3997/1873-0604.2017006.

[22] S. Beniwal, A. Ganguli, Defect detection around rebars in concrete using focused ultrasound and reverse time migration, Ultrasonics. 62 (2015) 112–125. https://doi.org/10.1016/j.ultras.2015.05.008.

[23] A.O. De La Haza, A.A. Samokrutov, P.A. Samokrutov, Assessment of concrete structures using the Mira and Eyecon ultrasonic shear wave devices and the SAFT-C image reconstruction technique, Constr Build Mater. 38 (2013) 1276–1291. https://doi.org/10.1016/j.conbuildmat.2011.06.002.

[24] Surendra Beniwal, Localized evaluation of interface bond of rebars in concrete using focused ultrasonic imaging, IITD, 2016.

[25] S. Beniwal, D. Ghosh, A. Ganguli, Ultrasonic imaging of concrete using scattered elastic wave modes, NDT & E International. 82 (2016) 26–35. https://doi.org/10.1016/j.ndteint.2016.04.003.

[26] D. Ghosh, S. Beniwal, A. Ganguli, A. Mukherjee, Reference free imaging of subsurface cracks in concrete using Rayleigh waves, Struct Control Health Monit. 25 (2018) e2246. https://doi.org/10.1002/stc.2246.

[27] S.T. Kuchipudi, D. Ghosh, An ultrasonic wave-based framework for imaging internal cracks in concrete, Struct Control Health Monit. 29 (2022). https://doi.org/10.1002/stc.3108.

[28] M.C. van Wijk, J.M. Thijssen, Performance testing of medical ultrasound equipment: fundamental vs. harmonic mode, Ultrasonics. 40 (2002) 585–591. https://doi.org/10.1016/S0041-624X(02)00177-4.

NDE PATENTS

Dr.Shyamsunder Mandayam

Through this feature every quarter, we intend to provide you a snapshot of some latest and important patents in the world of NDE. We also intend to use this feature to encourage the Indian NDE community to file more patents based on your innovations. We will be happy to provide guidance and assistance in different ways – Answering queries, Conducting Tutorials and webinars, One-on-one discussions, Networking with Intellectual property experts, etc.

Need help understanding? What are Patents? Why to Patent? When to Patent? What is the Patenting Process? …… Please feel free to reach out to me by email at mandayam.shyamsunder@gmail.com

Here we list below a few interesting patents related to a mix of different modalities in ***NDE and Inspection.***

United States Patent 20230251228A1

System and Method for Real-time visualization of Defects in a Material

Inventors: David A. Jack, Benjamin M.Blandford, Nathaniel J.Blackman

Assignee: Verifi Technologies, LLC, Waco, TX, USA

The present disclosure provides a system and method for real-time visualization of a material during ultrasonic non-destructive testing. The system includes a graphical user interface (GUI) capable of showing a three-dimensional (3-D) image of a composite laminate constructed of a series of two-dimensional (2-D) cross sections. The GUI 1s capable of displaying the 3-D image as each additional 2-D cross section 1s scanned by an ultrasonic testing apparatus in real time or near real time, including probable defect regions that contain a flaw such as a hole, crack, wrinkle, or foreign object within the composite. Furthermore, in one embodiment, the system includes an artificial intelligence capable of highlighting defect areas within the 3-D image in real time or near real time and providing data regarding each defect area, such as the depth, size, and/or type of each defect.

United States Patent 011703477B2

Nondestructive Testing Method and device for Detecting and Distinguishing Internal defect and external defect of wire rope

Inventors: Dong Lai Zhang, Shenzhen, En Chao Zhang, Wei Gao, Xiao Lan Yan, Shi Min Pan

Assignee: Harbin Institute of Technology (Institute of Science and Technology Innovation), Shenzhen (CN)

A nondestructive testing method for detecting and distinguishing internal and external defects of a wire rope includes: acquiring a magnetic flux signal and a MFL signal of a detected wire rope; preprocessing the magnetic flux signal and the MFL signal of the detected wire rope; comparing a pre-processed magnetic flux signal and a pre-processed MFL signal with a preset magnetic flux signal threshold and a preset MFL signal threshold respectively, and calculating a defect position; extracting a magnetic flux signal of a defect and an MFL signal of the defect based on the defect position; calculating a defect width of the detected wire rope based on the magnetic flux signal of the defect and the MFL signal of the defect; calculating a defect cross-sectional area loss of the detected wire rope based on the defect width; and determining whether the defect 1s the internal defect or the external defect.

NDE PATENTS

United States Patent 011719672B2

Application Specific Excitation of Ultrasonic Probes

Inventors: Thomas Wuerschig, Johannes Buechler

Assignees: Baker Hughes Oilfield Operations LLC

Systems and methods for improved ultrasonic testing are provided. An ultrasonic testing system can include an ultrasonic probe and an ultrasonic controller in electrical communication with the ultrasonic probe. The ultrasonic probe can include a plurality of ultrasonic transducers. The ultrasonic controller can be configured to generate one or more driving signals operative to cause the plurality of ultrasonic transducers to generate respective ultrasonic waves. A combination of the ultrasonic waves can form an ultrasonic waveform having one or more characteristics specified by the one or more driving signals. The ultrasonic controller can be further configured to change the one or more driving signals to adjust at least one characteristic of the ultrasonic waveform.

United States Patent 011680857B2

Ultrasonic Test Device and Test method for Service Stress of a moving Mechanical Component

Inventors: Chunguang Xu, Shuangyi Li, Yuren Lu, Peng Yin

Assignee: Beijing Institute of Technology, Beijing (CN)

An ultrasonic test device and test method for service stress of a moving mechanical component, where the device comprises an ultrasonic probe, a coupling fluid, a pressure-maintaining cover and universal wheels. The cover is arranged above an inspected position of an inspected component, an interior of the pressure-maintaining cover is filled with coupling fluid, a bottom of the cover is provided with a structure permeable to the coupling fluid to form a coupling fluid film between the inspected position and the bottom of the cover, and a top of the cover is equipped with the ultrasonic probe. A detection part at a lower part of the ultrasonic probe extends into the coupling fluid of the cover and is vertical to the bottom of the cover without contact. The distance between the ultrasonic probe and the inspected component is kept unchanged through the universal wheels.

United States Patent 20230143492A1

Ultrasonic Phased Array transducer for the NDE Inspection of the Jet pump riser welds and welded attachments

Inventors: Charles R. Barrett, Kevin J. Foley

Assignee: Westinghouse Electric Company LLC, Cranberry Township, PA (US)

An ultrasonic phased array transducer assembly having a single housing in which a plurality of phased array transducer subassemblies are mounted at a skewed angle relative to a leading face of the housing and to each other, with each transducer mounted on composite wedge(s) at different orientations within the housing.

Indian Society for Non-destructive Testing (ISNT)
Enriching Lives through NDE

CIRCULAR

No: ISNT/2023/01 **Date: 2nd January 2023**

Schedule of ISNT meetings
YEAR: 2023

Month	Meeting	Day/Date of mtg.	Timing	Mode / Venue
JANUARY 2023	Past President's Meeting	Sunday, 8th January	03:30 pm–05:30 pm	ONLINE
	Finance / Treasurers Meeting	Saturday, 21st January	03:30 pm–05:30 pm	ONLINE
FEBRUARY 2023	Byelaw Enforcement & Advisory and RA Committee	Saturday, 4th February	03:30 pm–05:30 pm	ONLINE
MARCH 2023	Chapter Chairmen Meeting	Saturday, 4th March	03:30 pm–05:30 pm	ONLINE
	PFMB	Saturday, 11th March	10.00 am– 11.30 am	HYBRID Online / ISNT HO, Chennai
	TMB		11.45 am – 1.30 pm	
	NCB		2.30 pm – 4.30 pm	
	NGC	Sunday, 12th March	10.00 am – 3.30 pm	
MAY 2023	Finance / Treasurers Meeting	Saturday, 20th May	03:30 pm–05:30 pm	ONLINE
JUNE 2023	PFMB	Saturday, 10th June	10.00 am– 11.30 am	HYBRID Online / ISNT HO, Chennai
	TMB		11.45 am – 1.30 pm	
	NCB		2.30 pm – 4.30 pm	
	NGC	Sunday, 11th June	10.00 am – 3.30 pm	
JULY 2023	Past President's Meeting	Sunday, 9th July	03:30 pm–05:30 pm	ONLINE
AUGUST 2023	Byelaw Enforcement & Advisory and RA Committee	Saturday, 5th August	03:30 pm–05:30 pm	ONLINE
SEPTEMBER 2023	Chapter Chairmen Meeting	Saturday, 2nd September	03:30 pm–05:30 pm	ONLINE
	PFMB	Saturday, 9th September	10.00 am– 11.30 am	HYBRID Venue to be decided by March NGC
	TMB		11.45 am – 1.30 pm	
	NCB		2.30 pm – 4.30 pm	
	NGC	Sunday, 10th September	10.00 am – 3.30 pm	
	Finance / Treasurers Meeting	Saturday, 16th September	03:30 pm–05:30 pm	ONLINE
OCTOBER 2023	Award Committee	Saturday, 14th October	03:30 pm–05:30 pm	ONLINE
DECEMBER 2023	PFMB	Wednesday, 6th December NDE 2023	02.00 pm– 03.00 pm	PHYSICAL NDE 2023 Venue, Pune
	TMB		03.00 pm - 04.00 pm	
	NCB		04.30 pm– 0530 pm	
	NGC		05.30 m - 07.30 pm	

Notes: 1. Separate notifications will be sent to the members of the committee / Board for each meeting
2. Each meeting should be attended only by the members and invitees

Bikash Ghose
Hon Gen Secretary, ISNT

The First International Conference on NDE 4.0 - April 2021 in Virtual Mode



The Second International Conference on NDE 4.0 – October 2022 at Berlin, Germany



And Now Proudly Announcing

The Third International Conference on NDE 4.0

to be held during

February 2025 in INDIA !

Watch this space for more details

ORGANISED BY

INDIAN SOCIETY FOR
NON-DESTRUCTIVE TESTING

NDE 2023

DEC 7-9, 2023 • PUNE

33rd Annual Conference & Exhibition on
NON DESTRUCTIVE EVALUATION



theme

Transformative NDE:
Unleashing the Power of Advanced Technologies

VENUE

The Orchid Hotel, Pune
Maharashtra, INDIA

OUR SPONSORS

PRINCIPAL SPONSOR

Waygate Technologies
a Baker Hughes business

PLATINUM SPONSOR

EVIDENT

GOLD SPONSORS

TECHNOFOUR
THE HOT TECHNOCRATS

TELEDYNE FLIR

MR CHEMIE
HOT MATERIALS

SILVER SPONSORS

VisiConsult

3 Eminent Engineering & Electronics Pvt. Ltd.

BLUE STAR
INDUSTRIAL SOLUTIONS

Eddyfi Technologies

ECH
the best in ndt

MODSONIC

ndtt

MAGNAFIELD
Electronics & Engineering

UPAC

www.isntnde.in









Find out more

Your Reliable Partner for Workflow Solutions

For enquiries, please contact:
marcomms.evidentindia@evidentscientific.com

EVIDENT